DISCRETE SAMPLE INTRODUCTION DEVICES IN

ANALYTICAL OPTICAL-EMISSION SPECTROMETRY

BY

Yuk Ying Cheung

A thesis submitted for the degree of Doctor of Philosophy in the University of London.

Department of Chemistry

Imperial College

London SW7 2AY

Dedicated to

        My Family

        Wai Sun

        Sai

        Kin

        Yvonne

        With love and affection

ABSTRACT

This thesis is divided into two parts. The first part deals with the adaptation of a graphite tube electrothermal vaporization device for the introduction of discrete liquid samples into an argon hydrogen air-entrained flame in which the phenomenon of chemiluminescence was studied. The superiority of the vaporizer/flame combination in terms of detection limits and ease of operation over other methods of sample introduction is discussed. The possibility of introducing organic compounds is studied briefly. The use of a horizontal quartz tube placed over the circular burner in line with the optics to enhance the emission intensity of S_2 species is described.

The second part of the thesis describes the use of a graphite rod electrothermal vaporization device for the introduction of discrete liquid samples and solid samples into an inductively-coupled argon plasma (ICAP) used as a source for optical emission spectrometry. The concentrations of the trace elements in cadmium mercury telluride determined by electrothermal vaporization and nebulization are presented to serve as standards for future studies in solid sampling. The thermal decomposition of cadmium mercury telluride and the effect of the vaporization temperature on the analyte emission signal shapes are examined. Empirical calibration curves are obtained for manganese and silver. Statistical analysis is employed to fit the best straight line to those graphs relating the relative emission intensity to the mass of cadmium mercury telluride vaporized into the inductively-coupled plasma. The possibility of employing cadmium and tellurium as internal standards is explored.

CONTENTS

ACKNOWLEDGEMENTS

The work described in this thesis was carried out at the Chemistry Department, Imperial College, between October 1977 and August 1980. It is entirely original except where due reference is made and no part has been previously submitted for any other diploma or degree.

CHAPTER ONE

SOME METHODS OF SAMPLE INTRODUCTION

1.1 Introduction

Since the development of the Bunsen burner[1] over a hundred years ago, premixed flames have played an important role in analytical chemistry. Their popularity for use in spectrometric techniques is due to several advantages:

1) Flames are convenient to use, reliable and relatively free from memory effects.

2) Burner systems are simple to construct and are inexpensive, sample solutions can be introduced into the flames by nebulization.

3) Both metals and non-metals can be determined by choosing a suitable flame composition.

4) The signal to background ratio obtainable is sufficiently high to allow adequate sensitivity and precision to be obtained.

1.2 Nebulization

The samples to be analyzed are usually in a liquid form or in solution after chemical pretreatment. Therefore, the most common and convenient technique for introducing liquid sample is by aspirating the sample to form an aeresol. On entering the flame (or plasma), the aerosol droplets are desolvated and the resultant particles are then dissociated and atomized. Any event that inhibits any processes associated with the final concentration of free atoms in the flame will decrease the sensitivity of the analysis.

Early designs employed for introducing liquid

samples into the flame were rather primitive. The apparatus

shown in Fig. I was utilized to introduce sodium chloride

into the flame as a suspension of fine droplets produced

by the effervescent reaction between the hydrochloric

acid and a zinc rod[2]. The rod could be inserted into

the acid or be removed at will. Beckmann [3-5] utilized

the eletrolysis of the analytical solution to produce

fine droplets.(Fig. 2)

It was apparent that these techniques were not

able to produce a constant and reproducible delivery of

the analyte to the flame. It was Gouy[6] who first attempted

to devise a prodedure for adequately controlled introduction

of samples. The introduction of the sample was based on

the principle of pneumatic nebulization.
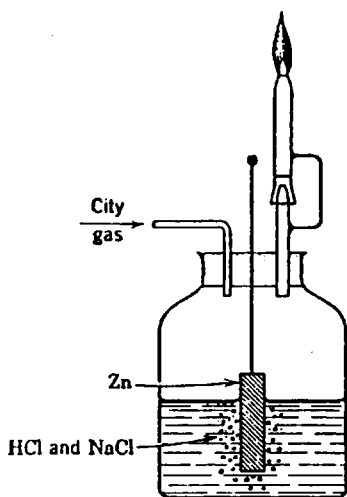
Fig. 1 Schematic description
of the procedure used by
Kirchhoff and Bunsen for
supplying their flame
with a solution.
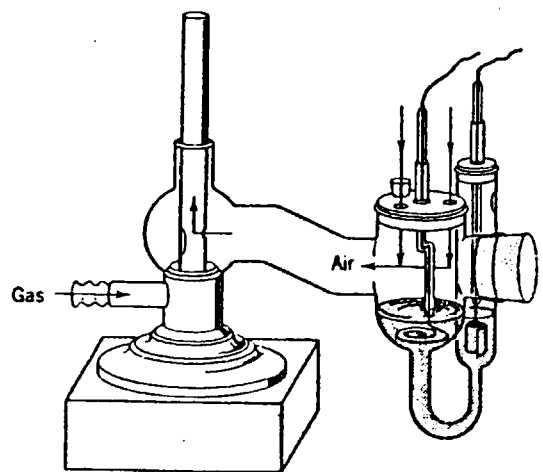
Fig. 2 Schematic description
of the apparatus used by
Beckmann to supply the
flame with a liquid
sample.

1.2.1   Pneumatic Nebulization

The simplest instrument which can be   used to disperse a liquid into a suspension of fine droplets is illustrated in Fig. 3 .   This pneumatic nebulizer consists of two tubes, one for the gaseous stream,and the other for the uptake of the solution, placed at right angles to each other.   The contact surface between the gaseous stream and the liquid can be enlarged by surrounding the gas outlet with a circular outlet for the liquid, thus increasing the output of the atomizer.   The resulting instrument is shown in Figs. 4 a and 4 b.   These schematic diagrams illustrate two concentric units in which the nebulizing gas enters through the central duct as in 4 a, whereas in 4 b, the liquid flows through the central tube. In both cases, the stream of air emerging from its nozzle with a high velocity entrains the liquid through the corresponding nozzle and tears from its surface fragments which are subsequently dispersed into a cloud of fine droplets.
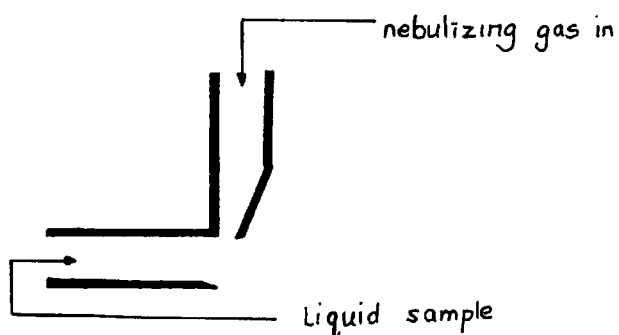
Fig. 3   A schematic diagram of a simple pneumatic atomizer

(a)   (b)
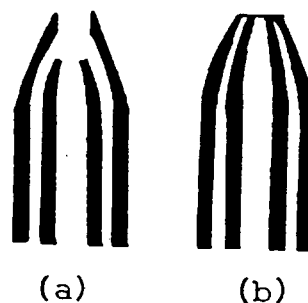
Fig. 4   Schematic diagram of concentric pneumatic nebulizers

The popular types of nebulizers employed are
the crossflow[7] and the concentric glass nebulizers[8].
Both devices have capillary tubes in their design to
generate an aerosol using gas at low flow rates. These
nebulizers function efficiently in aerosol generation.
Sensitivity may be affected, however, by the varying
viscosity of the sample. It is also possible for the
capillary tubes to become blocked, especially when analyzing
high salt content samples. Table 1.1 summarizes the
advantages and disadvantages of using a pneumatic nebulizer.

Table 1.1

Advantages	Disadvantages
1) Simple to construct. 2) Relatively low cost. 3) Simplicity in operation.	1) Low transport efficiency. 2) Uptake rate is affected by viscosity. 3) Unsuitable for liquids of high solid content. 4) Matrix and analyte are simultaneously nebulized.

Owing to the rapid growth of atomic absorption,
emission and fluorescence spectrometry with respect to
increased powers of detection, a need has arisen to in-
crease the efficiency of the pneumatic nebulizers to a
wide variety of samples such as biological fluids,
metallurgical and forensic samples to be analyzed.

For example, the Babington design[9] has been
used to nebulize solutions with high percentages of

dissolved solids and/ or suspended solids. Basically, the nebulizer consisted of a glass surface with a slit cut into it. A liquid flowing over the surface and across the slit was converted to a fine spray by pressurized air flowing through the slit. Since solutions to be nebulized were introduced on the outside of the nebulizer, there was little or no chance for clogging due to suspended particles or solutions of high viscosities. Thus, a wide range of complex materials including fuel oil, paints and food products can be nebulized. The Babington design produced a dense aerosol with a droplet size distribution of mean   diameter of 3.6μm with 95% of the refined droplets being below 5μm in diameter.

Similar procedures based on the Babington design were employed by several researchers. Fry and Denton[10] employed a modified Babington nebulizer for aspirating high solid solutions into a flame used for atomic absorption spectrometry. The large flow rates for sample solutions (20-25ml min^{-1}) and aspirant gas (8-12 L min^{-1}) made the Fry-Denton design undesirable for direct application to an ICP system.

The Suddendorf-Boyer[11] device was constructed from a piece of stainless steel. A 'V'-shaped channel was cut through the centre. A gas inlet port of 0.23mm in diameter was drilled perpendicularly to the centre of the channel . The liquid sample was introduced into the channel via a sample introduction tube. Aerosol was produced when the liquid flowing down the channel

was ruptured by the gas introduced from the gas inlet port. The dimensions of the walls of the stainless steel nebulizer were determined in such a way to prevent aerosol deposition. The sample solution uptake rate was 5ml min^{-1}. and the gas flow rate was compatible with ICP systems. However, the metal components were a potential source of contamination. The efficiency of this nebulizer was 5%. The cleanout time in between samples was about 90 seconds which ensured complete rinsing of all surfaces in contact with the sample solution.

Savage and Hiefje[12] reported a novel technique for reducing the size of aerosol droplets produced by a pneumatic nebulizer. The performance for theirelectric-field pneumatic nebulizer (EFPN) system was based upon the interaction of electric field forces and molecular forces within a charged liquid jet as it was pneumatically disrupted, resulting in an effective decrease in the surface tension of the liquid. This electric field-induced reduction in the surface tension led to the pneumatic formation of smaller droplets. Applying an electric field to the nebulizer resulted in a 63% reduction in aerosol volume mean diameter,thus enhancing the atom-ization process in the plasma.

1.2.2 Ultrasonic Nebulization

The ultrasonic nebulizer is specially designed to produce a fine spray of aerosol[13 - 23]. Nebulization is effected by pumping solutions onto a transducer plate oscillating at ultrasonic frequencies causing disintegration

of the sample solution into a very fine dense aerosol
which is subsequently swept into the plasma. These devices
offer the analyst greater powers of detection than those
obtainable using the pneumatic nebulizer, as the sample
solution input to the plasma can be greater by a factor
of ten. The aerosol particle size and its density are
independently controlled, unlike pneumatic nebulization
where particle sizes are reduced at the expense of density
because the carrier gas flow must be increased. In
ultrasonic nebulization, the aerosol density can be varied
simply by adjusting the gas flow past the liquid surface[24].
The size of the aerosol particles can be varied by changing
the ultransonic frequency[25,26]. The mean aerosol droplet
diameter obtained by ultrasonic nebulization is governed
by the ultrasonic frequency according to the relation[27]

$$d_o = \left[0.34 \frac{8\pi\sigma}{\rho f^2} \right]^{\frac{1}{3}} \qquad (1.1)$$

where σ is the surface tension of the solution (dyne cm^{-1}),
ρ is the specific gravity (g ml^{-1}) and f is the frequency
(Hz).

The increase in the efficiency of aerosol tran-
sport into the plasma may have an adverse effect upon
the lower power plasmas and it is often necessary to
employ desolvation apparatus to reduce the amount of
solution, but not the analyte entering the plasma. The
desolvation apparatus may, however, introduce errors into
the analysis. The loss of analyte due to the baking of
the dry particles onto the apparatus wall by high temp-
erature can lead to memory effects and decreased sensitivity.

The ultrasonic nebulizer is as versatile as the pneumatic nebulizer in the ability to nebulize sample of high salt matrix[28].

Many of the ultrasonic nebulizers employed are fed with a continuous flow of sample solution, but several reports have been published describing pulse sample delivery. Pulse introduction of sample limits the volume of liquid which goes into the flame or plasma[29,30] (see section 1.5).

1.3.1 Graphite Furnace Electrothermal Atomizers

Although aspiration into a flame is the most convenient and reproducible means of obtaining atomic vapour, it is one of the least efficient in terms of converting all the sample elements to atomic vapour and presenting this to the optical path of the spect-rometer. The overall efficiency of atomic conversion and measurement of atoms present in aspirated solutions has been estimated to be as little as 0.1%.

Analytical flames suffer from several problems, some which contribute to low efficiency in atom conversion.

1) the sensitivity of flame emission is limited by the amount of sample atomized and the extent to which the atom population is diluted by the flame gases.

2) loss in accuracy and precision results from uncon-trollable fuel to oxidant concentrations.

3) solid samples cannot be conveniently atomized in the flame.

4) the analyte residence time is short due to the chemically active environment of the flame.

In view of the above limitations, it became desirable to develop a device capable of high efficiency in converting the sample into atoms and in concentrating the resultant atomic vapour for spectrochemical measurement.

The first workers to achieve this using a so called "non-flame" atom cell for analytical purposes were L'Vov[31] and Massmann[32], although much earlier, King[33-35] had used a similar device to study atomic transition probabilities.

Instead of having a direct contact between the sample and the carbon tube, Woodriff and coworkers [36-38] introduced samples into the tube on a carbon cup inserted through the side arm of the tube.

Headridge and Smith[39] reported the use of an induction furnace for determining volatile elements in solutions by AAS. The furnace was inductively heated to 1350°C for routine use and it had been applied to the determination of cadmium in zinc base alloys.

West and Williams[40] pioneered the use of a graphite filament as an atom cell. The filament, 2mm in diameter and 20mm in length, could be raised to a temperature up to about 2500°C in 5 seconds by a passage of a current of ca 100 A. This device had been applied to determine a number of elements by Atomic Fluorescence Spectrometry[41] or by Atomic Absorption Spectrometry[42]. Other variations in carbon atomization techniques include atomization from a platform in graphite furnace [43] and graphite disc atomizers[44].

The initial response to the graphite non-flame atomizers was tremendous leading to an escalating quantity of publications on the applications of such atom cells. However, it was soon realized that carbon furnaces are prone to memory effects due to the porosity of the graphite and the formation of refractory carbides. Elements such as boron, vanadium, zirconium form carbides and require high temperature to effect complete atomization. The repeated use of the tube at high temperatures also degrades the performance and life-time of the tube or rod.

One improved version of the graphite tube is the pyrolytic graphite tube, which has the properties of low permeability to gases, low porosity, high purity and a higher sublimation temperature (3970K) than the standard graphite tube (3300K). Pyrolytic graphite, therefore, should offer improved sensitivity, detection limits, and precision due to improvement in vapour confinement, uniform heating and long life time. Sturgeon and Chakrabarti (44) , however, have demonstrated that there is no significant improvement in detection limits using the pyrolytic graphite coated tube. The precision values obtained for some elements measured with the coated and uncoated tube do not differ significantly, a fact also noted by Manning and Ediger[45]. Therefore, Chakrabarti recommends the use of pyrolytic tubes only on the basis of enhancement in sensitivities obtainable for nonvolatile elements and of the reduced atomization times for most elements.

1.3.2 Electrothermal Atomization from Metallic Surfaces

Atomization techniques in which a wire loop or sample boat carrying the sample is introduced into the hot flame above the primary reaction zone of a premixed flame can be traced back to the original work of Bunsen[1] in flame emission photometry. Several non-flame devices of the same type in which an electrically heated filament or a boat was used have been reported. In these open devices, the atom cloud released from the filament (or boat) passes into an unconfined volume in the absorption light path; transient analytical signals are recorded. Owing to the unconfined nature of the atom cell in these devices, any tendency towards memory effects due to analyte deposition may be minimized. Metallic atomizers are sometimes preferred because of their low background emission in the 200-350nm spectral region and of the need to avoid carbide formation.

The most commonly used metals for constructing filaments and boats are tantalum[46-48] and tungsten [49,50]. Other less common atomizers have been employed [51-53] which include   platinum filaments and tungsten alloy (97% tungsten,3% rhenium) wire loops. The former atomizer is expensive for routine purposes and the latter one, although recommendable for its high melting point (3200°C) and its pliability, does not reproducibly take up the same volume of solution each time it is used.

A device which is a combination of metal and graphite atomizers is the Filament In Furnace Atomizer

(FIFA).[54] The filament is a tungsten wire equipped with 5 to 10 sample locating coils and the graphite tube serves as a heat reservoir to the filament. 1-2 μl aliquots of sample are pipetted onto the coil and are evaporated and ashed in air outside the furnace tube. Each coil then passes through the graphite furnace sequentially for atomization.

The FIFA has been tested in a survey[54] in which the determination of the lead content in micro-litre volume of capillary blood samples and milligrammes of hair segments was reported.

The sensitivities of flameless atomic absorption with a tantalum ribbon atomizer and with a tungsten filament atomizer are similar in magnitude [55]. Groups of workers who have used tungsten filament atomizers claim that they are superior to carbon tube furnaces in terms of sensitivity and detection limits. Sychra et al,[56] however, have discussed this point in length and concluded that the characteristic concentrations, detection limits, optimum atomization temperatures, reproducibility and profiles of calibration curves obtained for silver, manganese, nickel, lead, vanadium are similar to those obtained with the graphite tube atomizer, because, for as long as the elements do not interact with the atomizer material, they will vaporize with equal ease, whether it is from a graphite surface or a metallic surface.

1.4 Electrothermal Vaporization into an Excitation Source

Exceptional relative and absolute powers of detection are achieved using furnace AAS. But in most cases, the technique is subject to many experimental constraints. They are as follows:

1) Critical experimental parameters must be optimized for each element.

2) The furnace tube porosity affects sensitivity; an effect which increases with increasing age of the tube.

3) Non specific absorption and light scatter neccesitates the use of background correction techniques which add cost to the instrument.

4) Analytical curves are limited to a small range of concentrations.

5) Recombination, nucleation of sample, incomplete vaporization of analyte lead to loss of sensitivity and detection power.

6) Simultaneous multielement determinations cannot be performed by conventional atomic absorption or fluorescence techniques.

In order to acheive higher sensitivity, ease and convenience of operation, freedom of interferences, novel techniques are evolving to meet the requirements of modern day analysis.

For the past two decades, the technological advances made on the inductively coupled plasma (ICP) optical emission spectrometry (OES) have firmly established the position of the ICP in analytical instrumentation.

It is well known that the ICP is relatively interference free due to its high temperature and the analytical curves obtained are linear over a concentration range of 4 or 5 orders of magnitude. The combination of electrothermal vaporization followed by plasma excitation of the elements offers the possibility of trace determinations on a multielement basis. With this arrangement, the problems of having to correct for the background and to critically optimize the parameters are eliminated.

The use of resistively heated vaporizer as a means of introducing samples into the plasma has several advantages over the pneumatic nebulizer.

1) The dry aerosol is introduced in a pulse which has the effect of increasing the density of the analyte per unit time. Hence sharp signal peaks of short duration are obtained, and detection power is increased by 1 or 2 orders of magnitude[57].

2) The element of interest can be arranged to be released before or after the vaporization of the bulk matrix by careful control of the heating programme. Thus elim-inating   interferences arising from the matrix.

Gunn[58] was the first at Imperial College to assess the capability of using a graphite rod as an electrothermal vaporization device for introducing samples into an ICP. Millard[59] furthered the work and applied the device to the determination of toxic elements in serum. It was fournd that using the graphite rod vaporizer, the

transport efficiency of cadmium in the presence of selenium (VI)
was 80% as compared to 39% in the absence of Se VI. It is
believed that after vaporization, the vapour aggregates into
geometric clusters which undergo elastic collisions with the
walls of the graphite rod enclosure and the transport tubing
and into the plasma[60]. In this manner, there is little
deposition of the analyte. As cadmium is a very volatile ele-
ment it requires a foreign substance to assist aggregation.

Nixon et al[61] described the use of tantalum
filament arrangement for the desolvation and subsequent
vaporization of 20μl sample volumes into an ICP. In later
studies[62], the Fassel authors found that the tantalum vaporized
together with the analyte at high temperatures and caused
spectral interference with some of the useful analytical
lines; undesirable refractory compounds were formed
between tantalum and matrices containing alkaline earths
as major constituents. Consequently, pyrolytic carbon
rods were preferred.

Another adaptation of electrothermal vaporization
followed by ICP atomization and excitation used a graphite
yarn[63]. Liquid samples ranging from 5 to 50μl could
be pipetted onto the yarn. The liquid distributed itself
over the length of the yarn by capillary action. The
sample was flash vaporized by passing a high current
through the yarn. The graphite yarn was incremented for
each sample into a chamber through which argon gas flowed
continuously to the ICP. The yarn incrementing mechanism
also provided electrical contact to the opposite ends
of the yarn in the chamber.

Aldous et al[64] described a platinum or tungsten
loop sample introduction device for introducing small
sample volume into a microwave induced argon plasma.
The loops were made from 10mm lengths of 0.1mm diameter
platinum wire. When dipped into aqueous solution, the
loop would pick up a sample volume of ca 0.12μl which
was in the form of a surface tension film. The aqueous
film was first evaporated by the passage of low d.c.
current, then the current was increased to vaporize the
solid remaining on the loop into the microwave plasma.
The relative standard deviation calculated for 0.25ppm
of cadmium was 10%.

Runnels and Gibson[65] employed a platinum
filament to dry and vaporize samples into a microwave
plasma. The filament was heated by means of a power
source consisting of a step down transformer. Taylor
et al[66] applied the platinum filament microwave induced
plasma system to the determination of sulphur using the
atomic emission line at 216.9nm.

1.5 Direct Analysis of Microlitre Solution Samples by Nebulization.

The use of furnaces and filaments is advantageous
in cases where there is limited sample available. But
if nebulization is preferred, the nebulizer may be adapted
to consume microlitre volumes. The techniques used for
nebulizing small volume of liquid were reviewed by Fassel[62].
The sample volumes nebulized ranged from 25μl to 200μL.

Samples such as organic solutions[67]and biological fluids [68] were nebulized.

Fry et al.[69] described a microsampling nebulizer technique based on an arrangement of small teflon funnels. These funnels allowed both micro dilutions and additions to be carried out on the sample. Uchida et al.[70] presented a 'one drop' method for flame atomic absorption spectrometry which allowed the analysis of $100\mu l$ portions of solution.

1.6 Hydride Generation

The technique of chemically treating the sample to generate a volatile product to be subjected to analysis by AAS has been applied to a series of elements which form volatile hydrides. The hydrides generated are carried into a flame where they are atomized and excited.

The success of hydride generation used with emission has been demonstrated by many applications[71-75] The technique has also been employed in the areas of flameless atomic absorption spectrometry[76-79] and Inductively coupled plasma spectrometry[80-81] to achieve high sensitivity and selectivity.

Introduction of the sample into the flame or plasma in the form of the hydride offers several advantages over the conventional pneumatic solution aspiration.
1) The separation process in the evolution step serves to eliminate practically all matrix effects by leaving the matrix materials behind in the reaction.

2) An efficient use is made of the sample because the entire amount of the element of interest present in the sample reaches the flame in a form suitable for efficient atomization.

3) The method allows a sensitivity improvement by factors from 50 to 200 because an intense and brief signal is obtained on introducing all the hydride into the flame.

4) Elements having their resonance lines in the vacuum UV can be determined sensitively by hydride generation into the flame or plasma.

The technique, however, suffers a few problems,

1) The generation process is more complex than direct nebulization.

2) Hydride evolution is limited to elements which form volatile hydrides.

3) The generation may suffer from reagent contamination problems.

4) Other materials present may compete with the analyte for the reagent.

1.7 Other Gaseous Generation Techniques

Alder et al [82-83] and Mermet et al [84-85] introduced various gases into an ICP to study spectroscopic processes occurring with the ICP. A generation technique had also been employed by Alder et al [57] in which the hypobromite oxidation of ammonium salts to ammonia has been used to determine exchangeable ammonium-nitrogen in soil samples

Snook and Kirkbright [86] employed a graphite rod [58] to vaporize refractory elements into the ICP. Instead of using pure argon gas as the carrier gas, a mixture of 0.1% trifluoromethane (Freon) in argon was used, so that, at high temperatures, the freon dissociated into fluoride radicals which halogenated the elements of interest. Excellent detection limits were obtained and memory effects which occur in electrothermal AAS were not observed in that system. Typical detection limits were 0.01ng for zirconium and 0.6ng for tungsten.

1.8 Conclusion

A number of ways by which samples can be introduced into the flame and plasma have been surveyed briefly in this chapter. Pneumatic nebulization, being the oldest used technique, is still widely employed in many laboratories and by instrument manufacturers despite its disadvantages. For as long as there is sufficient sample and the detection limits are not the critical factor, pneumatic nebulization remains the simplest and cheapest method of all.

Although ultrasonic nebulization has received praises for offering enhanced sensitivity and superior detection limits, its cost and difficulty in fabrication have prevented it from being added to the atomic absorption spectrometers and inductively coupled plasma system as an alternative to pneumatic nebulization. Furthermore a complete ultrasonic nebulization system is bulky and requires water cooling.

Graphite or metal furnaces and filaments are excellent atom cells in their own right when all the experimental parameters affecting the atomization process are critically controlled. Extreme care must be exercised in eliminating any background due to spectral interferences caused by scattered light from the incandescent graphite tube; formation of unwanted species having absorption lines close to the resonance lines of the elements of interest; or nonspecific absorption. Condensation is a major problem in furnace AAS as it decreases the atom population in the vapour phase. The problem becomes more serious with increasing height of observation. The commonly accepted theory is that in the presence of large amounts of excess foreign particles, cocrystallisation is likely to occur. The foreign ions occlude the element of interest, forming clusters and thus decreasing the concentration of neutral atoms available for absorption[87]. Occlusion can also occur on the surface of the carbon tube. Garnys & Smythe[88] presented some electron micrographs of carbon tube surfaces before and after atomization.

After several atomizations, surface irregularities are
evident which may trap elements, thus decreasing the
analytical sensitivity considerably. With improved
furnace atomizers designs, condensation and occlusion
may be reduced. Future developments in furnace AAS will,
undoubtedly, be towards more automation of the instrument
operations.

The electrothermal vaporization functions as well
as ultrasonic nebulizers in real terms when used for sample
introduction into the ICP. The carbon rod vaporizer has
been sucessfully employed to determine trace elements
such as lead,cadmium in blood and refractory elements.
More work is required in clarifying the mechanism of
analyte transport into the plasma. The effects of excess
concomitant ions on the vaporization of analyte should
be investigated in detail.

The hydride generation technique is an excellent
method for introducing elements forming volatile hydrides.
It can be adapted for use with a flame or plasma and a
wide range of elements can be determined. Furthermore,
the simplicity of the apparatus and freedom from matrix
interference render it an attractive alternative to other
available techniques.

CHAPTER TWO

THEORY OF CHEMILUMINESCENCE AND INSTRUMENTATION

2.1 Introduction

It has always been the desire of an analyst
to be able to carry out analyses in the simplest, most
efficient way possible given a set of experimental
constraints. The aim of this project was to apply the
phenomenon of chemiluminescence to the determination
of sulphur and phosphorus species in a flame. Having
decided to employ a diffusion flame on the grounds of
its merits (see Chapter 3), the next decision made
was on the choice of techniques for introducing the
sample into the diffusion flame.

In Chapter one, some sample introduction devices
have been described. Although nebulization is widely
used, the quantity of liquid introduced into the
diffusion flame will have an effect on the temperature
of the flame which is a critical factor in determining
the production of S_2 and HPO chemiluminescent species.
Also, the sample matrix together with the elements
of interest are simultaneously nebulized into the
flame and can, therefore, produce some undesired inter-
ferences due to the matrix.

Hydride generation works well for sulphur
but it has not been applied to generate the hydride
of phosphorus (PH_3). Hydride generation can be
prone to interferences due to the presence of other
elements which preferentially form the hydride. Extreme
caution must be taken to exclude foreign material (eg.
air) so as not to contaminate or decompose the reagent

used for generating the hydride. Finally, the hydride generation process requires lengthy chemical conversion of the sample prior to analysis making the technique unattractive for routine determinations.

The graphite-tube vaporizer and diffusion flame combination not only offers the advantages as disscussed in section 2.3, but the system can be automated by simply attaching an autosampler to the furnace, thus eliminating tedious manual injections by the operator. By suitable modifications to the signal detection system, simultaneous determination of phosphorus and sulphur can be achieved.

2.2 Theory of Chemiluminescence

Chemiluminescence is defined as the emission
of light as a direct result of a chemical reaction. When an
excited molecule emits radiation it undergoes an allowed
transition to a lower energy state. The relationship
between the change in energy (E) and the frequency of
the emitted radiation is given by the following equation.

$$\Delta E = E_1 - E_2 = h\nu \qquad (2.1)$$

where h is the Planck's constant and ν is the frequency
of the emitted radiation.

In an analogous way, an excited molecule due to
a chemical reaction will emit radiation in the following
manner[89] :-

$$A + B \longrightarrow C^* + D \qquad (2.2)$$

$$C^* \longrightarrow C + h\nu \qquad (2.3)$$

There are three conditions required for the
occurrence of chemiluminescence[90] :-

1) the chemical reaction must release sufficient energy
   to populate an excited energy state.

2) the reaction pathway must favour the formation of
   the excited state product.

3) the excited state product must be capable of emitting
   a photon.

Chemiluminescence (CL) reactions can be used for
chemical analysis by adjusting concentrations so that
the intensity, I_{CL}, is related to the concentration of
the reactant to be determined. Thus at anytime t, the

chemiluminescence intensity I_{CL} is given by equation (2.4)

$$I_{CL}(t) = \phi_{CL} \times \frac{dc(t)}{dt} \qquad (2.4)$$

where ϕ_{CL} is the efficiency of chemiluminescence which

is equated to $\qquad \phi_{CL} = \dfrac{\text{number of photons emitted}}{\text{number of molecules reacting}}$

and $dc(t)/dt$ is the reaction rate for the production of

an excited state.

I_{CL} can be measured as a function of time or it

can be integrated for a known time period. The integrated

equation with respect to t is of the following form,

$$\int I_{CL}(t)\,dt = \int \phi_{CL} \cdot \frac{dc(t)}{dt} \cdot dt \qquad (2.5)$$

$$I_{total} = \phi_{CL} \times C + constant \qquad (2.6)$$

$$I_{total} \propto C \qquad (2.7)$$

since ϕ_{CL} is also a constant for a particular system. In

the case of sulphur, as two atoms are required to form

S_2 molecules for excitation, $\qquad I \propto c^2$. (2.8)

Unlike many other light producing processes, CL

does not involve the intermediate formation of heat. The

necessary free-energy change of the CL reaction in Kcal/

mole (ΔG) is given by equation (2.9), [91]

$$-\Delta G \geqslant (hc/\lambda_{ex}) \qquad (2.9)$$

$$\text{or} \qquad ((2.86 \times 10^4)/\lambda_{ex}) \ \ Kcal/mole.$$

where λ_{ex} is the long-wavelength limit in nm for excitation of the emitting molecule. Hence for visible CL emission ΔG must be at least between 40 and 70 Kcal/mole[91].

2.2.1 The Flame Spectrum of Sulphur

Flames of burning sulphur, or compounds containing sulphur as additives emit bands of S_2, SO, SH, CS and a continuum. Bands of S_2 and SO_2 are sometimes seen in absorption. The various emissions are highly dependent on the nature of the flame. Conditions must be chosen carefully to bring out anyone of them.

2.2.2 Mechanism for S_2 Emission

The first observation of the blue emission due to sulphur in a hydrogen flame was made by Salet in 1869.[92] Sixty years later, it was confirmed that the emission spectrum was attributable to the presence of S_2 species[93]. The S_2 molecules are raised to higher energy levels by chemical reaction in the flame and emit their characteristic bands on returning to the normal sate.

In a hydrogen flame, combustion of H_2 and O_2 begins as the gases enter the reaction zone by chain branching reactions[94],

$$H + O_2 \rightleftharpoons OH + O \tag{2.8}$$

$$O + 2H \rightleftharpoons OH + H \tag{2.9}$$

$$OH + H_2 \rightleftharpoons H_2O + H \tag{2.10}$$
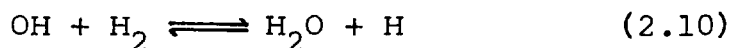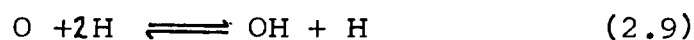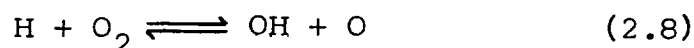
The concentration of H atoms produced in the reaction

zone is high as the recombination processes (equations

2.11 and 2.12) are slow in the forward direction and are

$$H + H + M \rightleftharpoons H_2 + M \qquad (2.11)$$

$$OH + H + M \rightleftharpoons H_2O + M \qquad (2.12)$$
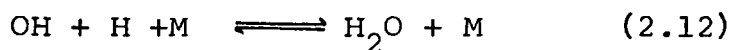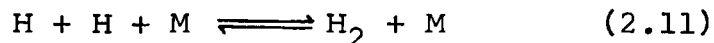
termolecular, and in the reverse direction because of

large activation energies.

Crone[95] proposed a possible excitation mechanism

for S_2 molecules,

$$H + H + S_2 \longrightarrow S_2^* + H_2 \qquad (2.13)$$
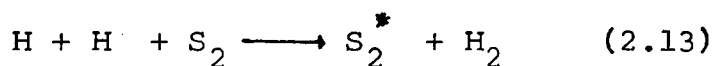
and for excitation to higher levels[96],

$$OH + H + S_2 \longrightarrow S_2^* + H_2O \qquad (2.14)$$
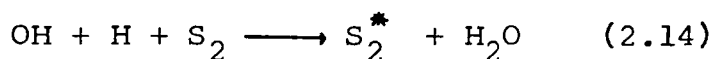
The excitation of S_2 via reaction (2.13) required only

4.5eV as compared to 5.1eV for reaction (2.14). It was

thought that reaction (2.13) was probably the dominating

process in the flame[97].

The following equilibrium[98] has also been

suggested to account for the formation of the S_2 species in

the flame.

$$2SO \rightleftharpoons SO_2 + \tfrac{1}{2}S_2 \qquad (2.15)$$
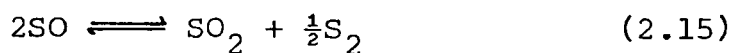
2.2.3 The Flame Spectrum of Phosphorus

Phosphorus in the flame emits four kinds of spectrum;

a greenish-white continuum, a band system in the green and

bands of the PO molecule in the ultraviolet belonging

to the beta gamma systems. Line spectra can also be

detected.

2.2.4 Mechanism for HPO Emission

In the cool hydrogen flame, the presence of green emission is due to de-excitation of excited HPO molecules[99, 100]. Possible excitation routes were proposed [100,101] to describe the formation of the species responsible for chemiluminescence.

$$P_2 + O \rightleftharpoons P + PO \qquad (2.16)$$

$$P + OH \rightleftharpoons PO + H \qquad (2.17)$$

$$H + PO + M \rightleftharpoons HPO^* + M \qquad (2.18)$$

$$H + PO^* \rightleftharpoons HPO^* \qquad (2.19)$$
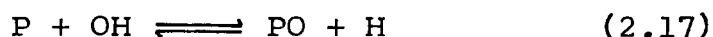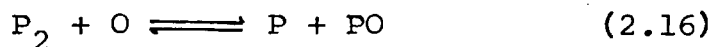
'M' has been included in equation (2.18) because it has been reported that the chemiluminescent intensity observed in the flame may be enhanced by nitrogen or a cooled surface[97, 102-104] (a fact also true for sulphur).

Two theories have been developed to account for the observed enhancement.

1) A third body "M" can be used to remove the excess energy from the newly formed PO molecules produced in reactions (2.16) and (2.17)[100,101] to give stable PO species.

2) H and OH radicals required in reactions (2.16-2.18) recombine slowly in the cool flame gases and therefore survive to a greater distance downstream in the cooled flame[97].

2.3 Instrumentation

Figure 5 represents a block diagram of the instrumentation employed for the observation of S_2 and HPO chemiluminescence. Species vaporized from the IL 555 furnace atomizer are passed into the argon hydrogen-air diffusion flame where chemiluminescence occurs. The IL 151 spectrometer monitors the radiation and the signal output is either displayed digitally on the spectrometer display panel or the analogue signal is recorded on a strip chart recorder.

This arrangement offers several advantages in the determination of phosphorus and sulphur over the conventional flame chemiluminescence techniques utilizing nebulization or gas generation procedures, ie:-

1) electrothermal vaporizers only require a few micro-litres of sample for each determination.

2) total content of the element is determined although a degree of speciation is possible with careful control of the tube temperature programme.

3) programmed heating of the sample can be performed with several temperature steps to allow evaporation of the solvent, pyrolysis and analyte vaporization. The programme can also be optimised for each sample type and superior detection limits can be obtained.

4) viscosity effects are negligible.

5) the speed of the analysis is similar to nebulization into the flame, but it is more rapid than gas generation.

6) the capability of direct solid sampling exists when electrothermal vaporizers are used.
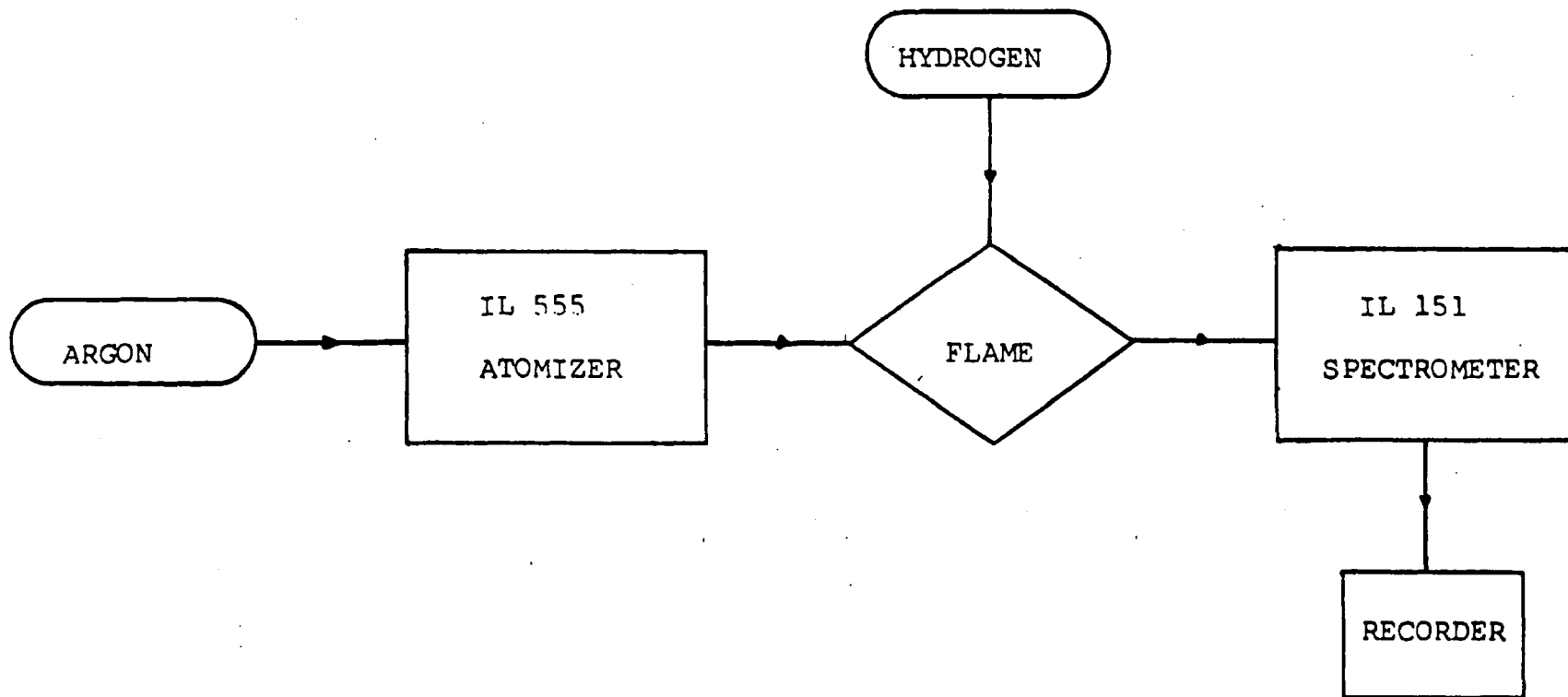
Figure 5   Schematic Diagram of the Instrumentation.

2.3.1 Sample Introduction Device

The sample introduction device used in this study was a commercially available furnace atomizer (Model IL 555 CTF. Instrumentation Laboratory Inc. Jospin Road, Wilmington, MA. 01887 U.S.A.). The atomizer consisted of a control module and an atomizer cell which contained a carbon tube. When used in an atomic absorption or emission mode, the atomizer would be positioned in the line of the optical path between the gas control box and the monochromator. As the atomizer was used only as a means of vaporizing the analyte into the flame, it was placed on the bench top as close as possible to the burner system to minimize the length of the connecting tubing. The features of the IL 555 which are relevant to this study are described below.

Control Module Front Panel (Fig. 6)

On the left of the panel is the gas flow control meter(2). The meter is graduated in litres per minute. The clean switch (7) enables a high temperature cleaning stage to be applied to the carbon tube to remove any post atomization residues. The mode switch (6) enables the operator to select three modes of operation; manual, auto and pressurized modes. The start/advance button (4) initiates and terminates each step in the manual mode or executes the entire programme in the automatic modes of analysis. The temperature set (3) is used to calibrate the temperature readout prior to operation. The slider (9) control on the power control panel sets the temperature
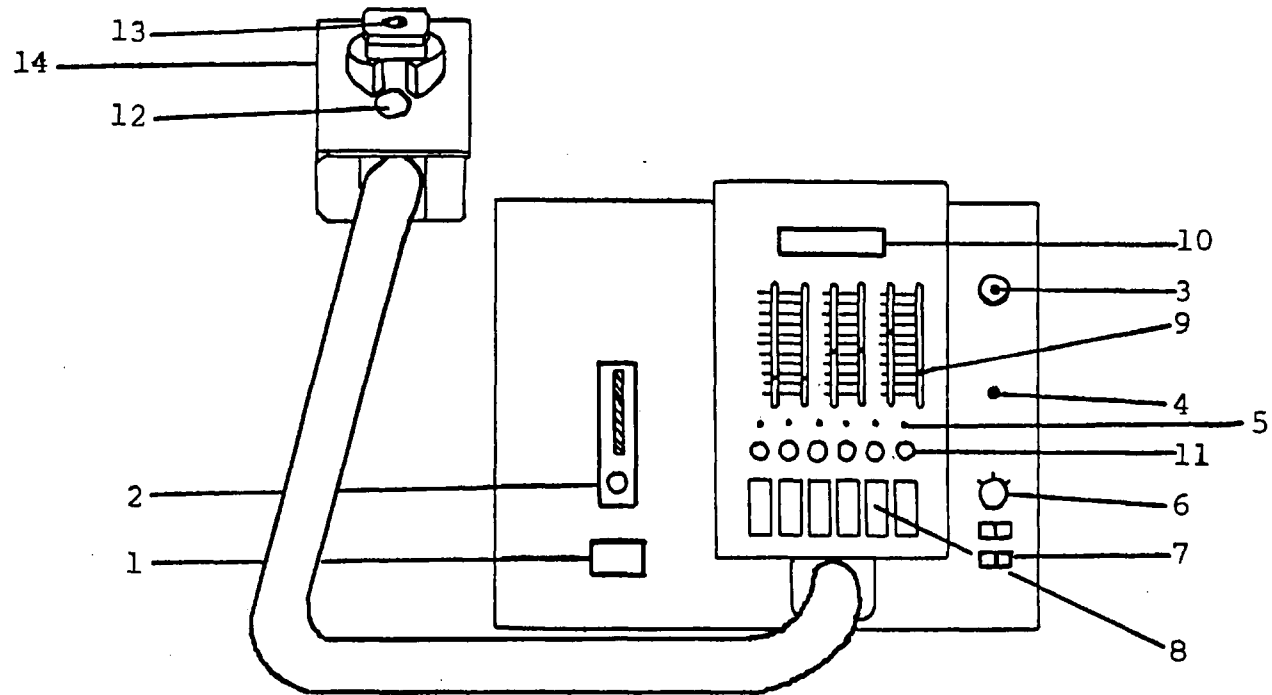
Fig. 6 Control Module and Atomizer Cell Front Panel.

for each stage of the analytical heating programme. Time intervals for each stage of the heating programme are selected by one of the six thumbwheel switches (8). Each integer on the wheel represents a time interval of 5 seconds. Figure 7 illustrates the flexibility of the IL 555 in executing a temperature programme.
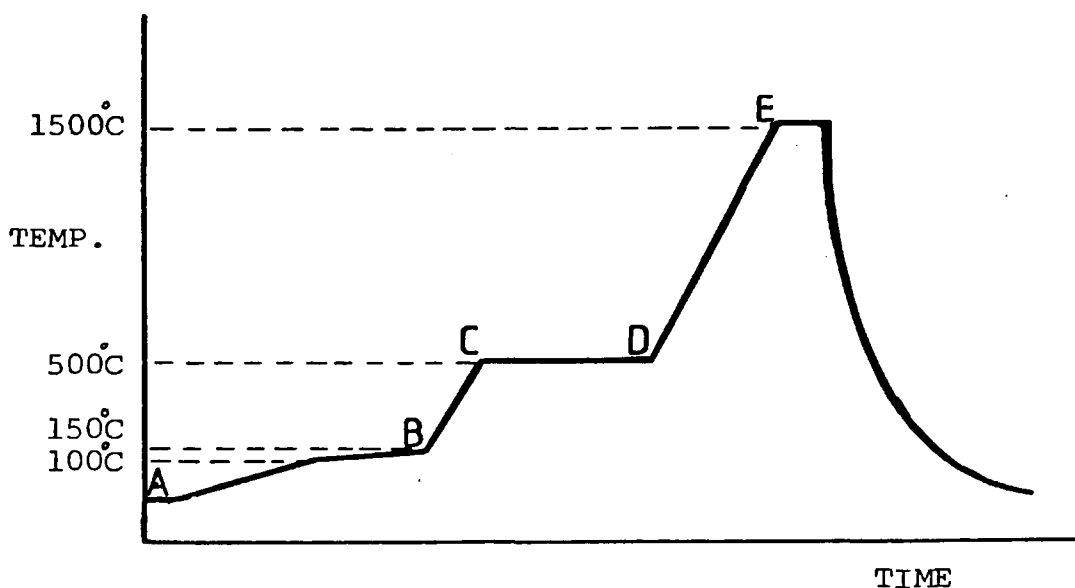
Fig. 7 A Typical Temperature Profile in the AUTO mode.

A slow drying stage from A to B enables the sample to be desolvated. A ramp from B to C is designed to pyrolyse the sample, a temperature hold stage C to D ensures complete pyrolysis. A ramp from D to E enables the sample to be atomized.

The temperature readout (10) displays the actual temp-
erature of the furnace betweem 25 and 3500°C. Above
each thumbwheel, there is an integrate start push
button (11) which when depressed will initiate peak
area integration of the analytical signal obtained
during atomization for a period of time which may be
selected on the spectrometer.
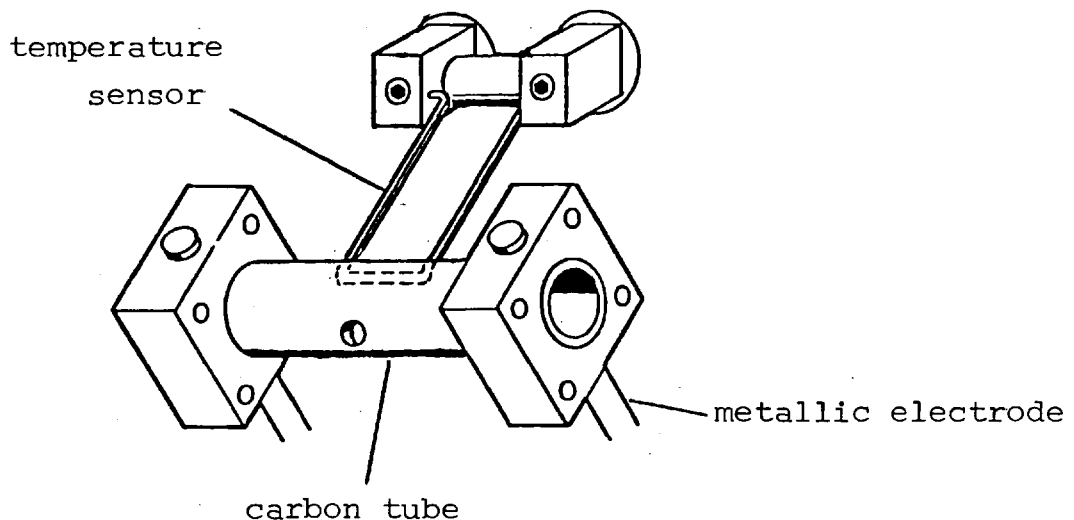
Fig. 8   The graphite tube and the temperature

sensor   assembly

The Atomizer Furnace

The interior of the atomizer furnace is shown
in Figure 8 .   Two metallic electrodes supply power
to the tube assembly,   the temperature of which is
continuously monitored by a tungsten alloy temperature
sensor in contact with the underside of the tube, (Fig. 8).

Argon enters the cell through two entrance holes, one on each side of the chamber base. The argon gas serves as a sweep gas to carry vaporized analyte into the flame and prevents oxidation of the graphite tube at high temperatures.

The face plate (14) (Fig. 6) is purposefully designed to ensure a gas tight seal. It can be removed for replacement of the carbon tube assembly or temperature sensor and for general maintanance purposes. The atomizer cell door (12) opens automatically when the heating programme is complete and closes upon the initiation of the next cycle. The teflon vertical access port (13) permits sample introduction. This white teflon cap is normally equipped with a quartz window. But for these studies it has been removed to allow connection of the atomizer to the burner with P.V.C. tubing to facilitate sample vapour transport to the flame (Fig. 9). The teflon cap and connecting tube can be removed for sample introduction to the tube by means of a micropipette.

2.3.2 The Spectrometer

The spectrometer used for the work described in this thesis was also a commercial instrument (Model IL 151 Instrumentation Laboratory Inc. 6, Jospin Road, Wilmington, Massachusetts. U.S.A.). The IL 151 is a single-beam atomic absorption (AA) spectrometer which can be used as an atomic emission (AE) spectrometer simply by selecting the flame emission (FE) mode at
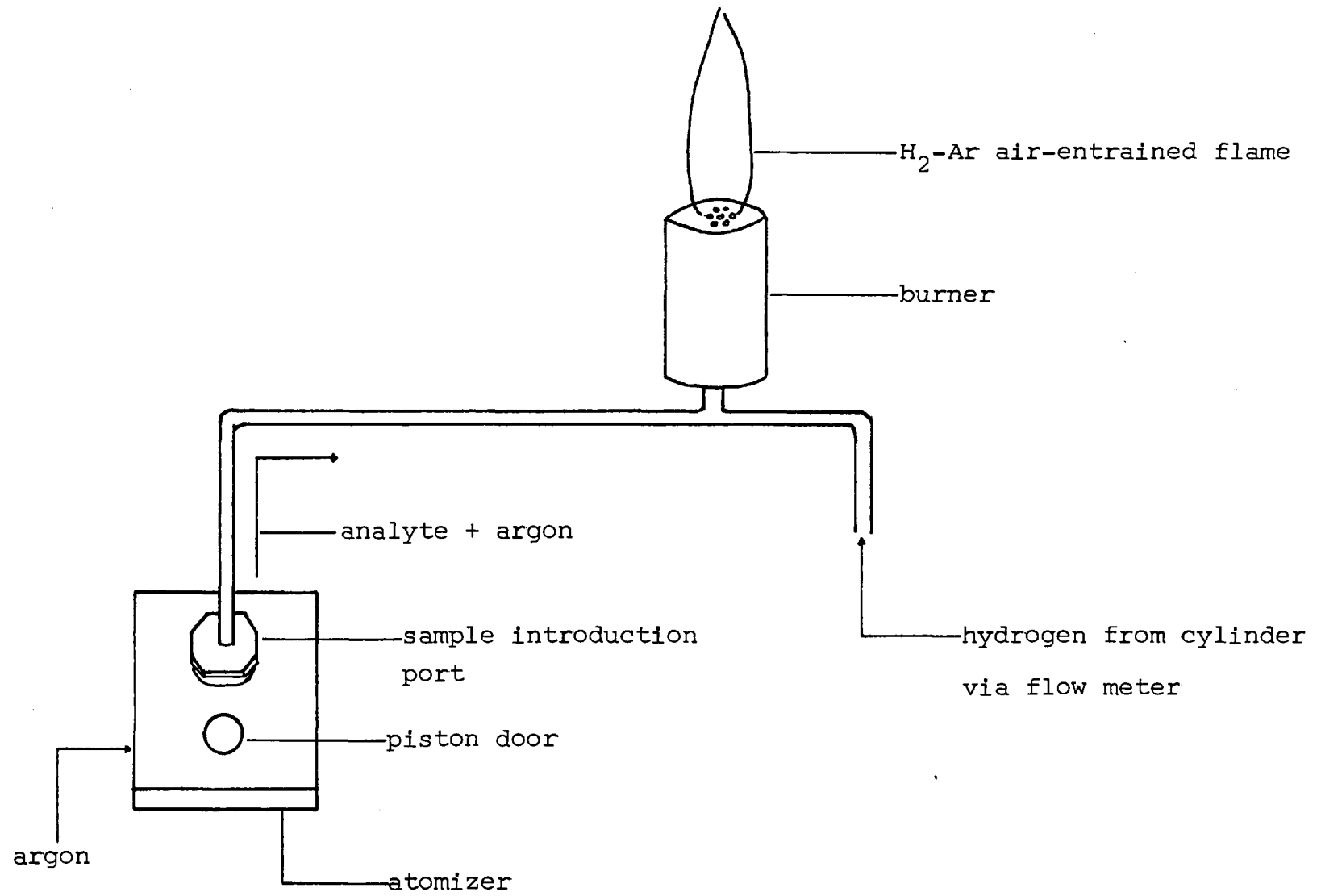
Fig. 9 Atomizer and burner configuration

GAS CONTROL

BOX
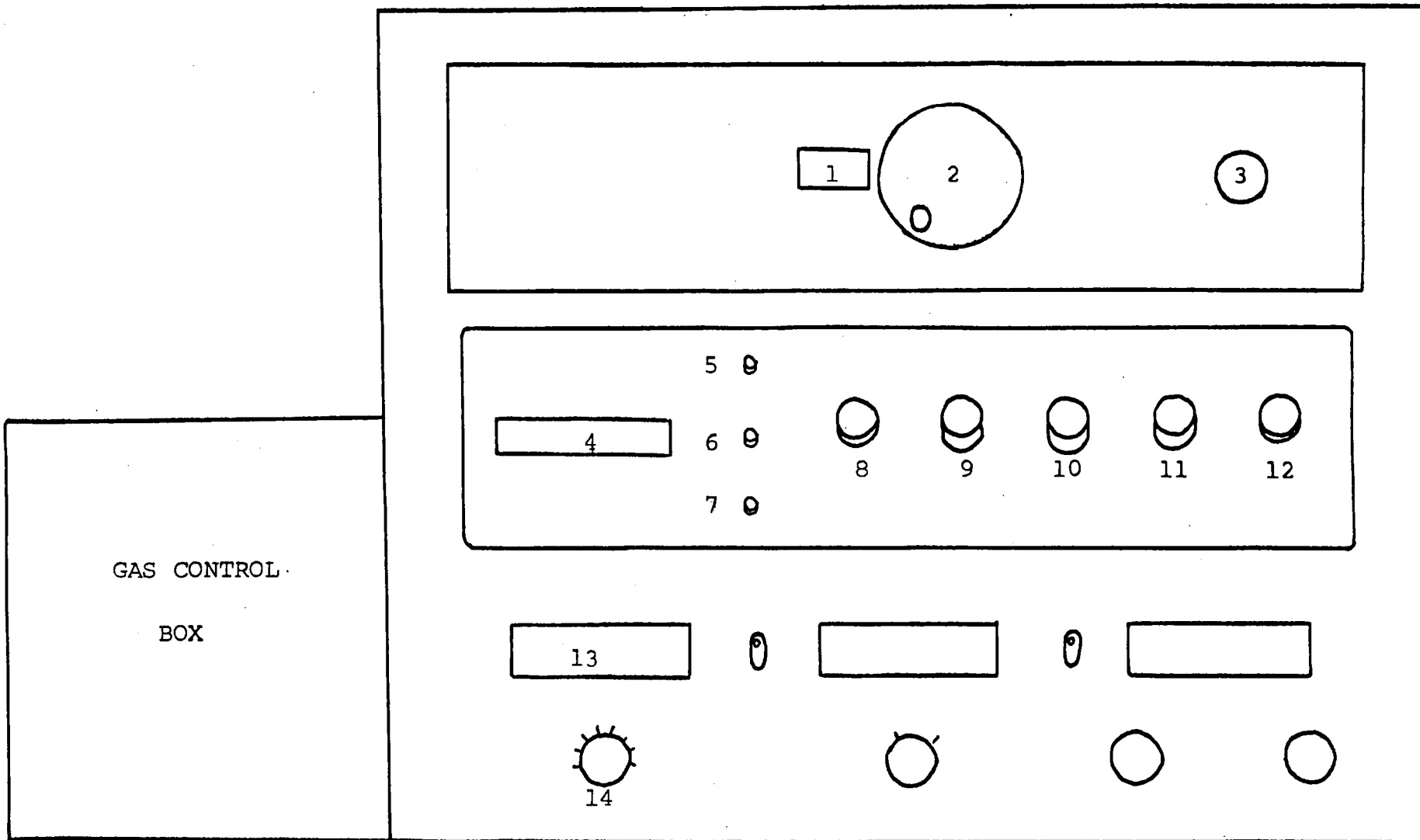
Fig. *10* IL 151 Instrumental controls and display.

the spectrometer. The IL 151 was designed for the analysis of many metals, metalloids and some non-metals present in solutions using either a pneumatic nebulizer/ flame combination or the resistively heated graphite tube atomizer.

Instrumental Description

Figure 10 shows the front panel of the IL 151. On the left is the gas control box, above which is the housing for the hollow cathode lamps for atomic absorption spectrometry (AAS). The burner and nebulizer system supplied with the instrument were removed and replaced with a circular burner used to support a diffusion flame. The flame employed was ignited manually (see section 2.4). Thus, the ignition controls were not used. The right side of the diagram illustrates the instrumental controls available for operating the spectrometer functions.

1) WAVELENGTH INDICATOR: displays the selected analytical wavelength in nanometres.

2) WAVELENGTH SELECTOR: a dial used to move the diffraction grating to change the wavelength focused on the photomultiplier tube (PMT).

3) SLIT WIDTH SELECTOR: selects in incremental steps, the curved entrance and exit slit widths of the monochromator. The selector is graduated in micrometres.

4) DIGITAL DISPLAY: displays values in absorbance units, concentration units or relative values (for emission work).

5) AUTO ZERO: resets the digital display to zero.

6) DECIMAL POSITION BUTTON: sets the decimal at any
   one of the five positions.

7) INTEGRATE INITIATING BUTTON: activates the inte-
   gration network for the selected integration period.

8) SCALE EXPANSION SWITCH: allows selection of the
   range of instrument readout.

9) INTEGRATE MODE SWITCH: the integration circuitry
   provides an analogue mathematical average of a con-
   tinously varying signal. There are four modes of
   integration.
   AUTO: used for the analogue readout mode.
   MANUAL: requires the use of the integration
   initiating switch to initiate a period of integration.
   PEAK AREA: mode used for acquisition of transient
   signals that have a short unsymmetrical signal peak.
   PEAK HEIGHT: mode used for acquisition of signals
   of short duration symmetrical peaks.

10) INTEGRATION PERIOD SWITCH: selects the time period
    for integration.

11) READOUT MODE SWITCH: selects the output for either
    flame emission or absorption analysis.

12) CURVE CORRECT SWITCH: adjusts the linearity of
    the concentration readout.

13) INTENSITY METER: displays light intensity measured
    by the pmt.

14) PMT VOLTAGE SWITCH: seclects various voltages applied
    to the PMT.

The Monochromator

The IL 151 uses a one-third metre Ebert mono-
chromator (Fig. II). Light is admitted into the mono-
chromator through the entrance slit. The parabolic
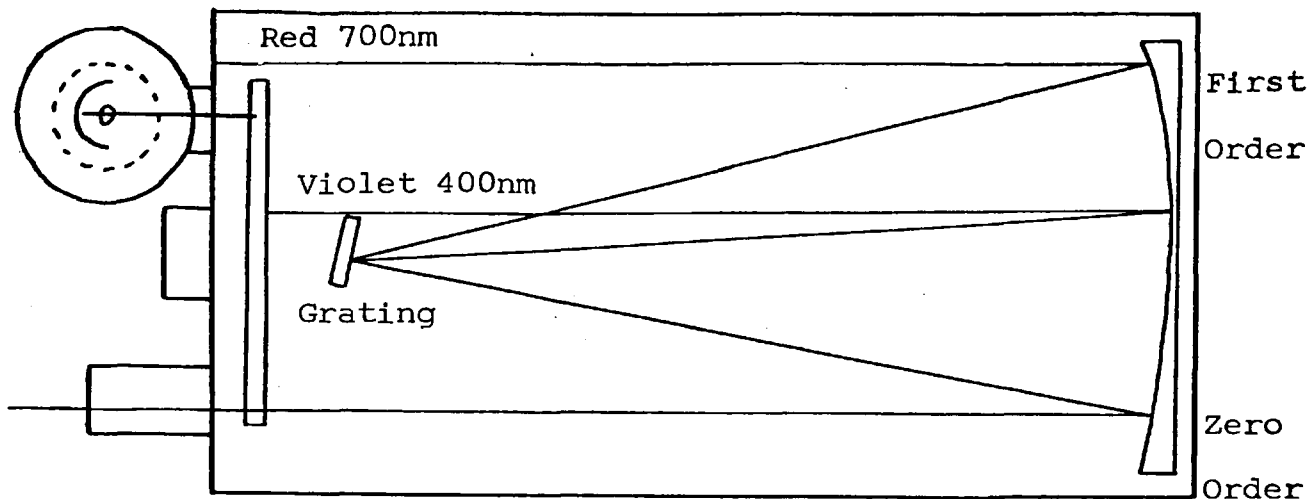
Fig. II Ebert Monochromator.

mirror reflects the slit image and focuses it onto a

diffraction grating where wavelength dispersion is achieved.

The component wavelengths are reflected back to the

mirror where the spectrum is re-reflected to the exit

slit onto the detector. The monochromator has two

external controls. One rotates the grating with respect

to the incident light, changing the wavelength of the

light falling on the exit slit (the wavelength selector).

The other selects the width of a curved slit, thus determining

the light through-put and spectral bandpass of the

monochromator (the slit width selector). The grating

is a 32X32mm plane square grating ruled with 1200 lines

per millimetre. The grating is blazed at 250 nm and has an effective spectral range from 190-750 nm. Table 2.1 summarizes the specifications of the monochromator.

Table 2.1 <u>Specifications of the Monochromator.</u>

Optical mount	EBERT
Focal length	$\frac{1}{3}$ metre
Effective aperture ratio	f/9
First order reciprocal linear dispersion	2.5 nm/mm
Scattered light	less than 0.02%
Slits	curved, variable from 10μm to 640μm
Entrance slit	640μm [1]
Exit slit	800μm [1]
Bandpass	2nm [1]
Slit height	10mm [1]
wavelength range(with interchangeable gratings)	190nm-1000nm
Grating	32X32 area 1200 grooves/mm
Blaze	250nm

2.4 The Argon Hydrogen Air-entrained Flame

Most types of flames used in flame spectrometry have bulk temperatures between 2000 and 3000K[105]. There are, however, analytical applications in which

(1) used in this study

a "cool flame" is desirable, for example, a hydrogen

diffusion flame with added nitrogen may be used for the

determination of non-metals such as sulphur and phosphorus

(106, 107). Such a flame burns as oxygen diffuses into

the combustion region from the surrounding air and

has a temperature of less than 1000K(107). In this

case, the analytical line or band is excited by chemi-

luminescence.

The burner used for the work described here

was of a Meker type. The burner consisted of a stainless steel

cylindrical tube as shown in Fig. 12 a. One end of the

tube had seven small outlet ports hexagonally arranged

(Fig. 12 b). The inert sweep gas (Ar) and fuel gas (H$_2$)
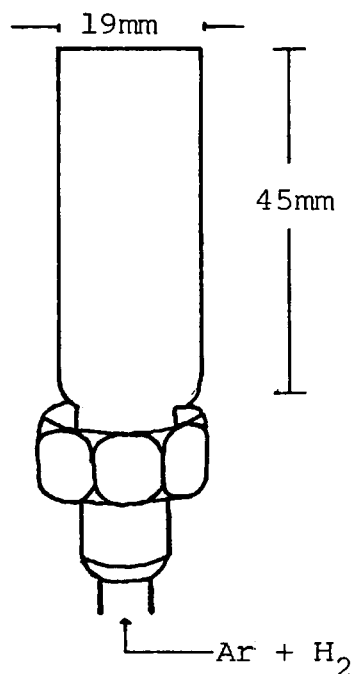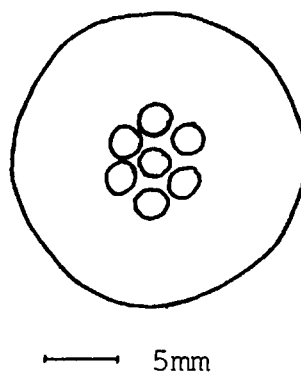
Fig. 12 b   the burner head

Fig. 12 a   the burner

were introduced into the burner from the base. This
arrangement produces above each port a separate primary
combustion zone while the burnt gases from each of these
zones merge into a single   flame surrounded by a
single secondary   combustion zone. The argon hydrogen
flame was supported by drawing oxygen from the surrounding
air and could thus be conceived as a limiting case of
the unpremixed hydrogen-air flame. When the fuel gas
ratios were optimised, the flame appeared to be tran-
sparent with an   occasional flicker of yellow light,
especially, near the top of the flame, due to entrain-
ment of dust into the flame.

The burner was positioned in front of the slit
so the radiation emitted from the flame was focused
onto the entrance slit. The position was located by
focusing   the image of a light bulb placed between a
concave mirror and the entrance slit. The burner
support   allowed vertical and lateral movement
for the burner. The whole assembly was mounted on an
optical bar.

2.4.1   Flame Ignition

To ignite the flame, the following procedure
is applied,
1) turn on the atomizer power supply and select the
manual mode.
2) depress advance/start push button to allow a
flow of argon through the furnace into the flame burner.
3) turn on the fuel gas supply to the burner,

4)   ignite the flame with a taper.

To extinguish the flame, turn off the hydrogen first, then the argon gas.

CHAPTER THREE

THE ANALYSIS OF SULPHUR

3.1 Introduction

Sulphur and phosphorus have their principal resonance lines in the vacuum ultraviolet region of the spectrum where the background absorption of the oxygen in the atmosphere and also of the burning flame gases is high. It is, however, possible to determine sulphur and phosphorus directly using their resonance lines both in atomic absorption and atomic emission spectrometry.

Kirkbright et al.[108] determined sulphur and phosphorus at their vacuum ultraviolet resonance lines by emission spectrometry employing an inductively coupled plasma source. To obtain an atmosphere free of oxygen, the authors purged the optical path and the monochromator with oxygen free inert gas. The detection limits (DL) achieved are shown in Table 3.1.

Table 3.1 Detection limits reported by Kirkbright et al.

Element	Wavelength (nm)	DL (ppm)
Sulphur	180.73	2.2
Sulphur	182.04	1.7
Sulphur	182.63	3.7
Phosphorus	177.5	>10
Phosphorus	178.78	3.0
Phosphorus	185.92	0.4

L'Vov determined sulphur and phosphorus in the vacuum ultraviolet region by flameless atomic absorption spectrometry. The sample on a graphite tube was vaporized at 1900K with an argon pressure of 1.2atm.. The sensitivities obtained are shown in Table 3.2.

Table 3.2   Non-flame AAS results reported by L'Vov[109]

Element	Wavelength (nm)	Sensitivity*(pg)
Sulphur	180.7	81.4
Sulphur	182.0	105.0
Sulphur	182.6	315.0
Phosphorus	177.5	3.4
Phosphorus	178.3	4.4
Phosphorus	178.8	7.4

*for 1% absorption

The disadvantages of using a vacuum system are:

1) inert atmosphere is expensive to maintain and is not suitable for routine analysis.

2) it is difficult to obtain an oxygen free atmosphere.

The most widely used direct method for determining sulphur and phosphorus is based upon the emission spectra of S_2 and HPO molecular species which are produced in an air-hydrogen flame.

The first observation of chemiluminescence due to the excitation of molecules was reported by Salet[92] in the middle of the nineteenth century. He detected traces of sulphur in a hydrogen flame by

the blue emission acquired by the flame when it was

allowed to impinge upon a vertical water-cooled surface.

In 1932, Fowler and Vaidya[93] described the S_2 band

spectrum as being the lines originating from transitions

between the lowest vibrational level of the electronic

ground state of S_2 and of the first excited electronic

state. The first analytical use of S_2 emission was

made by Crider[110] who quantified his findings by

relating the emission intensity to the concentration

of sulphur over the range 0.1 - 1.3ppm.

Dagnall et al.[111] investigated the behaviour

of different sulphur species in the flame and reported

that the emissive response in solutions for various

forms of sulphur was in the order:- sulphide $>$

sulphite $>$ thiosulphate $>$ ammonium sulphate $\gg$

sulphuric acid $\gg$ alkali metal sulphates. This series

was in accordance with the degree of volatility of the

samples introduced into the cool flame ($T \simeq 400°C$).

The cool flame was not sufficiently hot to vaporize

the metal sulphate and hence to excite the vaporized

species. To overcome the different emissive response,

a dual flame (Fig. 13) was used to determine sulphur

effluent from a Gas Chromatograph.[180] The effluent

was first burnt in flame 1 to vaporize all sulphur

species which were then passed into a diffusion flame;

S_2 chemiluminescence was observed through the window.

A novel technique for the determination of

sulphur and phosphorus called Molecular Emission

Cavity Analysis (MECA) was developed in the early
1970's by Belcher et al. [112,113] in which samples were
deposited into a small cavity at the end of a rod
which was then inserted into a hydrogen-air flame.
They determined the concentration of sulphur dioxide
and different sulphur anions. The technique of MECA
suffered interferences particularly from organic matrices
and it did not allow the evaluation of concentrations
of the total amount of sulphur in a sample because
different forms of sulphur were emitted at different
times after the initial introduction into the flame.
(This, however, could be a great advantage when some
degree of speciation was required.) Also the gradients
of the calibration curves varied from 1.5 to 2.1 and
were dependent on the different forms of sulphur. In
order to determine the concentration in the sample,
knowledge of its composition was required so that
standards could be prepared.
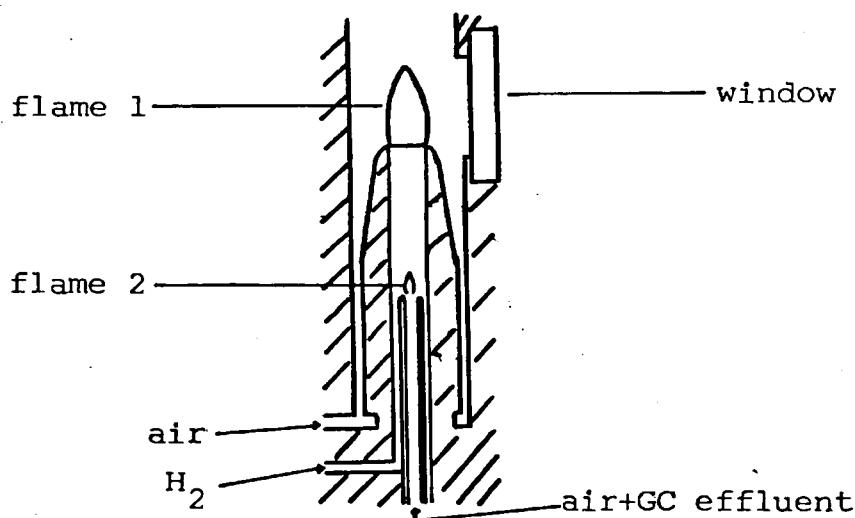
Fig. 13 Schematic diagram of the dual flame
Burner[110].

Everett [114] determined sulphur and phosphorus in oils by employing a Carbon Filament Atom Resevoir (CFAR) to vaporize the samples into the diffusion flame which surrounded the CFAR (Fig./4).
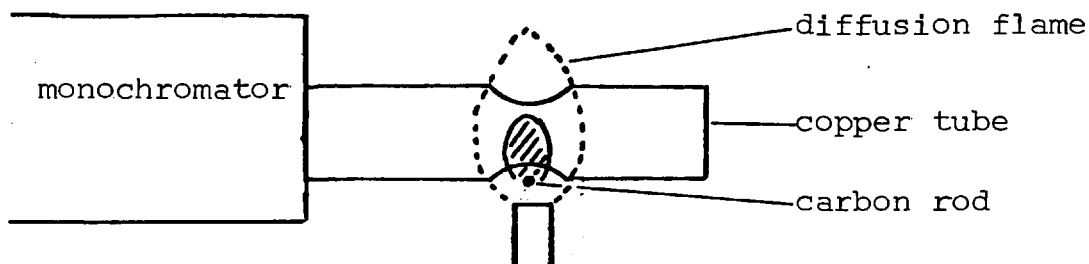
Fig. 14   The experimental arrangement for CFAR

The CFAR was positioned as close as possible to the entrance slit of the monochromator to cut down noise and to restrict the field of view. A copper tube (Fig./4) was placed horizontally over the filament. Two holes cut through the centre of the tube formed a chimney for the flame gases. One end of this tube was placed against the entrance slit of the monochromator and the other end was blocked. With this arrangement, the emission was confined to the area inside the tube and could be easily viewed by the monochromator with little interference from the continuum emitted by the glowing filament. However, the experimental procedure was cumbersome. Using a monochromator slit width of 0.6mm, Everett obtained a detection limit of 0.33ng for sulphur.

Hamouda[115] determined sulphur by generating

hydrogen sulphide into a diffusion flame and a detection

limit of 0.02ppm was obtained using 1mL solution sample.

Kagosha[116] also employed a generation procedure in

which SO_2 from petroleum fractions was generated by

combustion. The SO_2 was subsequently trapped in 0.02M

STCM/0.002M EDTA solution and on acidification with

hydrochloric acid the sulphur dioxide was released into

the cool flame.

Work presented in this thesis describes the

application of molecular emission spectrometry to the

determination of sulphur and phosphorus by observing

the chemiluminescence emission of the S_2 and HPO

species in an argon hydrogen diffusion flame. The use

of a graphite electrothermal atomizer to vaporize the

samples into the flame is described. The advantages

of using the atomizer/flame system have already been

discussed in section 2.3.

3.2 Experimental Optimization

3.2.1 Sample Introduction

The cylindrical carbon tubes supplied by

Instrumentation Laboratory were of 38mm in length,

4.75mm in diameter and 0.8mm wall thickness. Initially,

$10\mu L$ aliquots of 100ppm S $((NH_4)_2SO_4)$ were dispensed onto

the inside surface of the tube through an orifice positioned

directly underneath the piston operated door. The

sample was dried and vaporised into the cool flame.

Analytical signals obtained in this manner were broad
in shape and multiple peaks often resulted, making
peak height measurements unreliable. On rapid heating,
the analyte was released and confined in the tube as an
atom cloud. The atom cloud remained in the optical
path for a finite time and subsequently escaped through
the open end of the tube and orifice. Clearly, this
slow dispersion of analyte can be a disadvantage when
a rapid release of sample into the flame is required.
To overcome this problem, a section of the tube around
the orifice was removed to expose the inner surface
as shown in Fig. 15

Fig. 15 The carbon tube vaporizer

Thus 10µL of liquid sample was deposited onto the
inner surface of the carbon tube from a micropipette
equipped with a disposable tip. On vaporization, the
analyte was now released from the tube and swept into
the flame where deep blue radiation was observed for
sulphur in the cool region of the flame due to the de-
excitation of S_2 molecules.

3.2.2   The Argon Hydrogen Air-Entrained Diffusion Flame

The temperature of an analytical flame is an important factor in the production of molecular species for chemiluminescent reactions. The parameters effecting the temperature of the diffusion flame are the burner design and dimensions, flow rates of argon and hydrogen and the amount of air entrained into the flame.

As the temperature along the vertical axis is not uniform the viewing zone above the burner head was varied to determine the location for maximum chemiluminescent intensity based on signal to noise ratios.

3.2.3   Optimum Gas Flow Rates and Viewing Height

The gas flow rates and the observation zone were optimised by independently varying their values. Figures 16 - 18   show the effects of variations in these parameters. The optimum conditions are summarized in Table 3.3.

Table 3.3   The Optimum Parameters used

Ar flow rate	3 L/min.
H_2 flow rate	1 L/min.
viewing height	13mm above the burner head

The radiation originating from the centre of the flame was measured as at the flame edge the OH
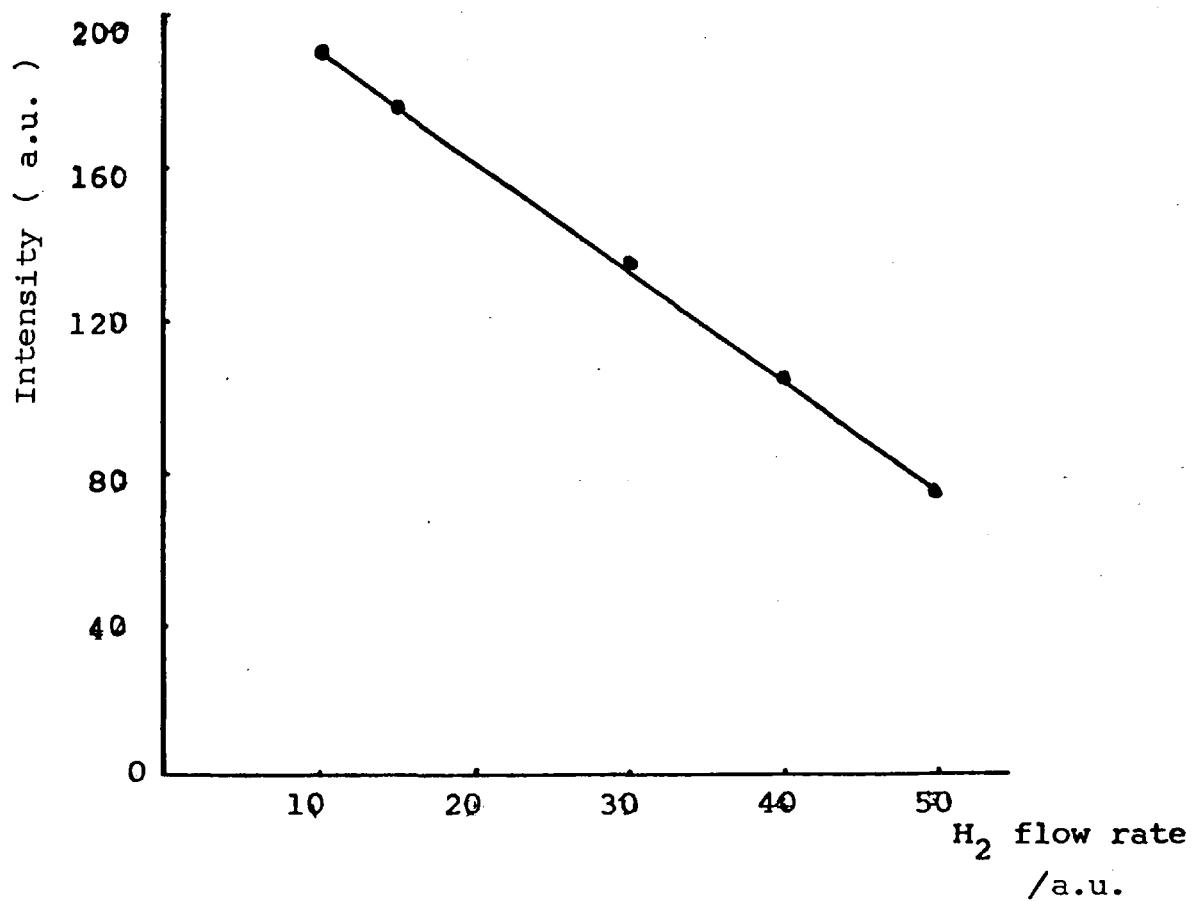
Fig. 16 The effect of the hydrogen flow rate
on the S_2 emission intensity at a
constant argon flow rate of 3 L/min.
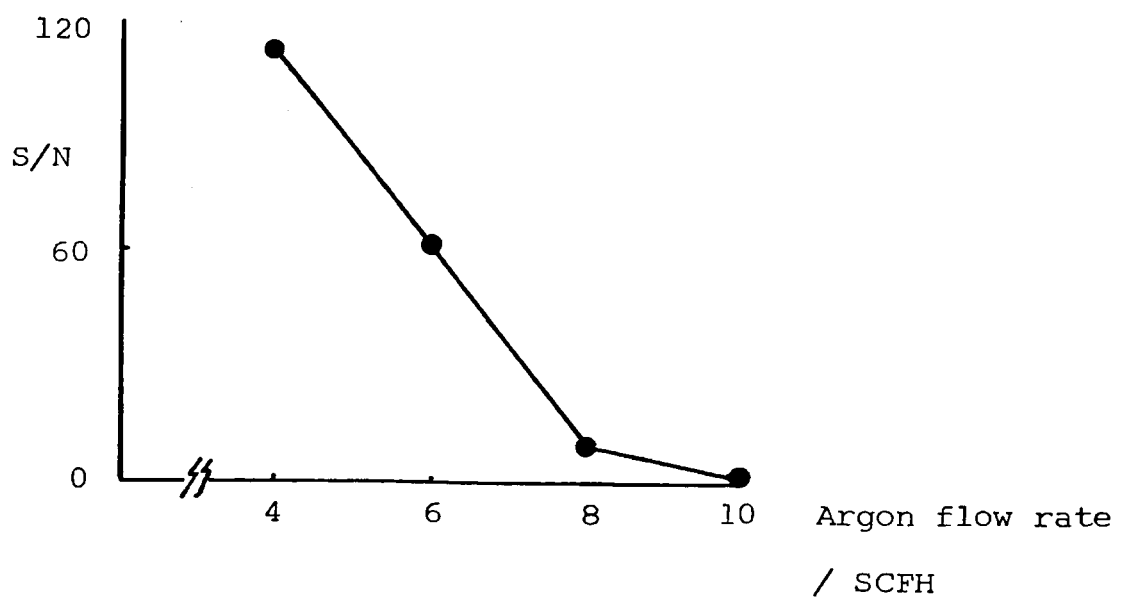
Fig. 17 The effect of argon flow rate on
the S_2 signals
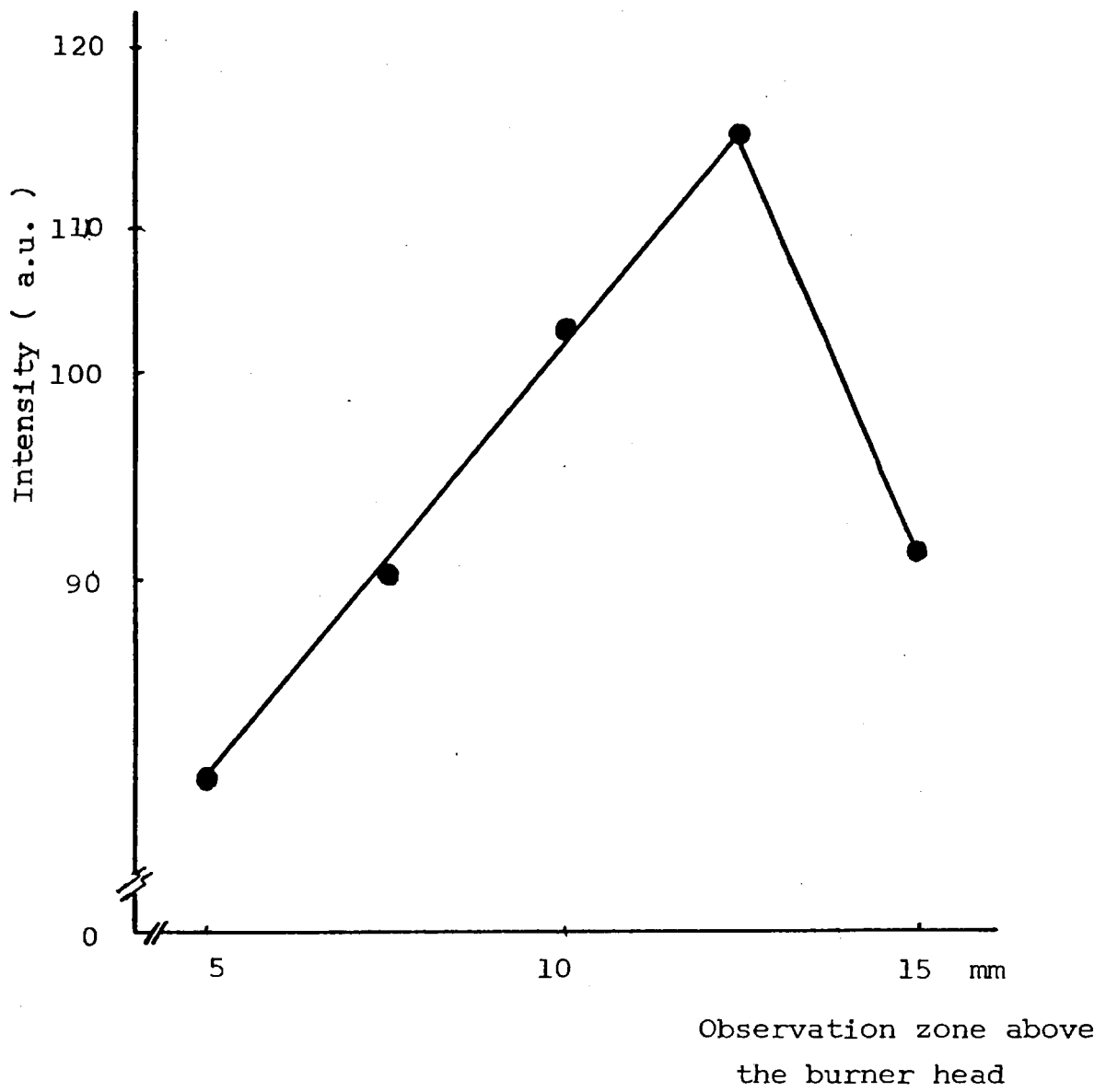
Fig. *18* Optimization of the viewing zone.

emission band head at 307nm is strong. As oxygen quenches chemiluminescence, no S_2 emission was observed near the flame-air boundaries (Fig. 19)

OH emission at 307nm

S_2 emission

flame boundaries
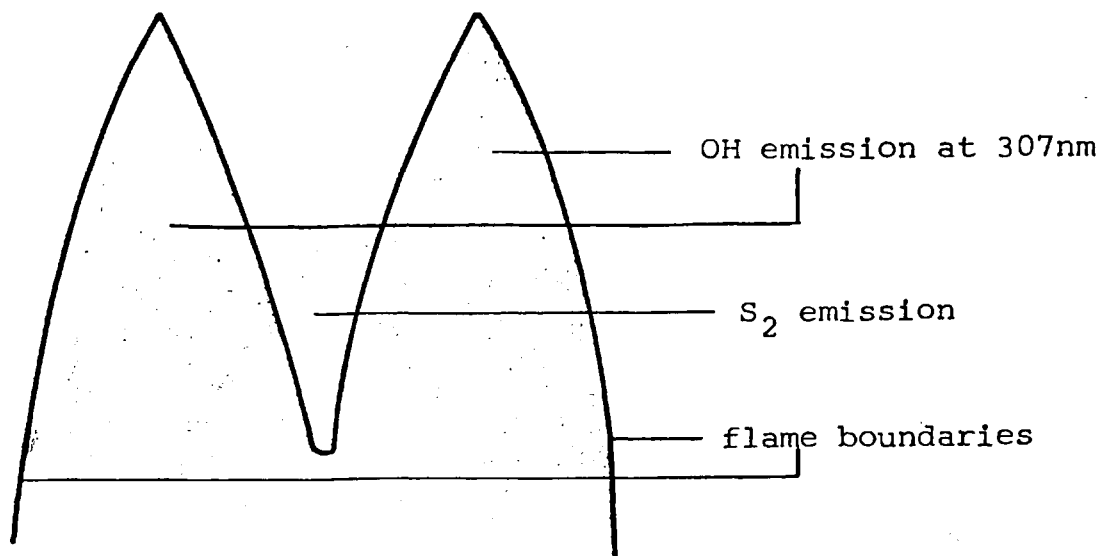
Fig. 19 Schematic diagram of the various emission zones in the diffusion flame.

3.2.4 Optimum Bandpass

The S_2 emission is a relatively wide band system (Fig.20). For this reason it is advantageous to use a wide band pass at the spectrometer rather than a narrow band width as is commonly employed for observation of line emission. Thus, Hamouda[115] used an interference filter of 70% peak transmission to observe the S_2 band system at 384nm. The largest bandwidth available on the spectrometer (2nm) was selected for maximum light throughput (Fig.21).
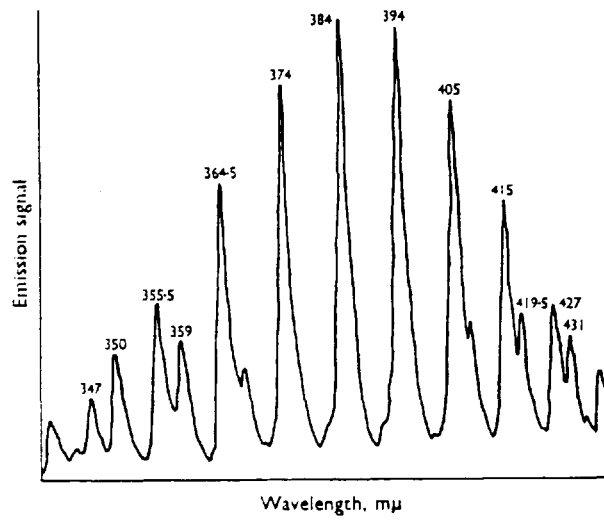
Fig. 20   Molecular chemiluminescence spectrum of S_2
bands in a nitrogen hydrogen diffusion flame[111]
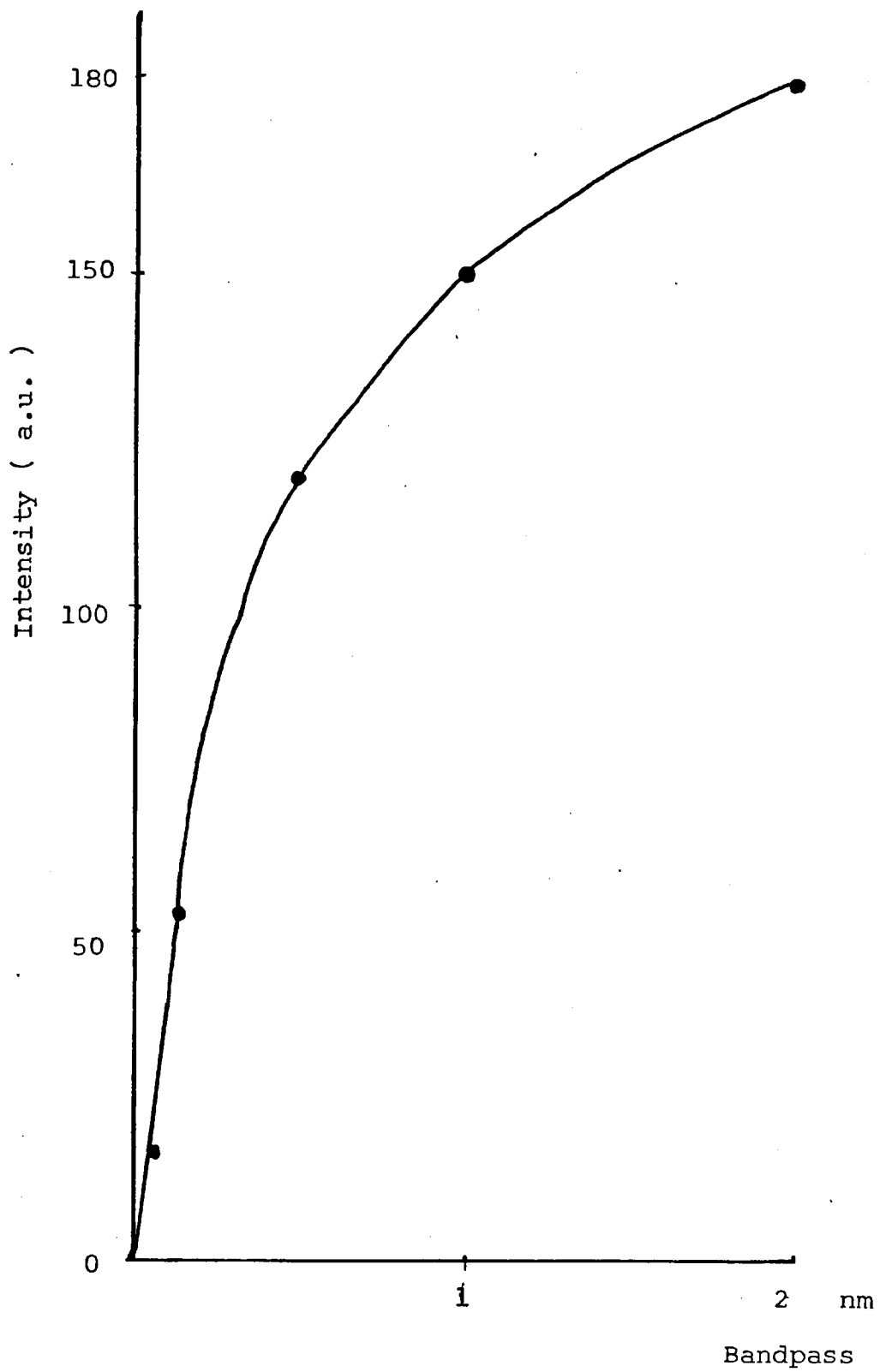
Fig.**2l** The relationship between the bandpass
and emission intensity.

3.2.5 Optimum Heating Programme Applied to the Carbon Tube Vaporizer

Table 3.4 Optimized temperatures for analysis of Sulphur and Phosphorus.

Stage	drying	vaporization
temperature °C	100	1700
time sec.	15	5

The optimum temperature and time used to effect the vaporization of sulphur compounds from the carbon tube are shown in Table 3.4. A rapid rise in temperature between the drying and vaporization steps caused a pulse release of the material into the flame. A transient emission signal was observed in the diffusion flame.

1 sec.

←——→

20μL of 100ppm S

$(NH_4)_2SO_4$
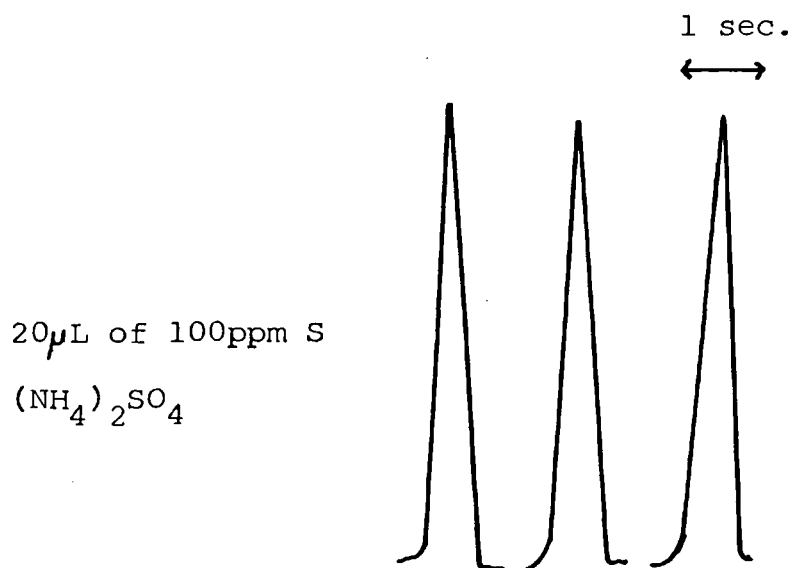
Fig. 22 Typical Peak Shapes

3.3   Procedure for Obtaining Calibration Curves

A working solution of 1000ppm S was prepared (made from dissolving 4.1211g of ammonium sulphate in 1000ml of distilled water) from which working solutions were prepared. The diffusion flame was ignited as instructed in section 2.4.1. 10μL aliquot of sample was pipetted into the carbon tube. On depressing the start/advance button, the atomizer executed the heating programme as selected prior to the analysis. Analytical signals obtained at the optimum conditions previously described were recorded on a strip chart recorder.

3.3.1   Results and Discussion

Figure 22 shows some typical peaks obtained by the procedure described in section 3.3. A detection limit of $10\mu g \ ml^{-1}$ of sulphur was obtained from an emission signal equal to twice the noise on the background intensity. The relative standard deviation calculated from 12 replicate determinations of 20ppm sulphur was 0.04.

Calibration curves were obtained for pure aqueous solutions of ammonium sulphate. A non-linear calibration graph was obtained when peak height intensity was plotted against the S_2 concentration as shown in Fig.23 . When the graph was replotted on log-log scale (Fig.24), the resultant curve could be separated into two parts. The linear portion obeys the square law relation of S_2 concentration to emission intensity and has a slope of 2 as the following mechanism is responsible for excitation of sulphur.
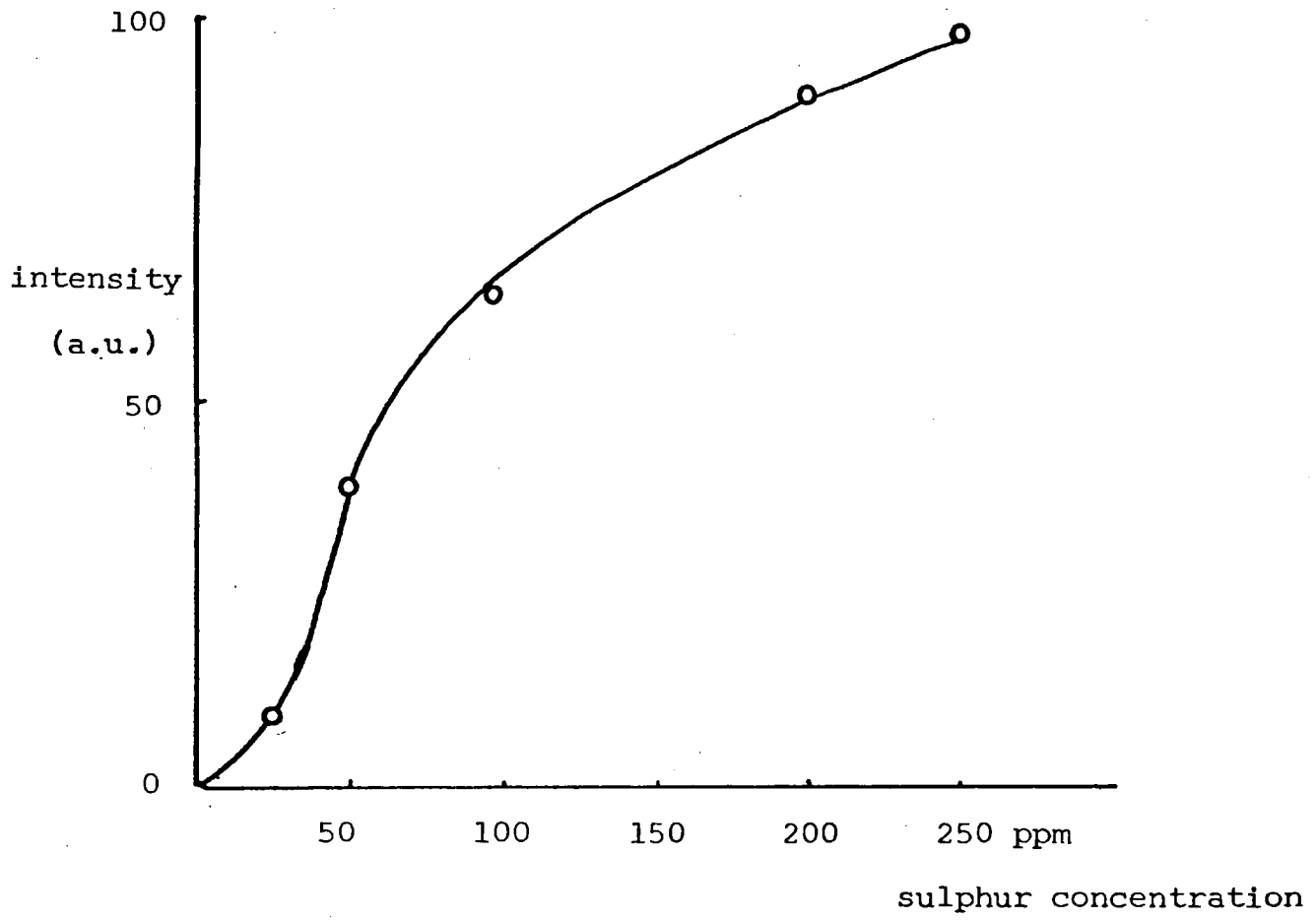
Fig. 23 Calibration Curve for Sulphur
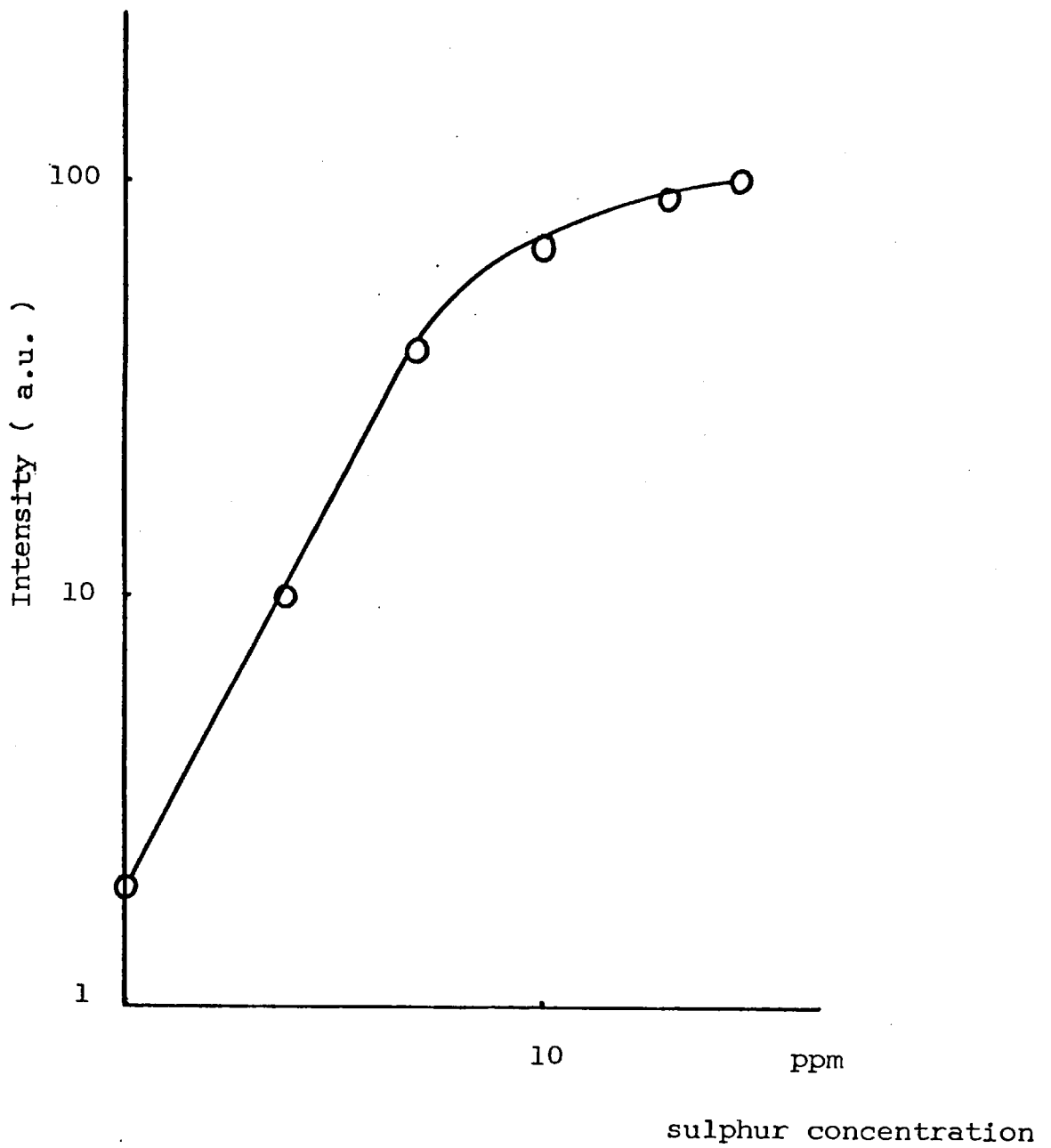
Fig.24   Calibration Curve for Sulphur on log-log scale

<u>viz.</u>

$$S_{(compound)} \longrightarrow S_{atomic} \qquad (3.1)$$

$$S + S \longrightarrow S_2 \qquad (3.2)$$

$$S_2 \xrightarrow[collisional]{} S_2^* \qquad (3.3)$$

$$S_2^* \longrightarrow S_2 + h\nu \qquad (3.4)$$
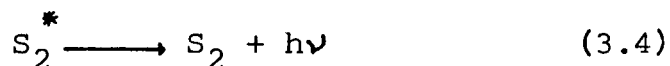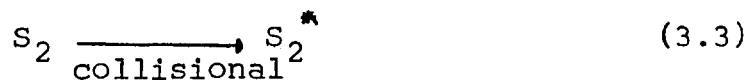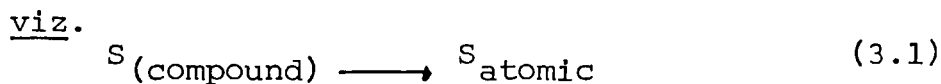
Thus $\qquad I \propto (S)^2 \qquad (3.5)$

and $\qquad \log I \propto 2\log(S) \qquad (3.6)$

The square relationship is only valid if the blank signal is negligible. The second part of the calibration curve shows a curvature towards the concentration axis. This is due to a combination of several factors, ie. signal broadening, self-absorption and quenching.[115] Attempts have been made to straighten[114,179] the top part of the curve without much success and it is recommended that the straight line part of the curve should be used for calibration.

3.4 Improvements in Analytical Sensitivity in the Determination of Sulphur

The use of a circular Meker burner head with seven holes (6 holes hexagonally arranged with one in the centre) drilled in the centre to support the argon hydrogen air-entrained flame causes a considerable degree of air entrainment[135]. The presence of oxygen quenches the emission of S_2 due to an increase in flame temperature and the formation of SO_2.

The sensitivity and detection limit in the

determination of sulphur by cool flame using electro-
thermal vaporization may be achieved by decreasing the
amount of air entrained. It has been reported by
several authors that the temperature of the flame and
the amount of air entrained into the flame are critical
factors in determining the intensity of the observed
chemiluminescence from the S_2 species. Thus Gilbert$^{(117)}$
shielded the flame with a water-cooled pyrex chimney
to decrease the quantity of air entrained and to cool
the flame. Similarly, Dagnall et al.$^{(111)}$ placed a
borosilicate glass tube 15cm in length vertically over
the stem of a circular burner to obtain a similar
result.

Dĕdina and Rubeška$^{(118)}$ reported the use of
a cool, fuel-rich, hydrogen-oxygen diffusion flame burning
in the inlet port of a T-shape tube for determining
Selenium after having generated the selenium hydride.
The advantages reported were:

1) the temperature in the optical tube can be controlled
   by the tube dimensions and quantity of oxygen
   introduced into the flame. For a tube of 152mm
   in length, 3.2mm inner diameter and if the oxygen
   and hydrogen flows were 25ml min^{-1} and 2.8ml min^{-1}
   respectively, the temperature at the junction of
   the inlet was 115°C, and only 45°C at the ends of
   the tube.

2) The analyte is confined to a well defined space.

In this study, for similar reasons, a horizontal
quartz tube mounted 2.0mm above the burner was found

to enhance the chemiluminescence in the flame and lower
the detection limit for sulphur. The tube used was
20mm in diameter, 70mm in length and had an orifice
8mm in diameter placed directly above the centre of
the circular burner to allow entry of the flame gases
into the tube (Fig.25). Using this device the flame
burnt above the 8mm hole and within the tube and at
both ends of the tube. The advantage was that the
optical path of the emitting species was longer in the
horizontal axis in front of the entrance slit of the
monochromator. The position of the quartz tube above
the burner was critical in controlling the amount of
air entrained into the flame. The height of the quartz
tube above the burner head was optimised. The optimum
position was 2.0mm above the burner head (Fig.26).

3.4.1 Results

A calibration curve was constructed using the
quartz tube attachment. On the log-log scale, the
curve is linear from 10ng to 100ng with a slope of 2
(Fig.27) The detection limit for sulphur was improved
two orders of magnitude to 2.5ng corresponding to 0.25ppm
using a 10μl sample. For comparison, a calibration
curve constructed using the circular burner head alone
and a calibration curve constructed using the quartz
tube were plotted along side each other as shown in Fig.28
The reasons for the observed enhanced sensitivity are,
firstly, the emission is concentrated in the optical
path; secondly, the intake of air is restricted by the
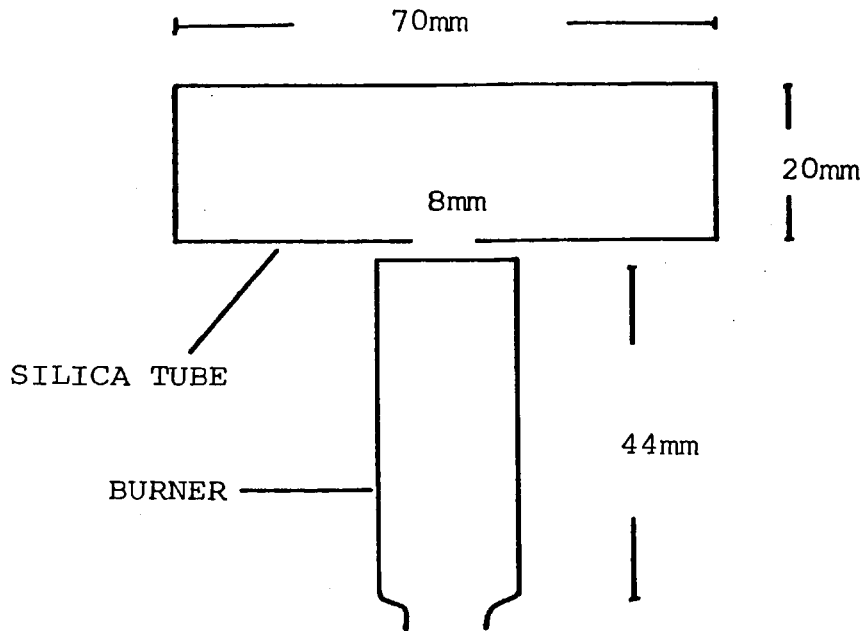
Fig. 25 The Configuration for the Circular
burner and the Silica tube.
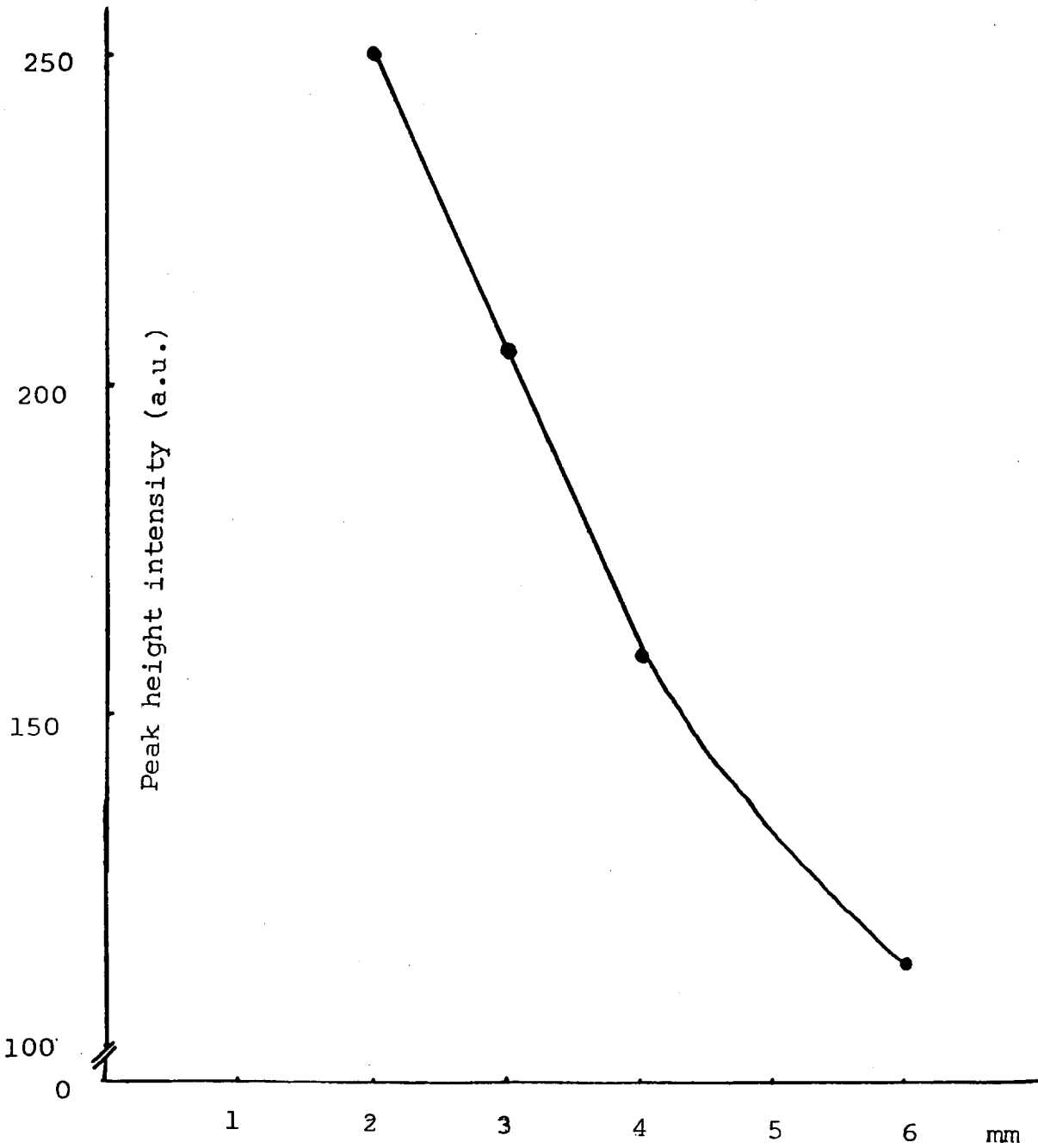
Fig. 2b Distance between the quartz tube and the burner head
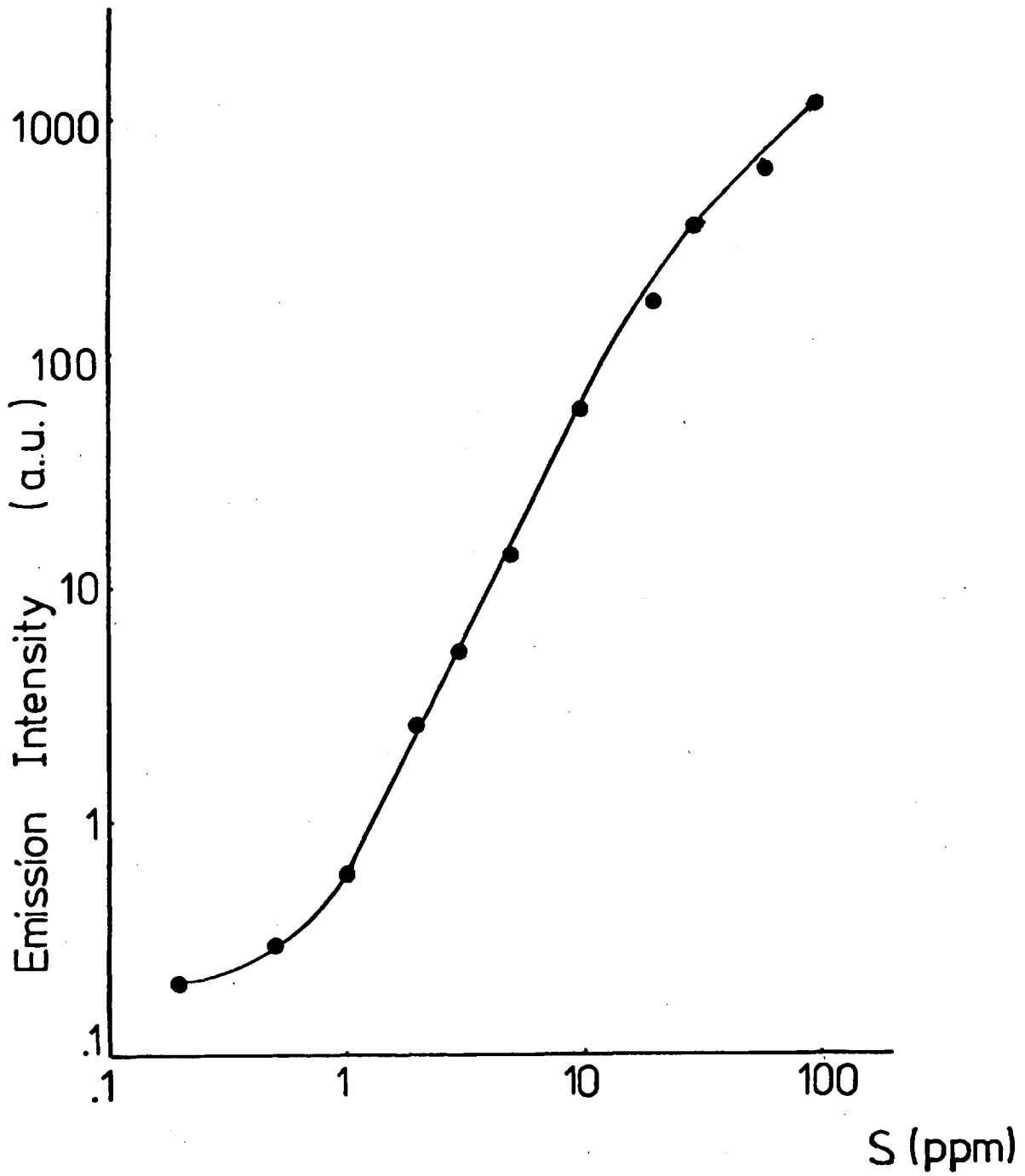
Figure 27   Sulphur Calibration Curve

on log-log scale
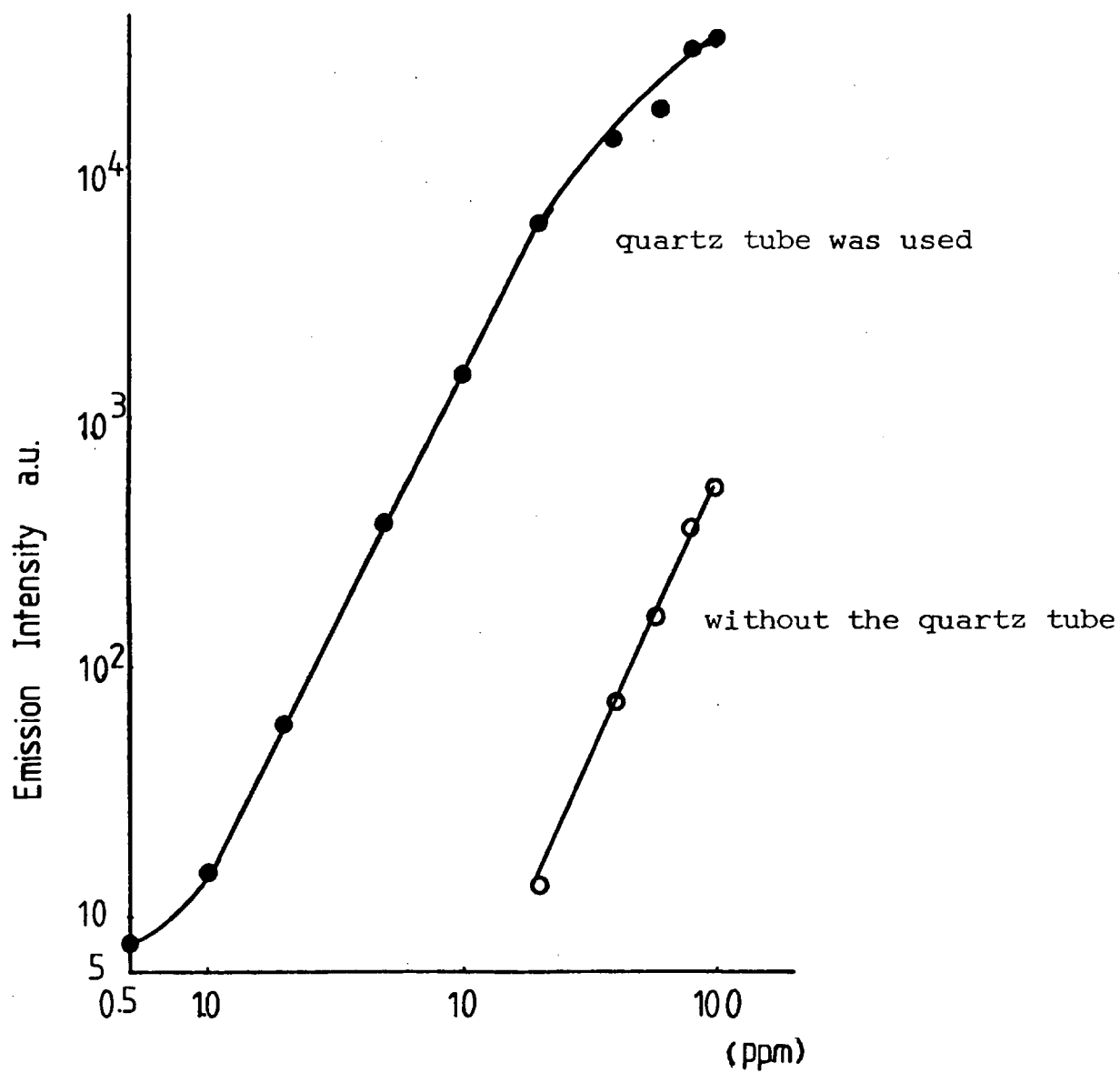
Fig. 28 A comparison for the calibration curves obtained with and without the quartz tube.

presence of the tube; thirdly, the tube may be acting as a cooling surface (see section 2.2.4).

3.5 Metal Sulphates

Various metal sulphates (magnesium, nickel, zinc, manganese) were vaporized into the flame resulting in the calibration curves shown in figure 29. All of the curves have a gradient of 2.
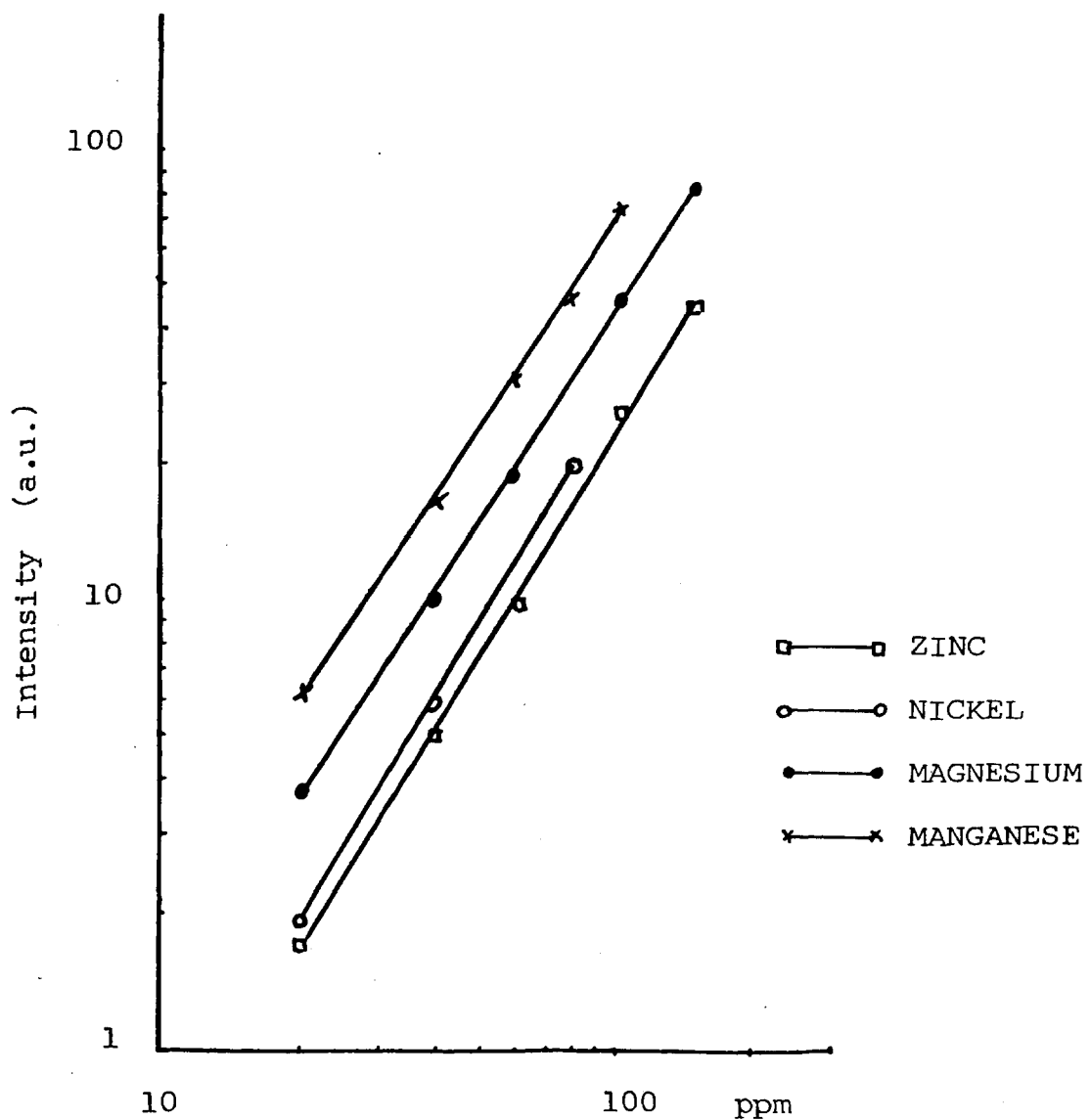
Fig. 29 Calibration curves for some metal sulphates

3.6   Interferences

For many elements determined by emission techniques under fixed instrumental conditions, there exists a relation between the optical signal and the analyte concentration which is represented in the simplest case by a linear analytical calibration graph and in the most general case by a curved one. The position and form of the curve may be affected by the nature and concentration of the concomitants present in the solution. An interference effect arises when the presence of a concomitant species causes a deviation in the measurement of an analytical signal. The interferences observed in flame or plasma emission spectrometry can be categorised into four major types:

1)   Spectral interferences: These interferences occur when the resolution of the spectrometer used is not sufficient to separate the spectral line of the element of interest from a line or a band emitted by the compounds in the matrix or by the source itself. For example, in the determination of phosphorus in phosphor bronze, the removal of copper was necessary as $CuCl$ and CuH bands emit in the proximity of the HPO band emissions.

2)   Ionization interferences: In the presence of a high concentration of a concomitant element of low ionization potential, the electron density and/or the temperature of the excitation source can be altered, thus causing a change in the equilibrium between the atoms and ions of the analyte element. As a result, the spectral line intensities may be enhanced or depressed.

3) Sample vaporization interferences: These interferences result from the formation of a stable species between the analyte and the interferent (the Ca-P system[173]) and/ or the occlusion of the analyte in a non-volatile matrix (the depression of Ca emission signal in the presence of an aluminium matrix.)[174]

4) Sample transport interferences: For the graphite tube vaporizer/flame system, transport interferences can be caused by the occlusion of the analyte on the surface of the graphite tube or by the formation of stable carbides. The transport efficiency is also dependent upon the degrees of interactions between the analyte element and the concomitants in the vapour phase.

In the present study, the problem of stray light was severe. The alkali and alkaline earth metals emitted intense radiation in the cool flame. Normally, one might not expect emission of alkali and alkaline earth metals in the flame. But, owing to the reducing properties of the cool flame, an induced chemiluminescence reaction can occur[122].

$$H + H + Na \longrightarrow H_2 + Na^* \qquad (3.7)$$
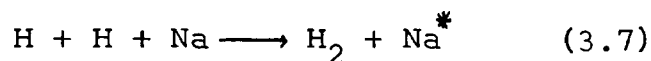
It is also possible that the temperature of the diffuse secondary reaction zone is high enough to dissociate the compound and excite the easily ionizable elements.

The stray light effects can be reduced or eliminated by some modification to the optics[175 - 178] or by employing appropriate filters located immediately in front of the detectors[175, 177] or ahead of the entrance slit of the spectrometer[177].

The effects of concomitant organic substances are complex and manifold. The types of interferences[119] observed include 1) background interferences, 2) sample aspiration, nebulization and desolvation interferences, 3) solute vol*i*tili*sation* interferences and 4) quenching interferences. It was reported that the presence of organic compounds in either the carrier gas or in the sample would cause a decrease in the observed emission signal[120].

The extent of interferences depend on whether the nebulizer is of the direct injection or chamber type, whether the flame is rich or lean, and whether the analyte is volatile or involatile. Many of these types of interferences can occur in the determination of sulphur and phosphorus. It was reported that the presence of organic compounds in either the carrier gas or in the sample would cause a decrease in the observed emission signal[120].

Sugijama et al.[121] suggested that the magnitude of the interference caused by organic compounds on the molecular emission due to the S_2 species increases exponentially with the concentration of volatile organic compounds. The decrease in the intensity of the S_2 molecular emission is based on the deactivation of the excited S_2 species by combination or collision with an organic compound. The intensity decrease is not due to temperature rise caused by presence of organic compounds and is independent of wavelength.

Veillon and Park[122] found that when solution

was directly nebulized into the flame, the S_2 emission

signal in organic solvents was considerably less than

that obtained in aqueous solvents. With alcohols, the

sensitivity decreased by about 4-fold, while in 4-butyl

acetate, it decreased by about 30 folds. The depression

was rapid at low concentrations of ethanol in water-

ethanol mixtures as shown in Fig. 30.
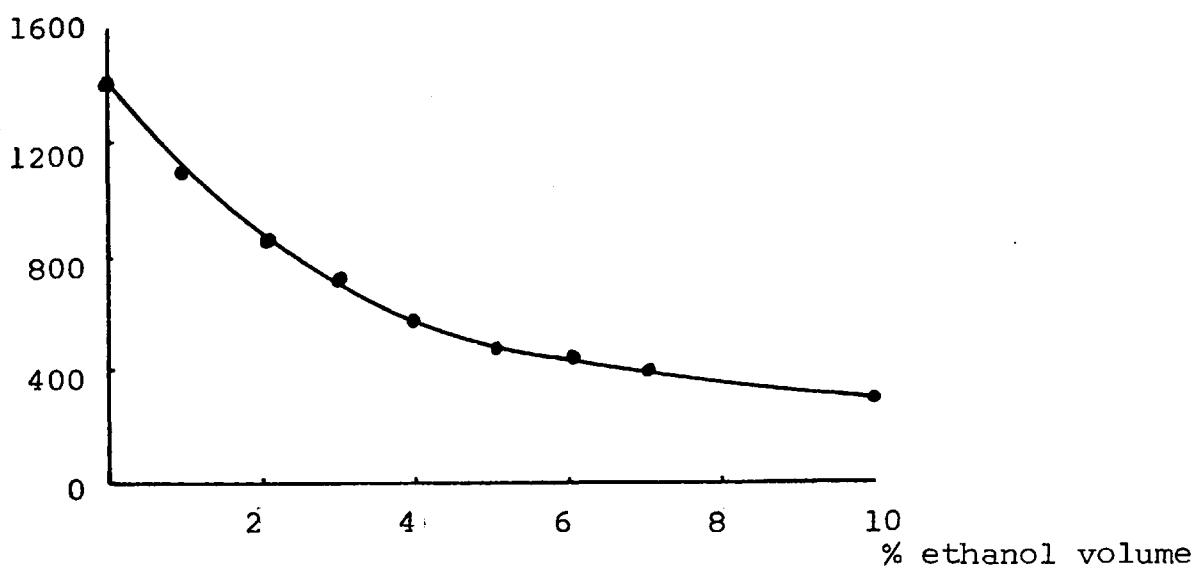
Fig. 30 Effect of Organic Solvent on S_2 emission.[122]

It was suspected by the authors that the depression

of S_2 (or HPO) emission by organic species was due

to either temperature of organo-radicals produced in

the flame.

Fredriksson and Cedergren[123] suggested that

the formation of thermodynamically stable gaseous CS

was probably responsible for the decrease in the cool-

flame signal from S_2 in the presence of hydrocarbons.

One of the advantages of using electrothermal

vaporization over nebulization and gas generation

technique into the flame is that organic sulphur

compounds can be determined directly without sample
pretreatment. The solvent, either water or organic
can be vaporized prior to the release of the analyte.
Also, organic matrices can be pyrolysed leaving the
element of interest to be vaporized into the flame
at a higher temperature.

Some preliminary experiment were carried
out to investigate the feasibility of introducing
vaporized organic sulphur compounds from the graphite
tube into the flame.

3.6.1 The procedure for obtaining calibrations

Analar reagent grade urea, sulphanilic acid,
aniline sulphate (their structures are shown in Fig.3/)
were dissolved in distilled water to make up stocks
solutions of 1000ppm. Suitable working solutions were
prepared from them.

$10 \mu L$ aliquots of the sample were introduced
into the flame using a micropipette. The samples were
pyrolysed at the highest temperature possible without
loss of sulphur

$$S = C \underset{NH_2}{\overset{NH_2}{<}}$$
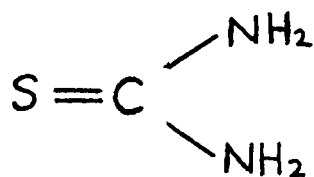
a) Urea.
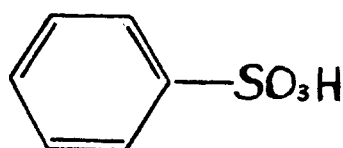
b) Sulphanilic acid.

$\frac{1}{2}H_2SO_4$

$-^+NH_2$
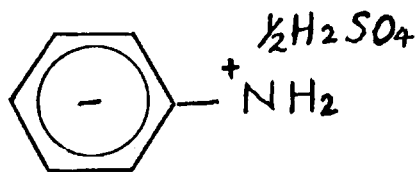
c) Aniline sulphate.

Fig. 31 Structures of Some Organic Sulphur compounds.

In the case of urea, owing to its low boiling point, (182°C), vaporization was observed immediately after desolvation.

Calibration curves are presented in Fig. 32 Urea gave a slope of 2, the gradient of the graph for aniline sulphate is 1.8 for concentrations up to 100ppm. (no quartz tube was used across the flame.) Sulphanilic acid, however, gave a gradient of 2 for the range 5-10ppm. At concentrations above 100ppm, all three calibration curves approached a plateau. This was probably due to quenching or self-absorption.

Diagram 32 indicates the possibility of determining organic sulphur compounds directly by observation of chemiluminescence when using electrothermal discrete sample introduction. However, further work is required before an affirmative conclusion can be drawn. For example, more complex organic compounds and other solvents should be investigated.
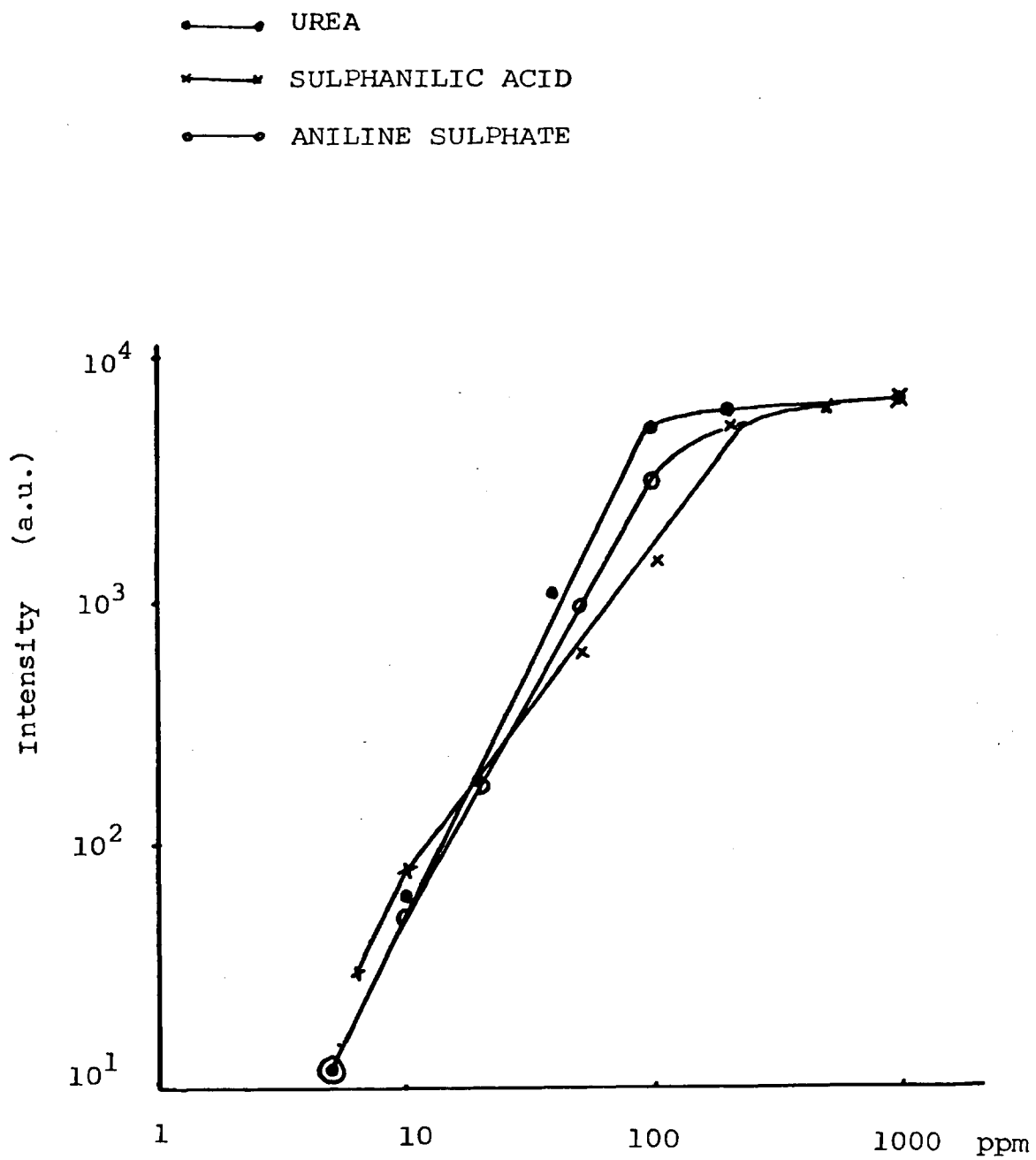
Fig. 32 Calibration Curves for some organic sulphur compounds.

3.7   The Analysis of Real Samples

The technique which has been described was applied to the analysis of sulphur content in well-water and herbage digests.

Well-water samples

Four well-water samples were supplied by Thames Water Authority and their sulphur content was determined.   The results obtained are shown in Table 3.5 and are compared with the results obtained independently by a turbimetric procedure.

Table 3.5   Well-waters

Sample	cool flame (ppm)	Barium Chloranilate (ppm)
Green Street	4	5.5
Bexley	16	16.5
Broxbourne	23	22.0
Wanstead	56	62.0

Some recovery experiments were carried by adding a knowNamount of sulphur to a water sample whose concentration in sulphur was predetermined.   Good re-coveries were obtained. (Table 3.6)

Herbage digests

Procedure for digestion: 0.5g of herbage was accurately

weighed into a large pyrex basin. 10ml of 95% W/V
magnesium nitrate was added to the sample. The mixture
was digested on a hot plate until no more brown fumes
were evolved. The resulting solid mash was ashed in
a muffle furnace at temperatures below 450°C until the
solid became white. The ash was dissolved in 10ml of
36% W/W hydrochloric acid and the solution was diluted
to 50ml with distilled water. The solution was passed
through a cation-exchange resin (Zeocarb 225 H) prior
to analysis.

Results

        Six herbage samples were prepared for analysis
by the procedure described above and their sulphur
contents were determined using the optimum conditions
as shown in Table 3.3. The concentrations determined
are presented in Table 3.7 and are compared to the
results obtained independently using the sample digestion
procedure and the barium chloranilate colorimetric
determination of sulphur. Good agreement between the
two methods of analysis was observed.

Table 3.6   Recovery of S added to Broxbourne well water

Broxbourne* ppm	ppm added	ppm detd.	%recovery
4.8	2	6.7	98
4.8	4	8.75	99

*Broxbourne well water was diluted 5 times.

In digesting the grass samples, magnesium nitrate was used . Magnesium, when present in a cool flame, can undergo induced chemiluminescent reaction.

$$H + OH + Mg \rightleftharpoons H_2O + Mg^*$$

Magnesium exhibits an atomic emission line at 383.0nm. Therefore, the digested samples were passed through an ion exchange resin column to remove magnesium prior to analysis.

Table 3.7   Herbage digests

Sample	cool flame %S	turbidimetry %S
2023	0.38	0.38
2024	0.305	0.30
2041	0.26	0.26
2020	0.24	0.24
2045	0.073	0.07
2076	0.105	0.12

CHAPTER FOUR

THE ANALYSIS OF PHOSPHORUS

4.1 Introduction

Like sulphur, phosphorus has its principal atomic resonance lines in the vacuum ultraviolet region of the spectrum (177.5nm, 178.3nm, 178.8nm) , thus making atomic absorption and atomic emission spectrometric measurement difficult. The usual method of determining phosphorus by emission spectroscopic techniques involve indirect procedures such as the depressive effect of phosphate on the emission of calcium and magnesium[124]. However, only a limited range of phosphate concentrations can be converted by using a given concentration of calcium. In addition, the sensitivity of this method is poor. If a 100ppm calcium solution is used, the minimum level of phosphorus which can be detected is about 30ppm.

Numerous colorimetric methods have been used in the determination of phosphorus[125]. These methods are based on the formation of a coloured complex whose colour density is proportional to the amount of phosphorus present. One example is the molybdenum blue method in which orthophosphate and molybdate ions react in acidic solution to give molybdophosphoric acid, which upon reduction with hydrazine sulphate ,produces a blue complex. This complex exhibits maximum absorption at 820-830nm.

Direct flame emission techniques utilising the phosphorus continuum at 540nm[126,127] are only moderately sucessful because the continuum emission is weak. Detection limits obtained were in the range 3-8ppm of phosphorus.

The determination of phosphorus by methods involving the measurement of the emission intensity from HPO molecules have been reported by several groups of workers[114,128-134]. A low temperature flame, termed the hydrogen diffusion flame (see section 2.4), was employed for the excitation of HPO species (see section 2.2.4). The formation of HPO molecules, however, is an equilibrium process and low temperatures shift the state of equilibrium to where the conditions for production of HPO species are favourable.

The techniques for determining phosphorus using a diffusion flame mentioned in references 128 - 134, 114 differ in one respect, that is, the manner in which the sample is introduced into the flame.

1)   Nebulization:

Dagnall et al[128] reported a detection limit of 0.1ppm by nebulising a solution of orthophosphoric acid into a diffusion flame. As band emission was obtained with phosphorus species, valuable sensitivity was lost by using a monochromated instrument that only recorded radiation within a narrow spectral region. Considerable increase in sensitivity was achieved by using a filter detection system[136]. A detection limit of 0.01ppm was obtained for aqueous phosphorus solution. The detection limit was further improved down to 0.007ppm by employing a heated nebulization chamber to dry the aerosol.

Prager and Seitz[132] employed a Mistogen EN 142 electronic nebulizer to introduce a fine aerosol into

the diffusion flame. However, a large sample volume
(100-150ml) was required for aerosol generation. The
minimum sample required was 10ml if the liquid was
contained in a nebulizer cup which fitted to the nebulizer
vessel. A detection limit of 0.003ppm was obtained for
phosphorus as phosphoric acid.

The low detection limits reported by these
authors demonstrates the utility of chemiluminescence
in the field of trace analysis. However, these authors
did not report any real life applications to assess the
usefulness of their techniques.

In nebulization, the analyte together with the
matrix are introduced into the flame. As the flame is
used to desolvate the aerosol as well as to dissociate
the dry particles, the temperature   needs to be
higher than is necessary for maximum formation of HPO
species. Thus a degree of sensitivity may be lost by
increasing the temperature. The matrix present may
also have an effect of degrading the sensitivity and
upsetting the equilibrium further.

2)   Electrothermal Vaporization

    a)   Graphite Oven   Flame Analysis (GOFA)[133]

        Campbell employed a Perkin-Elmer HGA 74 graphite
furnace atomizer to vaporize dried phosphorus compound
into a hydrogen-air flame where the chemiluminescence
due to HPO was observed. To reduce the interference
from calcium in the flame, a matrix of calcium and EDTA
was added to the samples and standards before introduction

into the furnace atomizer. This method gave a detection
limit of 3ppb for a 25µl aliquot of sample.

b)   Carbon Filament Atom Resevoir (CFAR) [132]

Everett attempted to use the arrangement
shown in Fig. 14 to analyse phosphorus in oil products.
A curve calibration graph was obtained in the range 0-100ng
(in the form of H_3PO_4). The detection limit was 4ng
using the HPO emission line at 526nm and a monochromator
slit width of 0.4mm. However, this method did not prove
to be sucessful in the determination of organic phosphorus
due to the limited workable range of the calibration,

loss of phosphorus in the pyrolysing stage and quenching
by the organic matrix.

c)   Silica-heated Graphite Furnace [134]

A graphite furnace was used in a similar manner
to the GOFA with the exception that the graphite furnace
was treated with silica to reduce its porosity and hence
to decrease the amount of analyte able to soak into the
graphite tube surface. This allows greater sample atom-
ization efficiency to be obtained in the same manner as
is achieved when pyrolytic carbon tubes are used.

3)   Gas Chromatography (GC)

In fact, GC is not intended to be a sample
introduction system for flame photometry. But because
of the unique characteristic of the GC/flame photometric
detector system,   it deserves a mention. A gas
chromatographic column when packed with a suitable

material can separate a mixture of compounds by virtue of their differing physical properties. Separation is achieved at the speed with which the component is eluted from the column.

Brody and Chaney[129] described an application of a flame photometric detector for organic phosphorus and for organic sulphur compounds. Organic vapours leaving a gas chromatographic column, with nitrogen as carrier gas, were mixed with a volume of oxygen to give the same nitrogen-to-oxygen ratio as occurs in air. The mixture was burned with hydrogen as the fuel gas in a flame-photometer burner. The emission from HPO was monitored using narrow band-pass interference filters and a photomultiplier tube, resulting in a very sensitive and selective detector. The response of the detector, for HPO monitored at 526nm, was reported to be linear from 6ppb to 60ppm. The sensitivity of the detector to phosphorus was 1×10^{-12}g sec^{-1}. The use of GC for sample introduction, however, is only applicable to organophosphorus compounds and to those which can be handled directly by gas-phase chromatography.

4)   Molecular Emission Cavity Analysis (MECA)[137]

Belcher et al introduced the phosphorus compound into the flame by depositing it into a steel cavity cavity which was then inserted into the flame. The sample was dried and vaporized in the environment of the flame. Nanograms of phosphorus could be measured in this manner.

4.2 The Spectrum of HPO

Fig. 33 ([119]) shows a molecular chemiluminescent spectrum of HPO in a cool hydrogen-air and nitrogen flame between 500 and 600nm. The spectrum exhibits maximum molecular band emission due to excitation of HPO at 526nm.

500   520   540   560 580   600   nm
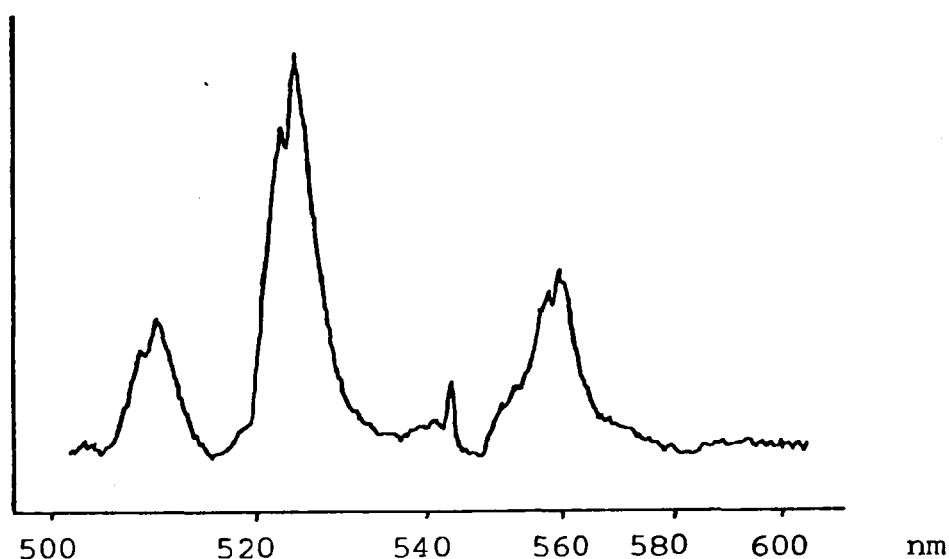
Fig. 33 Molecular chemiluminescence spectrum of HPO bands in a cool hydrogen-air flame between 500 and 600nm. Water-cooled burner was used.

4.3 Instrumentation employed in this study

The instrumentation used for the analysis of phosphorus was exactly the same as that used for sulphur and has been described in Chapter 2.

4.3.1   Optimization of the Experimental Parameters

The effects of experimental variables on the emission intensity of the species participating in chemiluminescence reactions have been discussed in Chapter 3. The variables are the choice of flame, the flame gas flow rates, the viewing zone in the flame, the slit widths and the vaporization heating programme. It was observed that the optimum conditions found for sulphur were applicable to the determination of phosphorus. This is not surprising as the emission intensity of the HPO band does not depend on the hydrogen flow rate once the critical flow of hydrogen has been reached at a certain flow of argon. A wide bandpass is required to gather sufficient chemiluminescence radiation from the HPO band emission. The bandpass chosen is subject to the signal to noise ratio and to the bandwidths available in the spectrometer. The analytical heating programme selected for vaporizing aqueous solutions containing sulphur could also be used for vaporizing aqueous phosphorus solutions as sulphur and phosphorus are fairly volatile elements and are readily released from the carbon tube. The best position in the flame for viewing the HPO emission was near the burner head as this portion of the flame was the hottest. The temperature of the flame at any one point is related to the fuel to air compositions, the concentrations of which become more and more diluted with the vertical distance away from the burner head. Hence HPO is observed at the base of

the flame and S_2 is observed higher up in the flame
which is consistent with the fact that HPO molecules
require higher excitation energy than S_2 molecules.
The optimised conditions employed for the analysis of
phosphorus are shown in Table 4.1

Table 4.1 The optimum conditions for the determination of P

Argon flow rate	3 L min^{-1}
Hydrogen flow rate	1 L min^{-1}
Viewing height	10mm above the burner head
Bandpass	2 nm.
Vaporization temp.	1700° C

4.3.2 Procedure for Obtaining Calibration Curves

A stock solution of 1000ppm P was prepared by
dissolving 4.2635 g. of analar grade of $(NH_4)_2HPO_4$
in 1000 ml. of distilled water. Working solutions
were prepared from this stock solution when required.
A 10μ1 aliquot of sample was pipetted into the modified
carbon tube (see section 3.2.1) where it was dried and
vaporized into the flame according to the preset heating
cycle. Signals obtained by monitoring the emission
intensities could either be displayed in an analogue
form on strip chart recorder or in a digital form displayed
on the spectrometer. For permanent storage of signals,
the strip chart recorder was required to be connected
to the recorder output (via an output jack) of the spect-
rometer.

4.3.3 Results and Discussion

An example of a calibration curve obtained for phosphorus following the procedure described in section 4.3.3 is depicted in Fig.34. The graph was constructed by taking the peak heights as a relative measure of emitted intensity and is linear between 1.0ng (the detection limit) and 2.0μg. The relative standard deviation calculated from introducing 10 replicate samples of 5ppm into the flame was 0.04. A linear response was also obtained up to

2μg by integrating the peak area over an integration period of 16 seconds.

4.4 Interferences

The type of interferences observed for sulphur in the diffusion flame/carbon tube vaporizer arrangement also affect the emission signal of phosphorus; namely, stray light, spectral interference (see section 4.5), and vaporization interference occurring at the surface of the graphite tube. To overcome these problems, ion-exchange procedure was employed to remove the interfering ions.
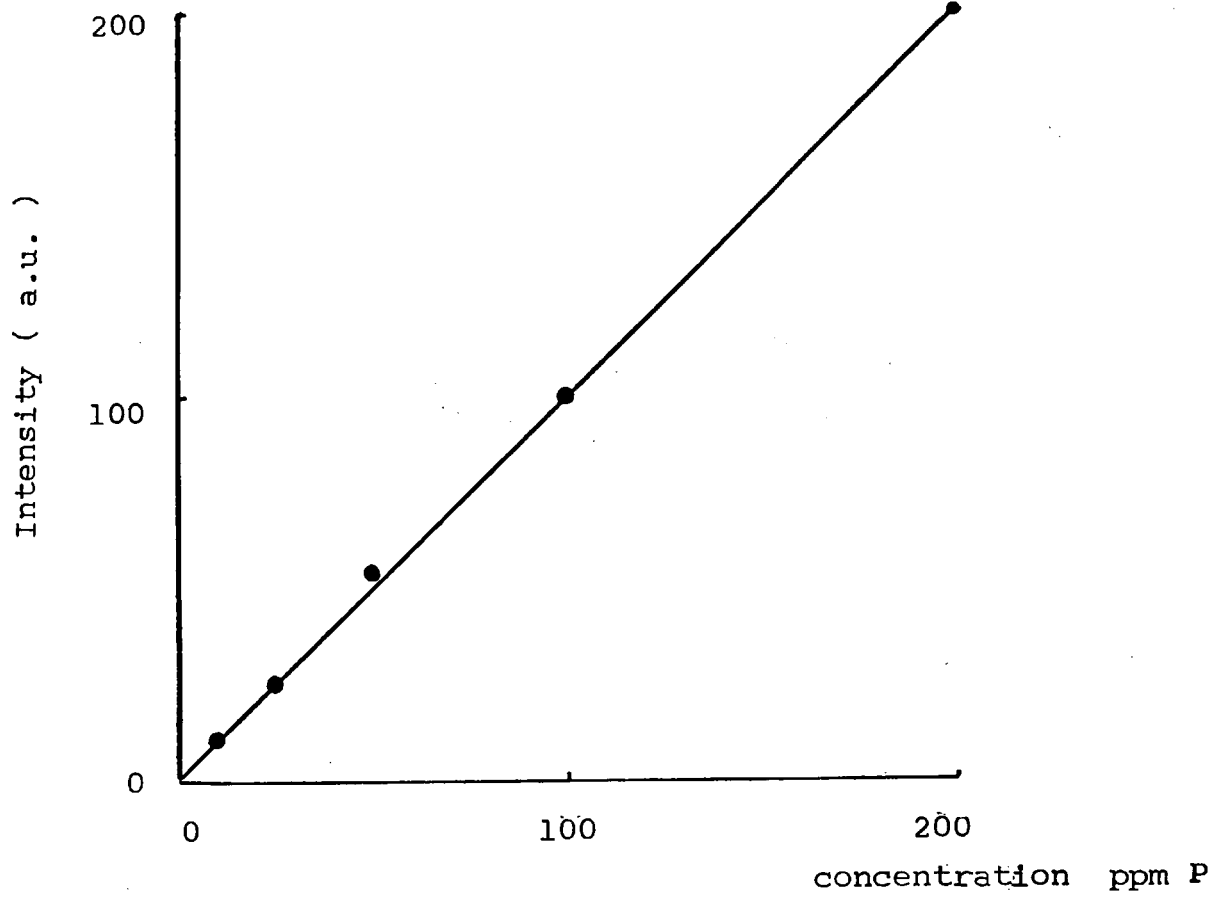
Fig. 34 A phosphorus calibration graph

4.5 Analysis of Phosphorus in Phosphor Bronze

The flame/electrothermal vaporizer system developed was applied to the analysis of phosphorus in phosphor bronze.

0.5g of bronze powder was weighed accurately and was dissolved in 20ml of _aqua_ _regia_ (prepared by mixing concentrated nitric acid, hydrochloric acid and water in the proportion $8HNO_3$: $3HCl$: $11.5H_2O$). The resulting solution was diluted to 50ml with distilled water. The solution was deionized using a cation ion exchange column (Zeocarb 225 in H form). After elution, the column was rinsed with 50ml of distilled water to ensure complete elution of the bronze solution. The concentration of the final solution was 0.5% bronze.The removal of copper was necessary as its presence gives a positive interference on phosphorus because the CuH and CuCl band emission coincide with the HPO emission[136].

The _aqua_ _regia_ had a depressive effect on the aqueous phosphorus emission. Fig.35 shows calibration curves obtained for phosphorus standards and standards spiked with nitric acid in the proportion that was used to dissolve the bronze. The depressive effect was reduced by introducing a pyrolysing step between the drying and vaporization stages to remove the _aqua_ _regia_. To ensure that there was no influence resulting from passing the solution through the ion exchange column, a standard addition procedure was adopted to determine
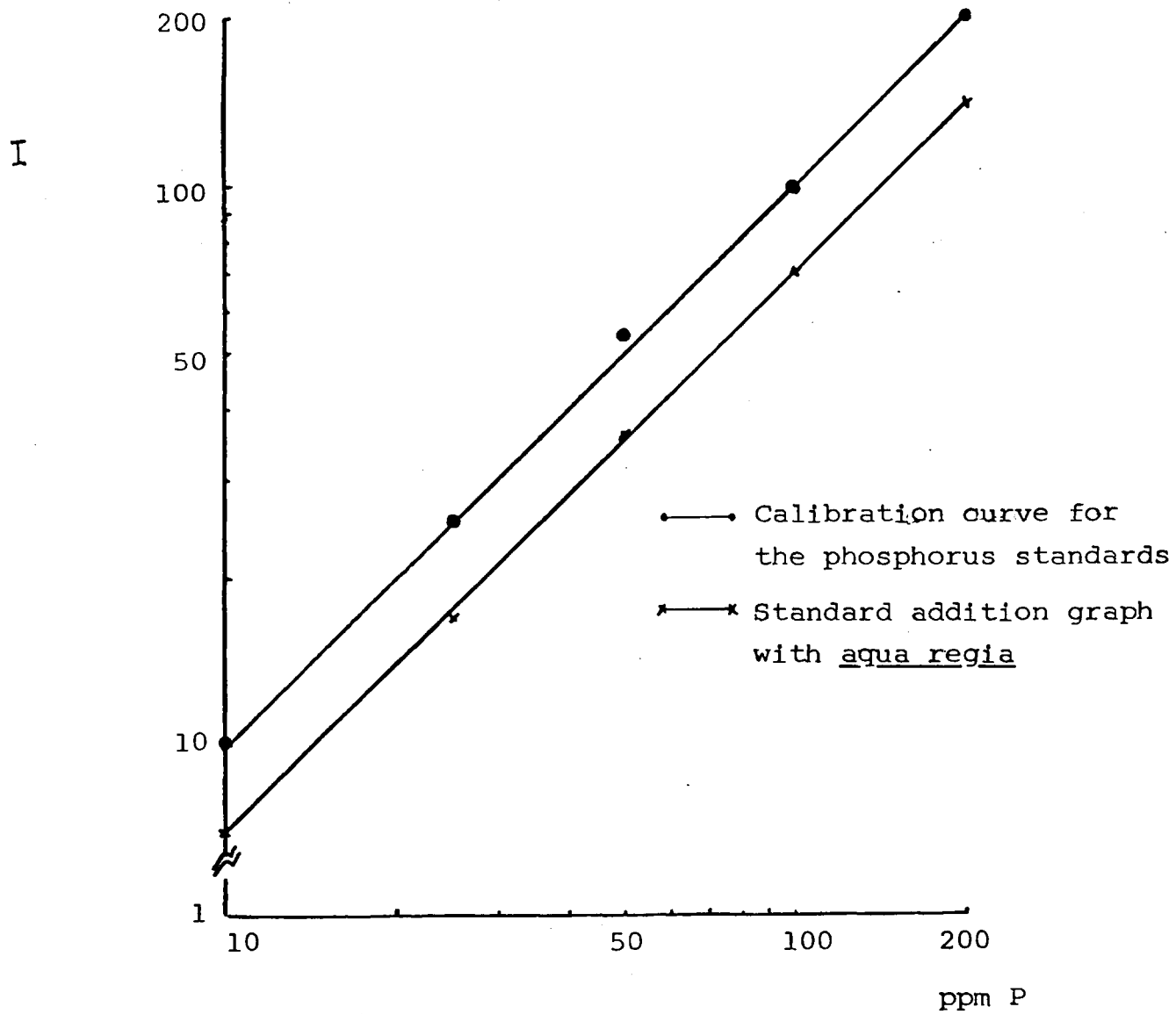
Fig. 35   The effect of aqua regia on the phosphorus intensity.

the content of phosphorus in one bronze sample. The
resultant standard addition graph depicted in Fig. 36
is parallel to the one constructed using aqueous phosphorus
solutions. Therefore further determinations were made
simply by taking the readings from a calibration curve.

The results of the analysis are shown in Table 4.2
and they are compared with those obtained by Molybdivanado-
phosphoric acid absorptiometry (MVPAA). The two sets of

Table 4.2 The Results for the Bronze Analysis

Sample	Cool Flame % P	MVPAA % P
A	0.24	0.26
B	0.28	0.30
C	0.32	0.35

results are in good agreement.
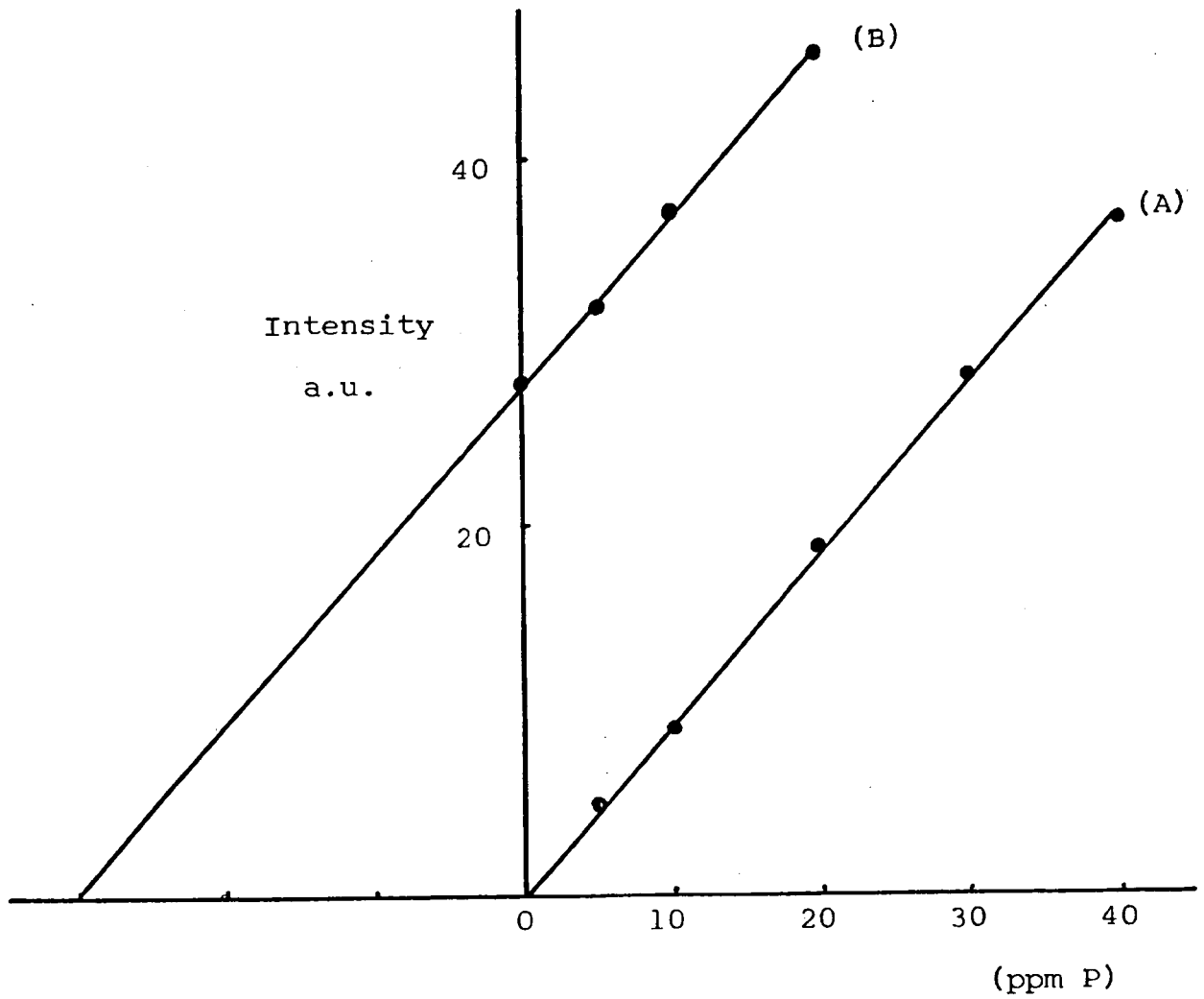
Fig. 36 Standard Addition Curve

(A) Aqueous Calibration curve for phosphorus.

(B) Standard addition curve.

Conclusions and Suggestions for Further Work

The adaptation of a commercially available electro-thermal atomizer as a sample vaporization device for the introduction of discrete liquid samples containing sulphur and phosphorus into a low temperature diffusion flame has been demonstrated to offer good sensitivity and convenience in operation. One of the drawbacks is the need to remove undesirable metal species which either cause spectral interference or stray light problems. The removal of cations by ion exchange is tedious and may discourage users from employing the technique for routine analysis.

The design of the atomizer is compact and suits the purpose of furnace atomic absorption work. Modification to the shape of the enclosure (triangular), however, is necessary for the use in sample vaporization as sample deposition on the underside of the face plate is a problem. Particle formation and solidification processes have been proved to influence the analyte transport efficiency[59]. Therefore, it is advantageous to increase the volume immediately above the carbon tube to allow greater degree of aggregation which in turn, will result in increased sensitivity due to a reduction of analyte deposition.

The use of a filter system to detect the emission signals will undoubtedly increase the sensitivity of analyses because sulphur and phosphorus exhibit band emission in the diffusion flame.

The graphite rod vaporizer posseses great potential in its ability to vaporize a wide variety of compounds.

This capability must be exploited to the full if the graphite tube vaporizer were to become competitive with nebulization, or gas generation for the determination of sulphur.

When a mixture of phosphorus and sulphur is vaporized into the flame, the emission signals of S_2 and HPO are temporally resolved. The blue radiation of S_2 is observed before the green emission of HPO. Therefore, it is possible to determine sulphur and phosphorus simultaneously as similar conditions are used to generate the S_2 and HPO molecules. Bowman and Beroza[131] described a dual flame photometric detector for monitoring chromatographic effluents which contained sulphur and phosphorus compounds (pesticides). The IL555 atomizer/flame system could be adapted to accommodate a dual detector system similar to that of Bowman and Beroza. The new setup would have to be a dedicated system and for it to become a commercial success, it would have to be extremely versatile and flexible in its ability to determine a wide range of samples.

CHAPTER FIVE

THE DETERMINATION OF SULPHUR AND PHOSPHORUS BY ICP-OES

5.1.1 Introduction

The basis of emission spectrochemical analysis is the observation of radiant energy emitted by atoms, ions and molecules which are excited in an emission source. The light emitted by the excited species passes through a prism (or a grating) which disperses the radiant energy according to wavelength, so that the characteristic spectra may be resolved and identified. In the ideal case, the intensity of the emitted light is proportional to the amount of emitting element in the emission source. The measurement of intensities of selected lines serves as the basis of a quantitive analysis.

The analytical emission source must be able to transform the sample from its initial state as solid, liquid or gas into a cloud of atoms, ions and or molecular species which can be electronically excited. A number of types of excitation sources are available for emission spectrometry. They are divided into two major types, flames and electrical excitation sources. An analytical flame is formed by combustion of a mixture of fuel gas and oxidant gas. The heat released by the combustion furnishes the energy required for vaporization and excitation of the sample. The temperatures of flames vary from 600 to 3000K depending on the fuel gas and oxidant mixture. A majority of the elements of the periodic table can be determined by emission and absorption spectrometry using a suitable flame as an emission source or absorption atom-cell. For instance, the oxy-acetylene flame is a

good atom-cell for some refractory compounds because of its high attainable temperature (ca 3000K). The presence of chemical and physical interferences, however, severely restrict the usefulness of a flame. Quite often, the detection limits obtainable by flame spectrometry are at ppm levels or higher, making analyses difficult or impossible to perform at trace and ultra-trace levels as required in clinical or environmental samples.

The electrical excitation sources are of the arc and plasma types.

5.1.2 Arc and Spark Sources

In the d.c. arc source, the arc is generated by striking momentarily two metal or graphite electrodes together with an electrical current flowing through them. The arc produced is maintained by a supply of electrons from the cathode and ions that are generated in the discharge gap. The temperature obtainable in d.c. arcs is about 4000K reaching to a maximum of 8000K depending on the distance between the electrodes and the quantity of current flowing through them. The high temperatures are sufficient to dissociate refractory compounds more efficiently than in a flame.

The spark source is typically produced by the discharge of a capacitor between the sample and counter electrodes. A capacitor of the order of nanofarads is charged to a high voltage and is then discharged to form a conducting spark between the electrodes. The sample

material is vaporized, atomized, ionized, excited and projected into the spark gap. As the excited atoms and ions travel away from the sample electrodes, they emit their characteristic spectra. As the spark current falls, the spark-discharge channel contracts, ions recombine into excited atoms, and the sample is deposited on the counter electrode. The process is repeated in subsequent half-cycles until the capacitor voltage is insufficient to maintain the spark discharge.

The arc and spark sources are valuable for qualitative analysis and multi-element quantitive analysis. They are commonly employed in industry because of their speed of analysis and their sensitivity. They are limited, however, in the way in which the sample is introduced into the region for observation of the spectra. The sample usually constitutes one of the electrodes and often using this arrangement the quantity of sample vaporized into the discharge region cannot be accurately controlled. The precision, therefore, can be poor. In the arc source, the evaporation of sample from the electrode and the consumption of the electrode during arcing causes the arc column to shift its position on the electrode surface. This movement of the arc relative to the optical axis of the spectrograph also reduces the precision of arc analysis.

5.1.3 Microwave Induced Plasma

The microwave induced plasma (MIP) is an electrodeless

discharge which is generated by ionizing an inert gas with a high voltage discharge. The inert gas ions and electrons are then accelerated in a microwave field. The discharge is confined in a quartz tube and is maintained by an electromagnetic wave resonating within a micro-wave cavity. The microwave induced plasma exhibits high electronic excitation energy although its gas temperature is low. Because the MIP cannot tolerate excess liquid or more than a few milligrams of solids per unit time, only volatile compounds or gases can be introduced into the plasma for excitation. For large volumes of liquid, nebulization is employed in conjunction with a desolvation apparatus. Other sampling devices using the electrothermal vaporization procedure are employed for microlitre volumes.

5.1.4 Inductively-Coupled Plasma

The inductively-coupled plasma discharge (ICP) as a source of optical emission spectrometry (OES) is a relatively recent development[138,139], and is perhaps the most promising emission spectroscopic source today.

The ICP discharge is generated in an inert gas flowing through a quartz tube, placed inside an induction coil connected to a high frequency generator. The high-frequency currents flowing in the induction coil generates an oscillating magnetic field whose lines of force are axially orientated inside the quartz tube and follow elliptical closed paths outside the coil (Fig.37)[140]. The axial magnetic field induces a seed of electrons, produced

by a Tesla coil, to flow in closed annular paths inside
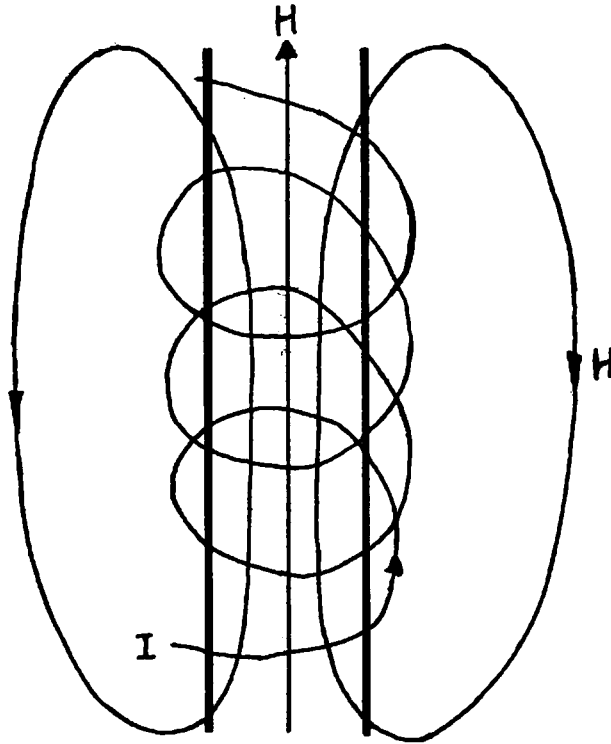
Fig. 37 Magnetic fields and eddy currents
generated by induction coil. (140)

the quartz tube space. The electrons and ions are ac-
celerated on each half cycle of the magnetic field. When
they meet resistance to their flow, heating and further
ionization occur resulting in an instantaneous formation
of a plasma. The plasma formed in this way attains a
temperature of over 8000K and it is necessary to cool
the surface of the confinement tube with a high velocity
gas flow introduced tangentially at the base of the
plasma torch. The tangential flow of gas streams upwards,
cooling the inside walls of the outermost quartz tube
and centering the plasma in the tube. It also has an

effect of vortex stablizing the plasma.

The plasma torch employed in research and in commercial instruments consists of three concentric tubes as shown in Fig.38 [141]. The coolant gas flow is

coolant gas flow

analyte and carrier gas flow
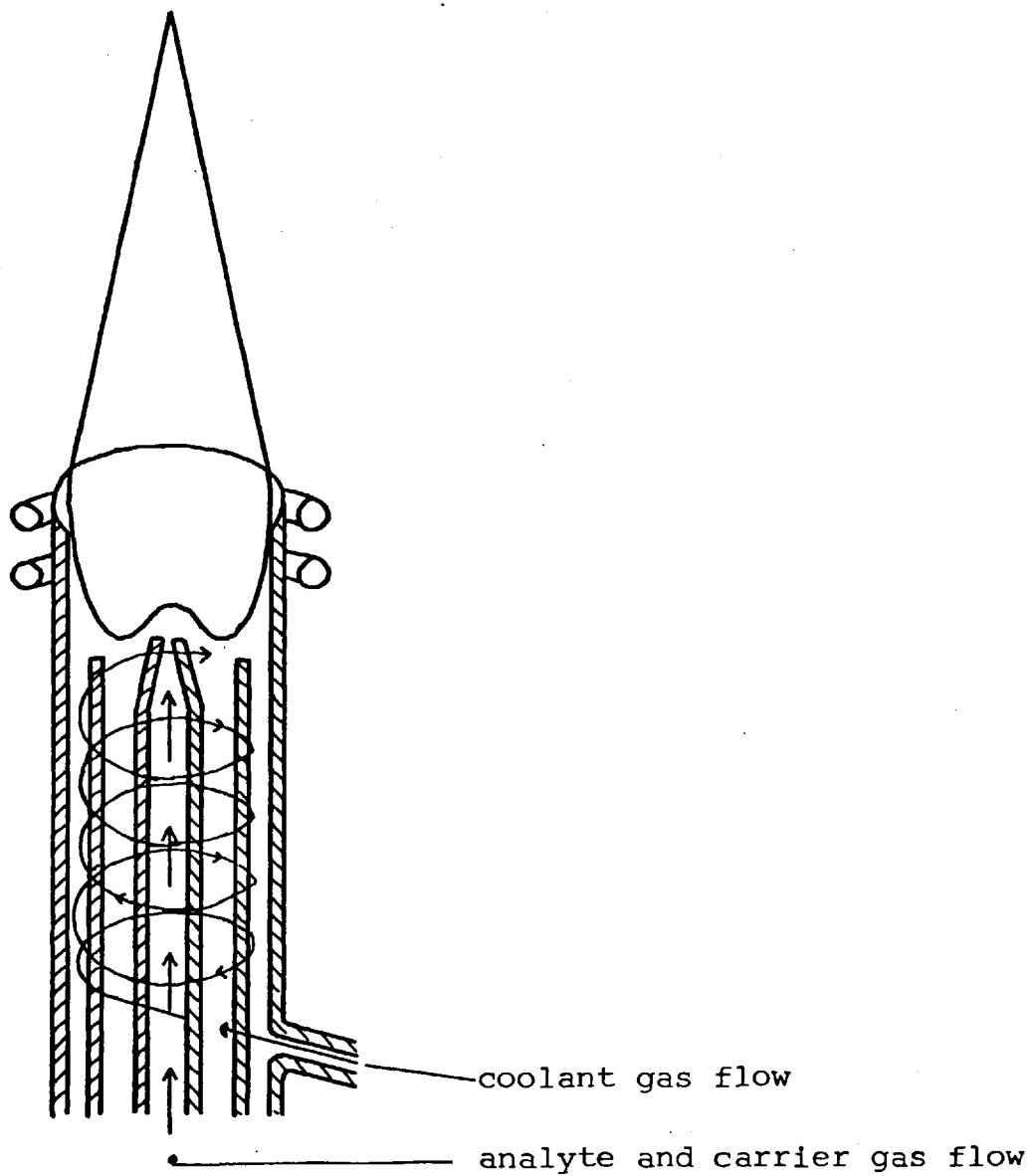
Fig. 38 A typical plasma torch

typically in the 10 Lmin^{-1} range, the plasma gas serves

to sustain the plasma and the injector flow carries the

analyte into the hot environment of the plasma. Without

the presence of an injector tube, the analyte introduced

would not penetrate efficiently into the plasma because

of a combination of two effects.

1) Thermal effect- this is due to the fact that the

plasma gases are heated internally, thereby, causing

them to be accelerated in a direction perpendicular to

the exterior surface of the plasma.

2) Magnetic effect- the decrease of the radial magnetic

field from the boundaries of the axis causes an inward

flow of plasma. This leads to a build up of kinetic

pressure in the core resulting in an axial flow of plasma

back to the boundaries, thus forming a barrier to sample

penetration (the magneto-hydrodynamic barrier).

Due to these two effects, most of the analyte

is deflected around the outside of the plasma where the

temperature is considerably lower than in the core (Fig.39a).

If, however, an injector tube of the shape shown in Fig. 39b

is used , the sample will emerge out of the narrow bore

tube with a velocity which is high enough to overcome

the magneto-hydrodynamic force. The resultant plasma

is of an annular shape (Fig.39b). The stream of sample

passes through the axial channel where the analyte is

vaporized and dissociated under extremely hot conditions.

Analytically useful emission is observed in the tail

flame where there is considerably less continuum emission

than from the region just above the magnetic coil.
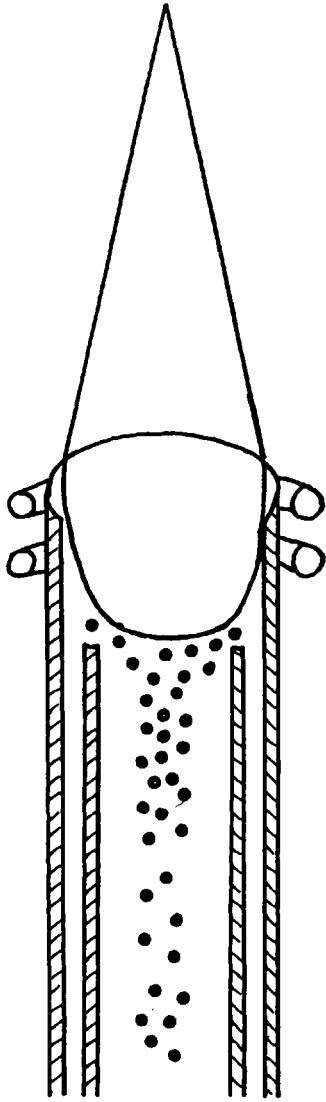
Fig.39a Without the injector,
the analyte is deflected
around the outside of
the plasma.
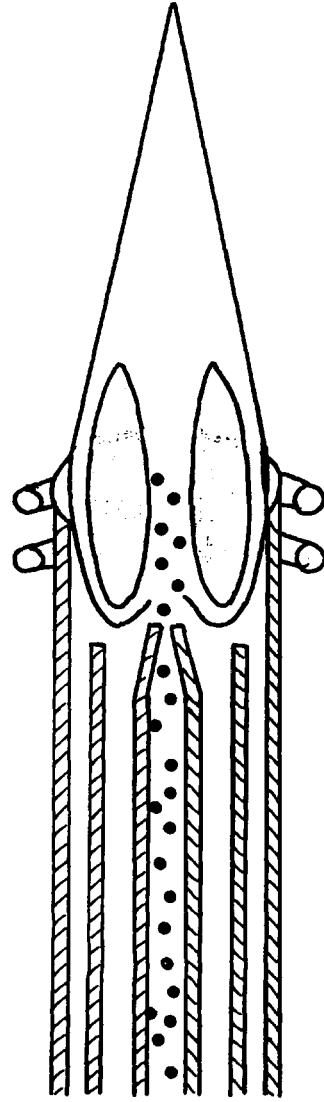
Fig. 39b The analyte penetrates
efficiently into the
core of the plasma in
the presence of an
injector.

5.1.5   The properties of the ICP as an excitation source

The properties of an ideal excitation source are:- [142]

1) Capable of exciting lines of a large number of elements.

2) High sensitivity.

3) High selectivity.

4) Good stability.

5) Freedom from spectral, chemical, ionization and con-tamination interferences.

6) Convenience in operations.

The ICP is applicable to the analysis of a large number of elements. The halogens, however, are not easily   de-termined and atmospheric gases such as oxygen and nitrogen present problems simply because the plasma is operated in air. Never-the-less, nitrogen present as ammonium nitrogen has been determined by ICP-OES using an extended torch[57] in which the outermost tube was extended by 40mm above the coil to exclude the entrainment of air into the discharge. The emission was viewed through the quartz wall. There are commercially available plasma systems which are equipped with an inert gas purging unit to remove air from the plasma torch box and the optical system, thus, making the determination of oxygen and nitrogen possible.

The ICP posseses high sensitivity due to the use of inert gas atmosphere to support the plasma, re-latively long residence time of the sample species in

the discharge and high excitation temperatures. The excellent sensitivity is demonstrated by the ppb levels of detection attainable[143,144]. Calibration graphs obtained using the ICP are rectilinear over 5 or 6 orders of magnitude with respect to analyte concentration as the ICP is an optically thin source (there is little self-absorption). After the initial warming up period, the short term and long term power stability is excellent owing to the availability of well designed RF generators.

The ICP is not as it was first thought, completely free of interferences, but by careful choice of incident RF power, viewing height, gas flow rates, the interference effects can be minimized to be considerably less than those observed in flame emission or absorption spectrometry, and also in flameless atomic absorption spectrometry.

5.2   Instrumentation for ICP-OES

The basic essential components in an ICP-OES
system are the high-frequency (HF) generator supplying
power to an induction coil via a matching network, the
plasma torch, a sample introduction system and a spect-
rometer to disperse and detect emitted radiation.   A
schematic diagram of the system used in this study is
shown in Fig.40

5.2.1   The HF Generator and the Matching Network

The HF generator employed was of the crystal
controlled type (Model HFP 2500D, Plasma-Therm Inc.,
New Jersey, USA.) operating at a frequency of 27.12MHz
with a maximum power output of 2.5KW.   The output of
the piezo-electric crystal oscillator was fed to a buffer
stage of the power amplifier to isolate the oscillator
from changes in the generator load.   The output of the
generator was monitored using a direction coupler in
the power line and was regulated by an automatic control
unit (Type APCS-3, Plasma-Therm Inc.) which closed down
the power amplifier if the ratio of reflected to incident
power exceeded a preset value.   An automatic impedance
matching network (Model AMN, Plasma-Therm Inc.)permitted
the matching of the impedance at the load coil to that
of the generator output, ensuing maximum power transfer
from the generator to the load coil.   This was achieved
by a servo-driven capacitor in the matching network
which was controlled by phase and magnitude detectors
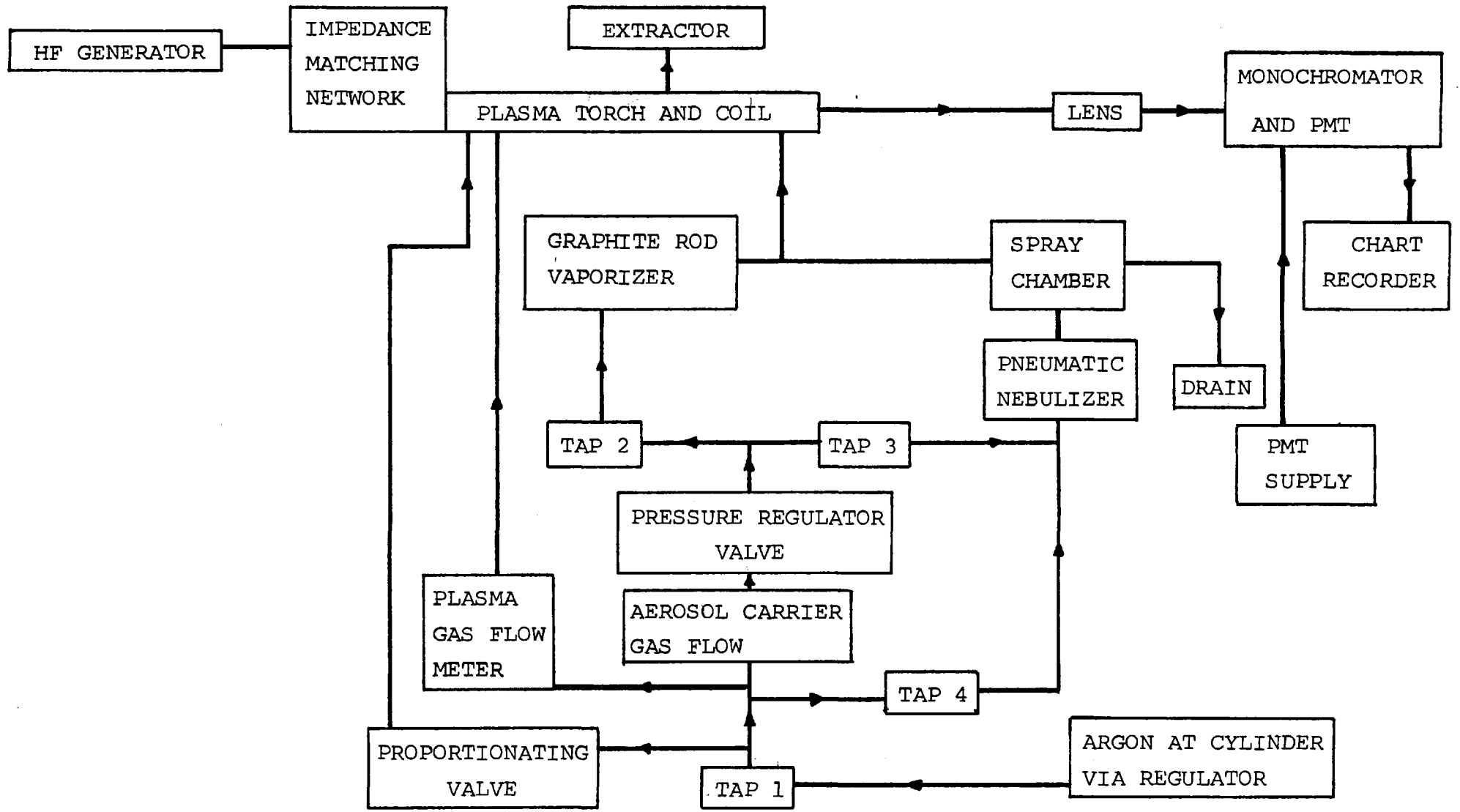
Fig. 40 Schematic diagram of the instrumentation in ICP-OES.

——Induction Coil

——Orifice Diameter 1.50mm

——18.2 mm i.d.

——16.2 mm o.d.

——3.7 mm i.d.

——Brass Base

——Coolant Gas

——Plasma Gas

——————— Aerosol Carrier Gas
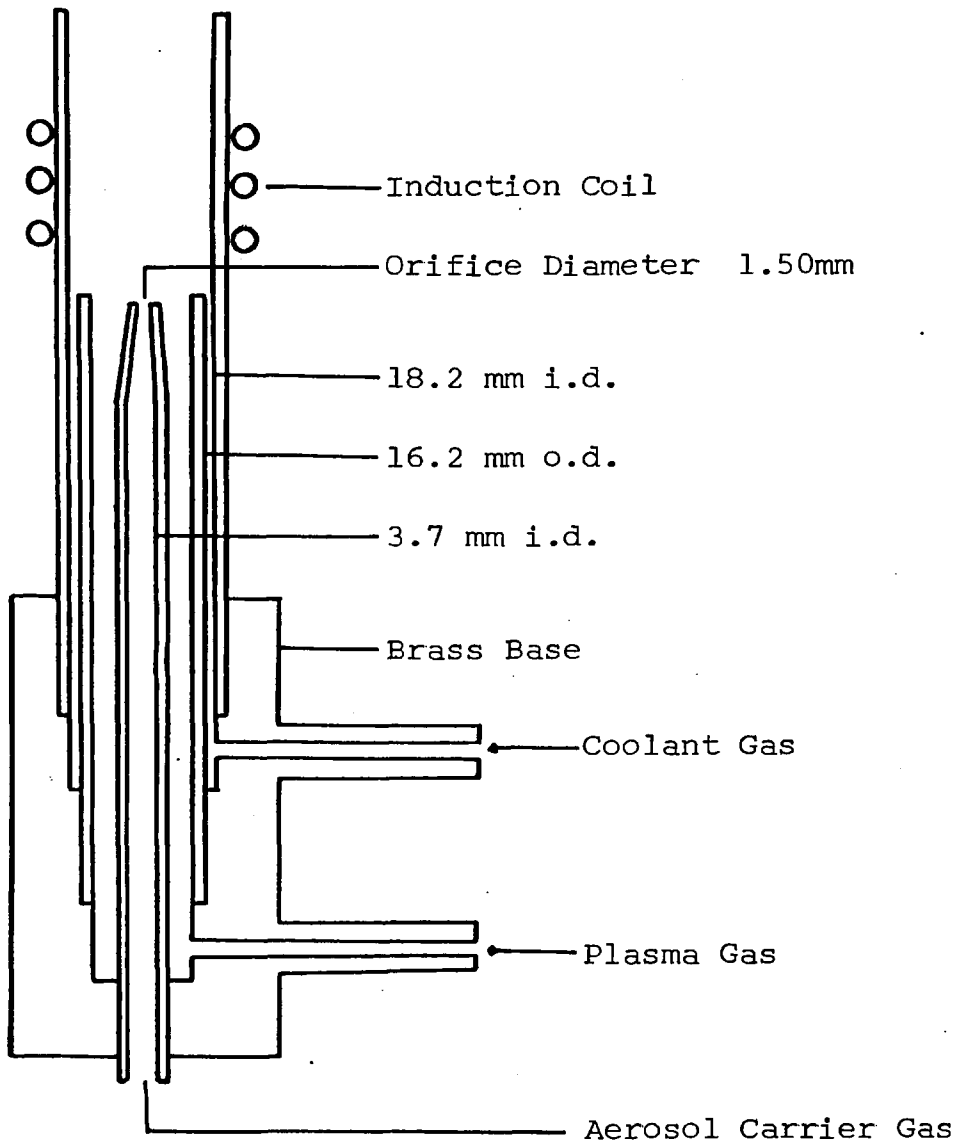
Fig. 41   The Demountable Plasma Torch

Adjustable Aluminium Rod——
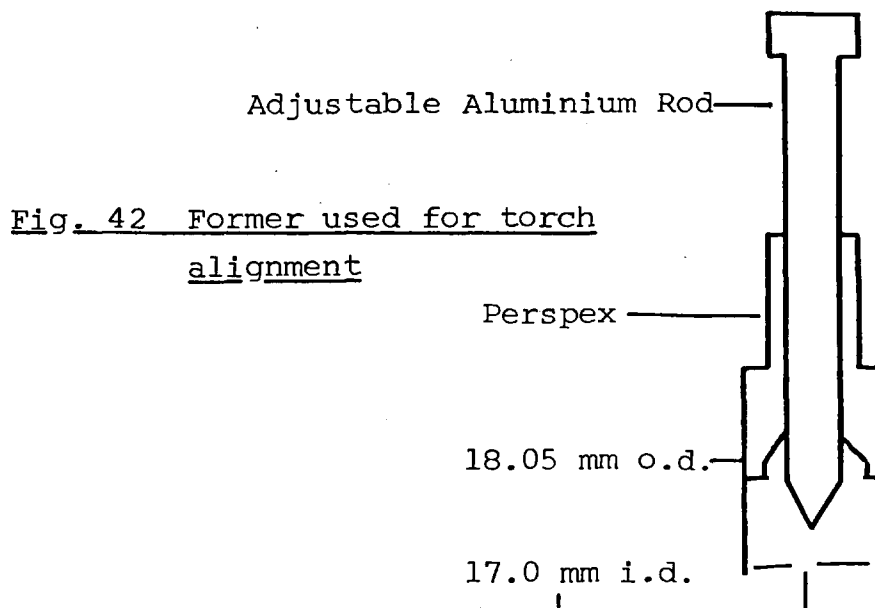
Fig. 42   Former used for torch
          alignment

Perspex ——————

18.05 mm o.d.——

17.0 mm i.d.

in the HF transmission line. After the ignition of the

plasma, the matching network returned itself automatically,

therefore, requiring no manual adjustment.

5.2.2 The Plasma Torch

A demountable tube of a design previously described

(*145*) was used. The torch consisted of 3 concentric

fused silica tubes firmly set into a brass base with

epoxy resin (Araldite rapid). The configurations of

which are illustrated in Fig.41 (*146*). A precision made

teflon former (*146*) (Fig.42) was used to ensure concen-

tricity of the silica tubes during the assembly of the

torch.

The outer silica tube was extended 13mm above

the load coil to prevent arcing between the centre of

the torch and the induction coil when igniting the plasma.

The brass-base was equipped with two tangential gas inlets

to allow the entry of the plasma gas and auxilliary

gas. The plasma gas had a vortex flow pattern up the

torch,which had the effect of stablizing the plasma, the

flow rate of which was variable. The auxilliary gas

was used to sustain the plasma and the gas flow was preset

at 1 lmin^{-1} via a proportioning valve. The innermost

injector tube served to introduce sample into the plasma.

The position of the injector tip from the load coil and

its inner diameter play a critical role in allowing the

efficient penetration of the aerosol into the plasma.

The plasma torch was positioned in a $2\frac{1}{2}$-turn

water cooled copper load coil which was mounted in an

aluminum housing, the interior of which was blackened

with a matt-black paint to avoid reflection of the plasma

radiation. The housing had a number of openings for

viewing the plasma, sample introduction, nebulizer

drain and removal of exhaust gases via an extractor.

The plasma torch and matching network assembly was mounted

on a screw-jack to permit the observation of different

zones of the plasma on a vertical axis.

5.2.3 The Pneumatic Nebulizer

The pneumatic nebulizer employed was of the

concentric all-glass type (Model GN-1, Plasma-Therm).

The spray chamber (Model SC-2, Plasma-Therm) allowed

small aerosol particles to enter the plasma. The optimum

operating pressure was 25p.s.i. which corresponds to a

solution uptake rate of 1ml min^{-1} at an injector flow

rate of 1 $1 min^{-1}$. In this study, the nebulizer served

only as a rapid means of locating analytical lines.

5.2.4 The Graphite Rod Vaporization Device

The graphite rod vaporization device (GRV)

(Fig.43) employed in this study is a commercially available

product and has been previously described[58]. A rod

(60mm in length and 3mm in diameter) made from spect-

rographically pure graphite was positioned between the

terminals of the power supply. The power supply was con-

nected to a programmer (Shandon Southern) which allowed

variation of voltage applied to the rod for the desolvation,

pyrolysis and vaporization steps. The graphite rod

Ball joint to plasma
torch sample inlet

To scale

Sample delivery port

Cylinder glass manifold

Water cooling
link

Circular
brass base

Tufnol insulating
blocks

Argon sample transport
gas inlet

Electrode terminals
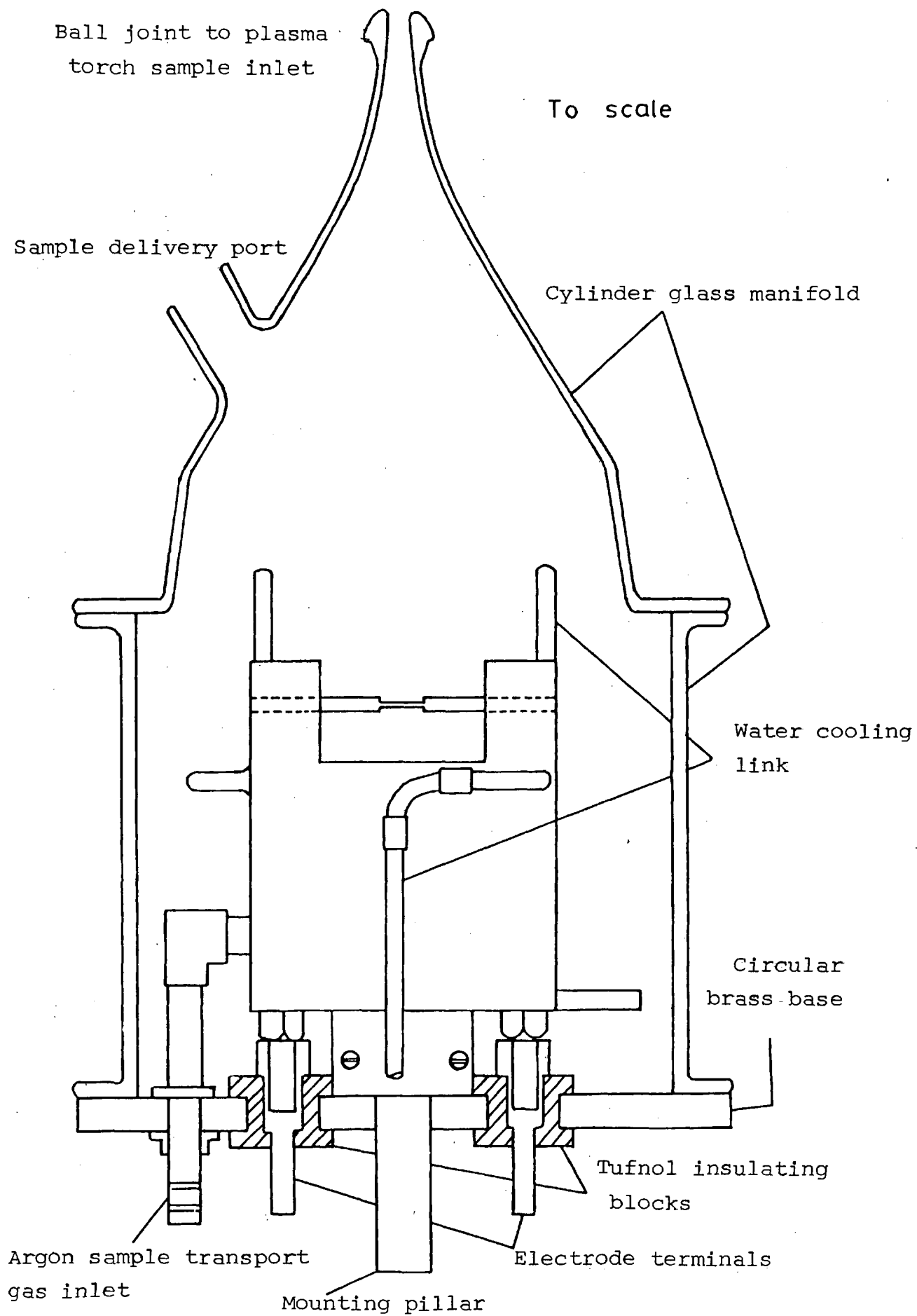
Mounting pillar

Fig. 43 Graphite rod vaporization device (146).

supporting pillars were mounted onto the brass base plate by means of Tufnol insulating blocks positioned as shown in the diagram. Inlets were drilled through the base to allow the entry of argon transport gas and the cooling water to the terminals. To facilitate sample introduction into the ICP, a glass enclosure was placed over the base plate. The enclosure consisted of two separate pieces, a cylindrical glass tube and a glass dome. The two pieces were held together by means of spring clips. A small amount of vacuum grease was smeared over the contacts to ensure leak-proof union. The glass dome was equipped with two ports, the inlet port on the side allowed the introduction of liquid samples by means of a micropipette and was closed with a plastic stopper which could be removed for sample introduction. On removal of the stopper, a back pressure was created causing the argon to flow out of the port. Therefore, air could not enter the glass chamber. The outlet port (for the exit of the carrier gas and analyte) positioned at the apex of the dome was connected to the plasma in-jector tube via a ground glass ball joint and a 0.5 metre length of P.V.C. tubing. On vaporization, the bulk of the dry aerosol entered the plasma as a discrete pulse. Thus the analytical signal obtained was sharp and short in duration allowing peak height measurement of emission intensity[58] to be taken.

5.2.5   The Fabrication of the Graphite Rod

High purity graphite rods were obtained (Type
RW 001 MCP Electronics Ltd., Middlesex.) and rod profiles
were made based on several designs previously reported
by colleagues at Imperial College[146,147]. Some of
the earlier designs made by Gunn[147] are shown in Fig. 44.
The type A rod had a deep well in the centre and could
only hold a maximum of 5 μl of liquid sample. The type
B and C rods were similar but could hold samples between
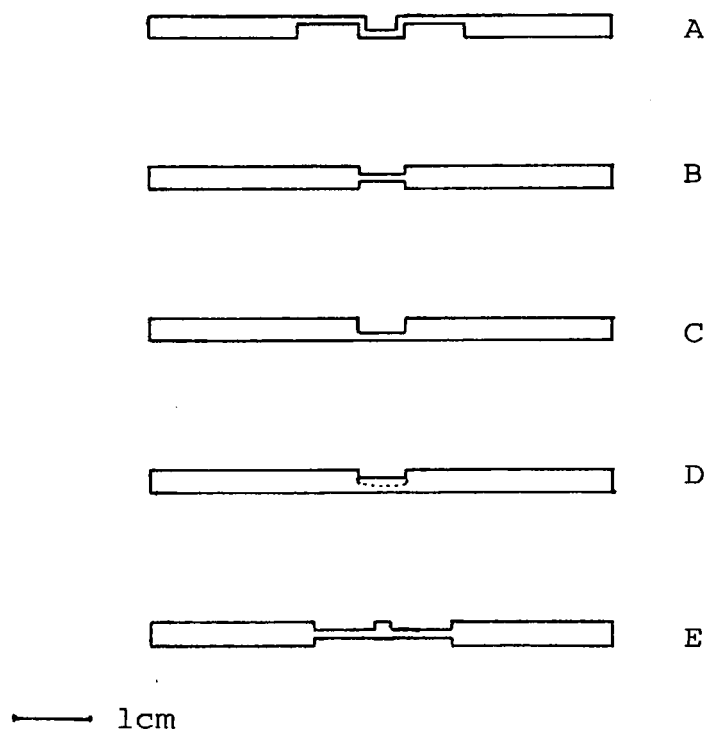
Fig. 44 Graphite rod vaporizers

20-30µl. Type D had a channel cut into the surface of the vaporization site to prevent sample loss during the analytical heating programme. The temperatures attainable at different rod voltages for the four versions were of similar magnitude$^{(147)}$. Rods B and C were preferred on the basis of sample capacity and simplicity in fabrication. Millard$^{(146)}$ fabricated a graphite rod with two separate depressions as shown in Fig.44 Type E   permitted simultaneous but separate vaporization of analyte and concomitant ions and was used to establish the origin of some interelement effects observed in the determination of toxic elements in biological fluids. For the work presented in this thesis, the graphite rods of the type A were used for liquid samples and type F were used *(page 136)* for solid samples.

5.2.6 Signal Detection and Registration

The arrangement for signal detection and registration was exactly as described by Millard$^{(146)}$. A 1:1 upright image of the plasma was formed on the entrance slit of a Czerny-Turner scanning monochromator (Monospek 1000 D400, Rank Hilger, Kent.) using two 7.5cm focal length silica lenses. The lens nearer to the ICP was masked down to a diameter of 1.88cm so that the collimating mirror of the monochromator was exactly filled by the incident radiation. The distance from the ICP to the entrance slit was 60cm. The spectrometer was fitted with a plane diffraction grating (1200 lines per mm) blazed at 300nm providing a reciprocal linear dispersion

of 0.8nm mm^{-1} and a 13 stage end-window PMT to cover

the wavelength range 180-620nm (Model 9789 QB EMI

Industrial Electronics, Middlesex.) The high voltage

input to the PMT was provided by a stablized power supply

(Model 475R, Brandenburg Ltd.,Surrey). The PMT output

was connected across a 10 K resistor to a fast response

(500ms) potentiometric chart recorder (Series 3000,

Oxford Instruments Ltd., Oxford). The entrance and

exit slits were set at 35μm for use with the GRV in order

to allow for the slight drift of wavelength due to tem-

perature variations in the laboratory[146].

5.2.7 Procedure for Initiation and Operation of the System

1) Turn on the extraction system

2) Turn on the water supply to the load coil and to
    GRV

3) Turn on argon at cylinder and open gas control
    valve (3) at plasma torch box (Fig. 45)

4) Turn on generator, when ready for use, the "RF off"
    button will light up, turn on associated electrical
    equipment

5) To purge air from the nebulizer and spray chamber,
    turn on the nebulizer gas control valve (1) and
    then nebulizer rotameter (N), To purge graphite
    rod chamber, turn off (N), then(1) and turn on GRV
    control valve (2) and then (N)

6) Select mannual at the tuning box mode switch (6)
    drive the values displayed to 00087 using the
    control buttons (7), return switch (6) to automatic

To initiate the plasma

7) Turn on coolant gas supply and adjust to 13-15L min^{-1}

8) Turn off nebulizer at rotameter (N) or GRV at (N)

9) Set the RF forward power at the generator to be approximately 500W.

10) Press the tesla (S) and "RF on" button (8) simultaneously .

11) After the ignition, adjust the forward power to the desired power

12) Introduce the injector flow into the plasma

1) Nebulizer

2) GRV   ON/OFF valves

3) Gas

4) Reflected power meter

5) Forward power meter

6) Auto/Manuel switch

C) Coolant gas

N) Injector gas   rotameters

W) Water

S) Tesla

8) RF ON
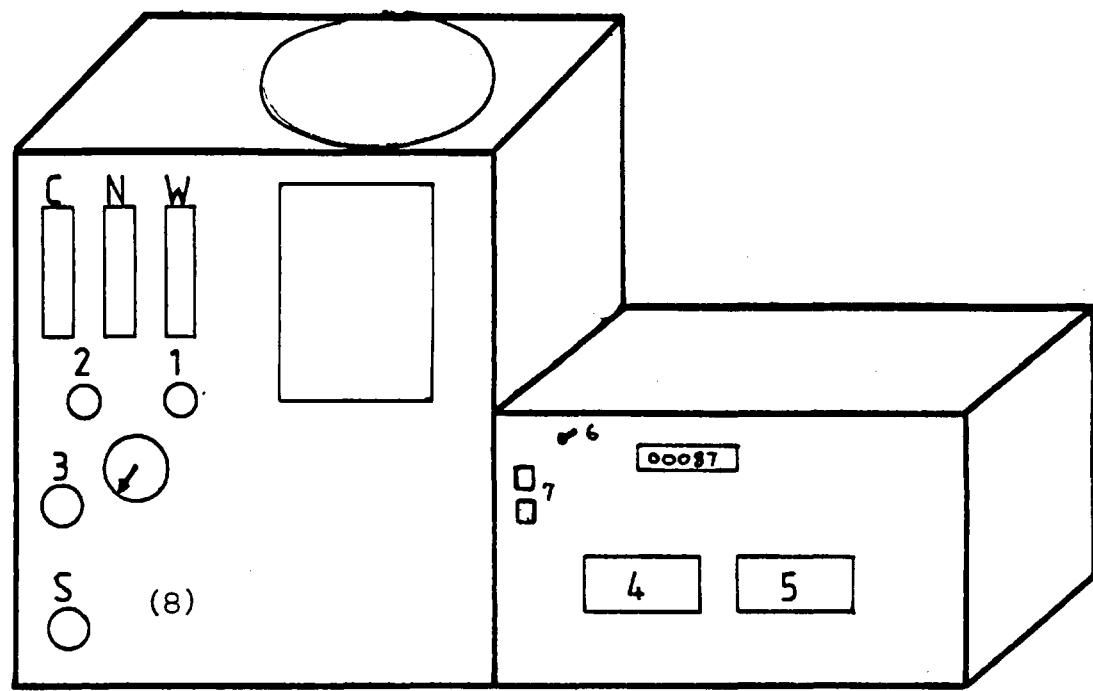
Fig. 45 Plasma torch box and the Tuning unit.

5.3 The Determination of Phosphorus and Sulphur by ICP-OES

The determination of phosphorus in aqueous solution by nebulization into an ICP source has been reported by several groups of researchers[140,141,148-150]. The technique has been applied to the determination of phosphorus levels in blood by Greenfield and Smith[67] and Kniseley et al[151], Kirkbright et al[152] have reported its use for the determination of phosphorus in ammonium acetate extracts of soils. Gunn et al[153] have reported the determination of phosphorus in milk powders.

The sulphur atomic emission lines observed in the ICP have been studied by Kirkbright et al[152], Alder and Mermet[154] and Bombelka[145]. The most intense analytical line observed is the resonance line at 180.73nm and this line has been used for the determination of sulphur in brine[155,156]. Alder and Mermet[154] studied the atomic spectrum of sulphur (S(I)) observed in an argon ICP and a number of lines which had not been previously assigned were reported. Bombelka[145] also made an extensive study of the S(I) spectrum over the wavelength range of 190-880nm. A number of new lines were observed and were assigned by Bombelka.

Some of the useful analytical lines for sulphur and phosphorus observed in the ICP are the lines at 180.73nm, 469.412nm for sulphur and those at 213.6nm, 214.91nm, 253.5 for phosphorus.

5.3.1 Optimization of Plasma Parameters for the Determination of Phosphorus and Sulphur

The experimental variables which affect the magnitude of the emission signal of an element in the ICP-GRV system are:

1) The viewing height

2) Argon injector flow rate

3) Incident HF power

4) Coolant gas flow rate

5) Plasma gas flow rate

6) The GRV heating cycle

7) The entrance and exit slit at the spectrometer

8) The length of the tubing connecting the GRV and the plasma torch

The effects of these parameters have been investigated in detail by colleagues at Imperial College based on the measurements of signal to background or noise ratios. It was found that the incident HF power, viewing height and sample transfer rate are critical factors affecting the intensity of the emitted radiation from the plasma. It was reported that[157] low viewing heights are suitable for viewing elements having high atomization energies and ionic spectra of easily ionizable elements; high viewing heights are suitable for elements having low atomization potentials. Higher powers have an effect of increasing the emission signal. Unfortunately, the noise increases more rapidly than the signal. Hence, S/N ratios degrade with increasing power.

All of the experimental parameters were optimized in the author's laboratory by previous researchers and a set of compromise conditions was adopted to give convenience in operation with the best overall sensitivity for possible application to simultaneous multi-element analysis (SMEA). The compromise conditions are summarised in Table 5.1

Table 5.1   Compromise Conditions Employed in this Study

Coolant gas flow rate	13 L min^{-1}
Plasma gas flow rate	1 L min^{-1}
Injector flow rate	1 L min^{-1}
Viewing height	27mm above the load coil
Incident HF power	1 KW
Spectrometer entrance and exit slit widths	35 μm
Vaporization voltage *	6 V
Connecting tubing	0.5 metre

* higher for refractory elements

5.3.2 Procedure for Optimization in This Study

The effects of the three critical factors mentioned in section 5.3.1 together with the effect of the rod vaporizer temperature were investigated. Aqueous sulphur solution ($(NH_4)_2 SO_4$) of 100ppm concentration and aqueous phosphorus solution ($(NH_4)_2HPO_4$) of 0.1ppm concentration were employed in the optimization study. Thus 10μL sample containing the element of interest was dispensed

onto the carbon rod and vaporized into the plasma under preselected conditions keeping one parameter under test variable at one time. The signal to noise ratios were calculated for each of the four variables and the best conditions found experimentally for sulphur and phosphorus are presented in Table 5.2

Table 5.2

Variable	Phosphorus	Sulphur
Incident power	0.7 kW	1.1 kW
Viewing height	15mm	20mm
Injector flow rate	1 L min^{-1}	1 L min^{-1}
Vaporization voltage	5 V.	3 V.*

*this value is optimum for ammonium sulphate, but is higher (6V.) for metal sulphates.

On close inspection, the S/N ratios obtained for the best conditions are not significantly superior than those obtained for compromise conditions. The detection limits (calculated from 2 times the standard deviation on the noise) obtained for compromise conditions are comparable to those obtained for the best conditions (Table 5.3). Hence, compromise conditions were adopted for the work carried out using the ICP.

Table 5.3 Detection Limits

	Best conditions	Compromised condition
Phosphorus (213.6nm)	0.008ppm	0.01ppm
Sulphur (469.412nm)	25ppm	25ppm

5.3.3   The Choice of Emission Lines used for Sulphur

The sensitive sulphur lines lie in the vacuum ultraviolet region (180.734nm, 182.036nm, 182.626nm). The most intense being 182.036nm with detection limit of the order of 1.7ppm [152]. The line at 469.412nm is found to be the best in terms of signal to background ratios [145] for an ICP operating in air. This line belongs to a multiplet and a scan of which is shown in Fig. 46

PMT   1200 V.

RF forward power 1 kW

⊢———⊣ 1 Å
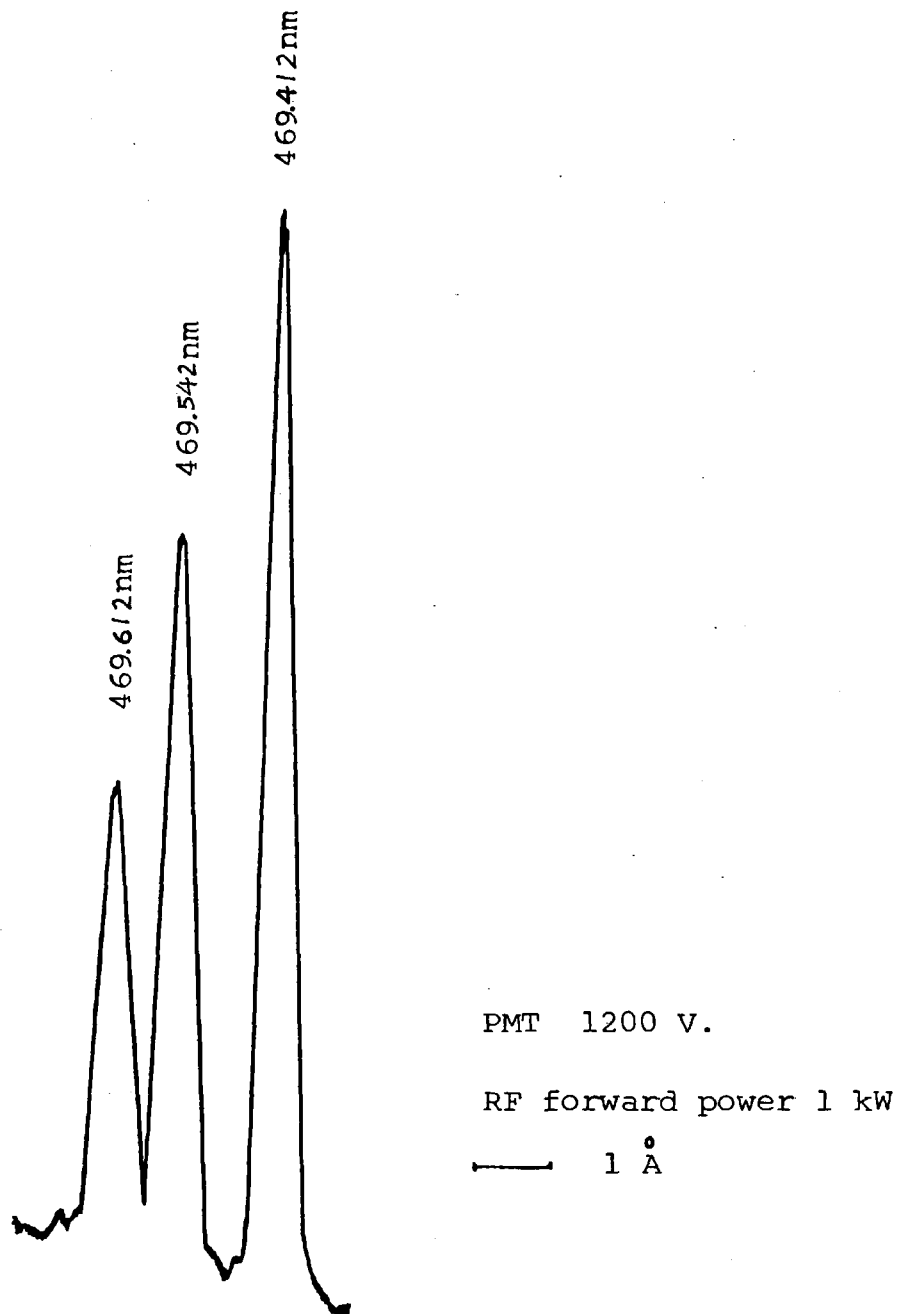
Fig. 46   The sulphur triplet at 469nm.

Bombelka[145] nebulized an aqueous 10% V/V sulphuric acid solution into an ICP operating at 1.2KW forward power and obtained a detection limit of 350ppm using the 469.42nm

line and a viewing height of 20mm. In the present study, I have attempted to improve the detection limit by improving the manner in which the sample was tranported to the plasma.

5.3.4 Calibration curves for Sulphur and Phosphorus

Following the procedure described in section 5.3.2 typical calibration graphs *for sulphur* are shown in Fig.47. Graph A was drawn taking peak height measurements and is rectilinear from 1μg (the detection limit) to 20μg. At higher concentrations, the peak broadened with respect to time. When these   peaks were integrated to give the calibration curve B, the linear range was extended up to 100μg.

Various phosphorus containing compounds were introduced into the plasma under the comprise conditions listed in Table5.I. The emission intensities for equal concentrations are similar irrespective of the nature of the compound introduced (Fig.48). The curves are rectilinear from 0.1ppm to 100ppm (the highest concentration tested.)

5. 4 Analysis of Phosphor Bronze

To assess the usefulness of the ICP-GRV system, it was applied to the analysis of phosphorus in phosphor
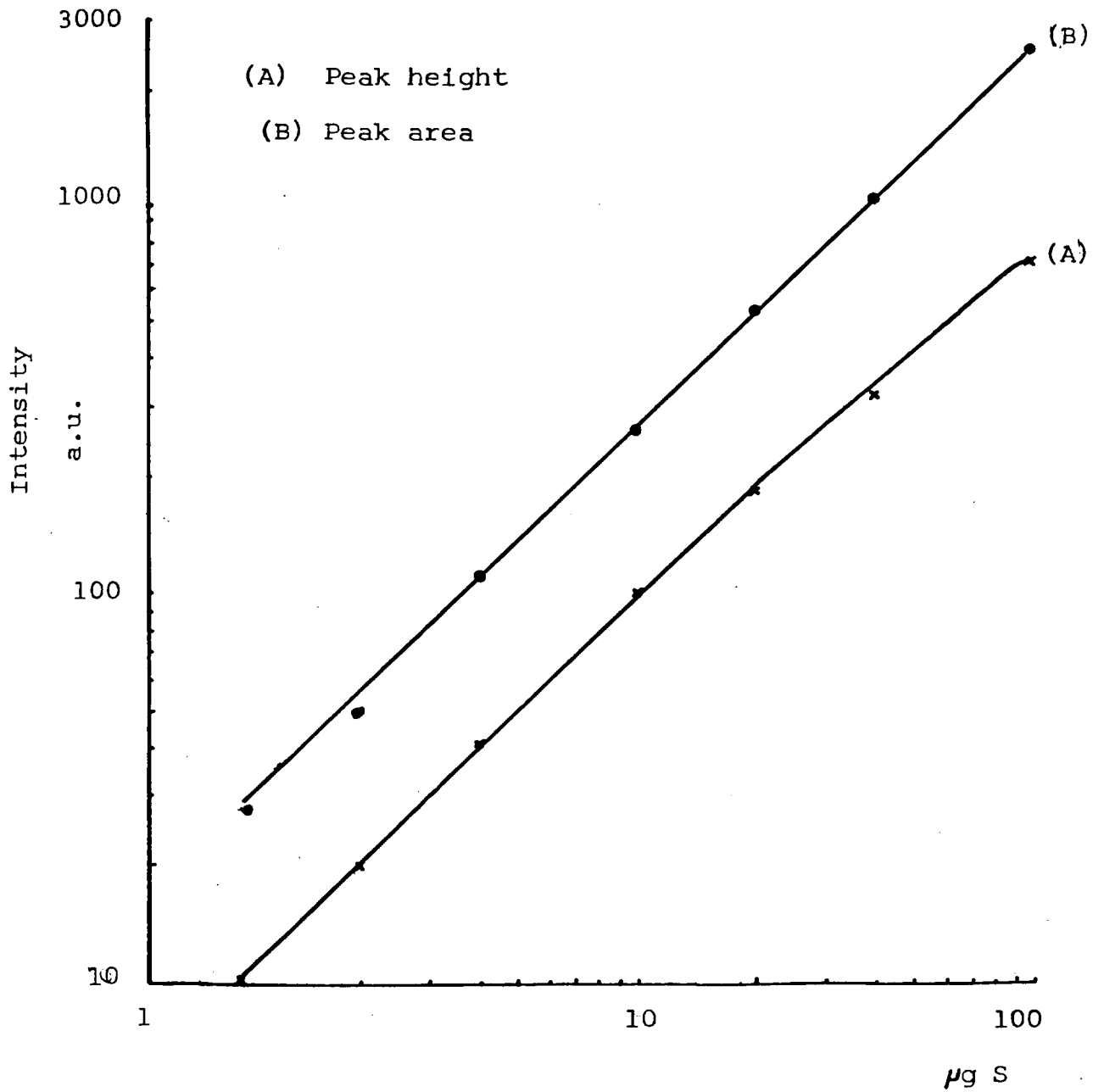
Fig.47 Calibration graphs for sulphur on log-log scale
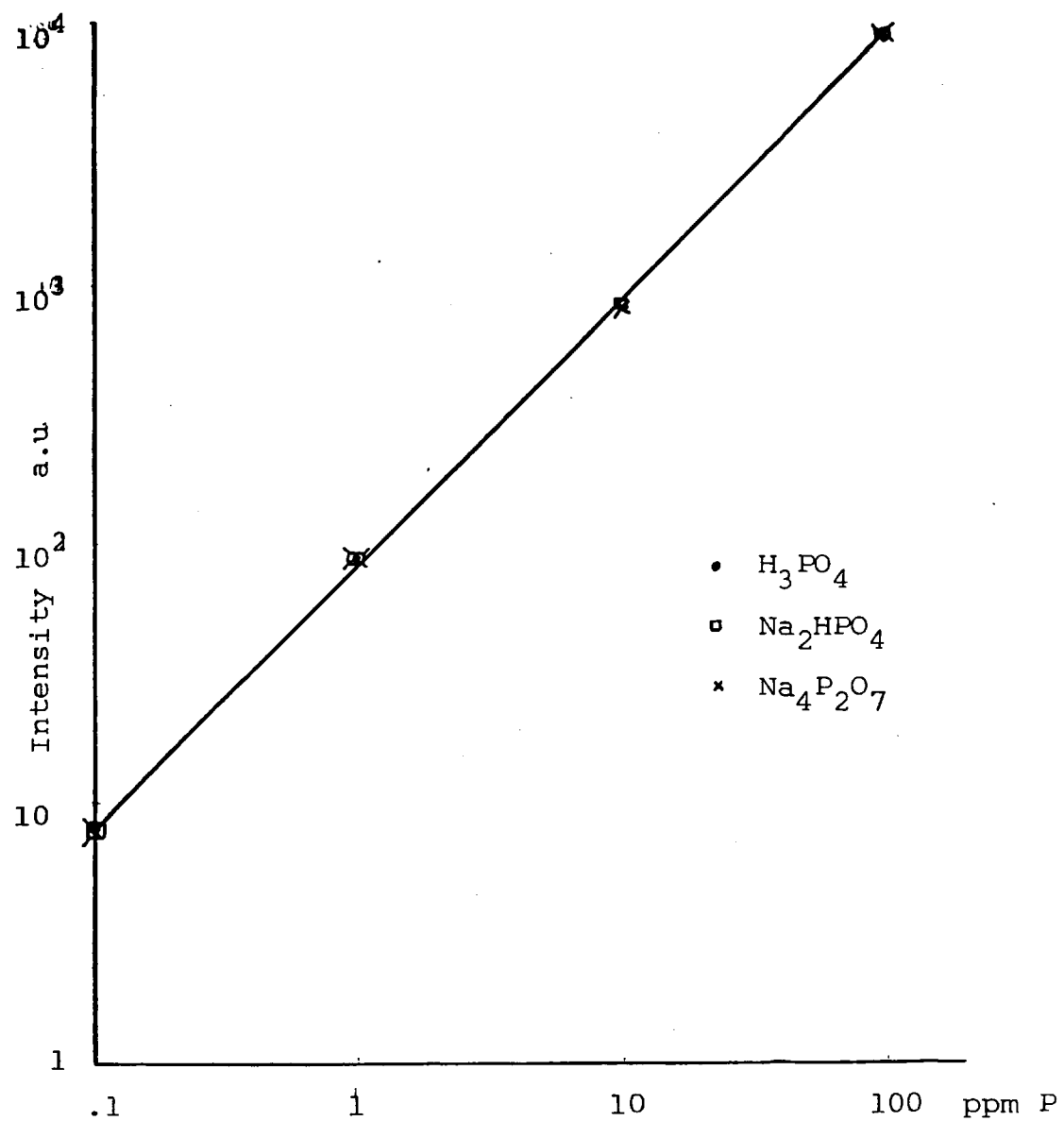
Fig. 46 Calibration graphs for different phosphorus compounds

bronze.

The bronze samples (kindly supplied by J.J. Makin (Metals) Ltd, Lancs, U.K.) were dissolved using the procedure as described in section 4.5 . The resultant solutions after dilution contained 0.1% of bronze. 10μL aliquots of sample were desolvated and vaporized electrothermally into the ICP source where the phosphorus atomic emission line at 253.5nm was monitored under the experimental conditions as shown on Table 5.1. A standard addition method was employed to determine the concentration of phosphorus in the bronze solutions

and to establish whether there were any matrix effects.

5. 4.1 Results and Discussion

The phosphorus emission line at 213.6nm was not used because of interferences due to copper. Interferences observed in the ICP-GRV system can originate either from the source or from the rod, sometimes it can be a combination of both. It has been established that there are few physical or chemical interferences in the plasma. The best well known and well investigated case is the interference of calcium on phosphorus (or vice versa). Research workers attribute this type of interference to the formation of Ca-P species in the plasma and the extent of this interference is independent of wavelength and is dependent on the viewing zone, ie, plasma temperature. such interference can therefore be minimized by careful choice of plasma conditions. However, another

type of interference arises because the spectral line
of the concomitant ion overlaps with that of the analyte.
In most cases, elements usually exhibit rich spectra in
the ICP due to the high energy of the source. Spectral
interference can usually be avoided by selecting another line.

Interferences originating from the graphite
rod include pre-vaporization losses, compound formation
on the rod and carbide formation. These effects can be
reduced by critical control of the heating programme
and addition of stablizers or reagents to inhibit or to
assist vaporization of the analyte $(86 , 172)$.

It was found that the interference due to copper
on phosphorus originated from the plasma source and
it is a spectral interference. Spectra obtained by
nebulising pure aqueous phosphorus solution and solution
of phosphorus containing copper over the spectral range
from 213.6nm to 253.6nm were compared. The relevant
sections of the spectra are shown in Fig. 49

Figure 49 shows that copper lines at 213.598nm.
and 214.9nm. interfere with the phosphorus atomic emission
lines at 213.618nm. and 214.914nm. respectively. There
is, however, no spectral interference observed at the
phosphorus line of 253.5nm. The sensitivity of this
line is relatively high and affords a detection limit
of 0.5ppm. Hence, this line was selected for the analysis
of bronze in the ICP.

(A)

(B)

(C)

(A) P 213.618nm
     Cu 213.598nm

(B) P 214.914nm
     Cu 214.9nm

(C) P 253.5nm

phosphorus solution

copper solution
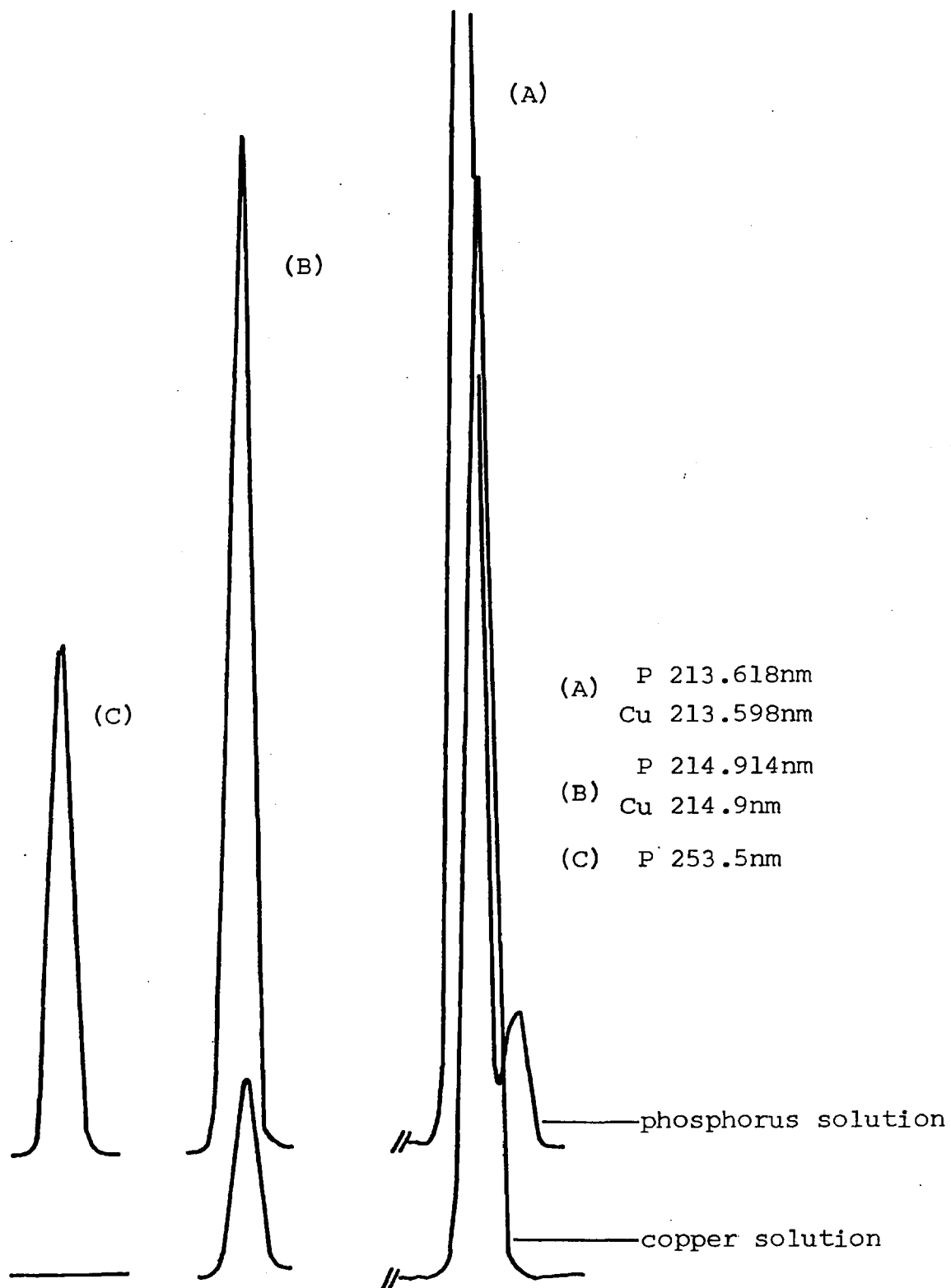
Fig. 49   A scan of the phosphorus and copper emission
          lines over the region 213.4nm to 253.7nm.

The results for the determination of the bronze samples
are presented in Table 5.4.

Table 5.4   The Results for the Bronze Analysis

Sample	ICP-OES % P	MVPAA % P
A	0.25	0.26
B	0.30	0.30
C	0.35	0.35

As can be seen from the table , the results obtained by
ICP-OES are in good agreement with those obtained by MVPAA.
Thus, by careful control of the experimental conditions,
the capability of the ICP can be exploited fully.

CHAPTER SIX

THE ANALYSIS OF TRACE ELEMENTS AND DOPANTS IN

CADMIUM MERCURY TELLURIDE BY SOLID SAMPLING

6.1 Introduction

Semiconductors can be considered as systems of electrons and nuclei whose properties are defined by a particular energy distribution of the electrons. According to the band structure theory, electronic energy levels are grouped together in bands in which the energy separation between levels is infinitesimal. The band-gap energy is defined as the difference in energy between the valence band and the conduction band. Based on the band structure theory, the distinction between a semiconductor and a metal is that semiconductors have non-zero band-gap energies, while for metals, the energy gap is zero. At temperatures above the absolute zero, some electrons will be thermally excited from the valence band to the conduction band. The absence of an electron in an energy level is defined as a hole. As a result of thermal excitation, therefore, holes are produced in the valence band.

The degree of impurities can effect the properties of a semiconductor. If foreign atoms or molecules (impurities) are added to a pure system, they can introduce energy levels which modify the properties of the material. The levels introduced by the impurity generally are different in energy from the levels of the pure system. Thus an addition of an impurity (doping) usually introduces levels in the band-gap. If some of the new levels are occupied and lie just below the conduction band, thereby increasing the number of electrons , the impurity is called a donor. If some of the new levels lie just above

the valence band and are unoccupied, valence band electrons can be thermally excited to these levels. This excitation increases the number of holes and the impurity is called an acceptor.

Because conduction is a function of the number of holes and electrons, it is possible that by controlling the addition of impurities, the conductivity of a semiconductor can be increased. Thus, a pure matrix is required to begin with in order to dope to a prescribed level.

Cadmium Mercury Telluride ($Cd_{0.3}Hg_{0.7}Te$-CMT) is made by reacting cadmium telluride with mercury telluride. It is used as an infra-red radiation detector because of its relatively small band-gap energies. The purity of this material is important as the amount of impurities can alter the energies of the band-gap. The CMT semiconductor employed commercially has impurity levels of the order of 0.05 ppma. Such a low level necessitates the direct introduction of the sample in the solid form as dissolution will dilute the impurities to below the limit of detection of most spectroscopic techniques.

There are a number of techniques available for determining impurities both qualitatively and quantitatively. These include emission spectrography, mass spectrography, neutron activation analysis, calorimetry, X-ray spectrography, chromatography, polarography and fluorimetry. Of these methods, the first three are more suitable because they offer relative freedom from contamination and also yield direct multielement analytical results.

6.2 Solid Sampling

Despite the amount of research and publications devoted to ICP-OES with nebulizers used as sample introduction devices, there has been relatively little progress made in the introduction of solid sample into an ICP source. The main problem lies in producing an aerosol of uniform sized particles from the solid sample. A commercial portable aerosol generator was developed by Dahlquist et al[158] in which an arc was maintained between the conducting solid and an annular electrode. The particles generated were transported by argon into the plasma source via ca 20 metres long tubing. Several minor and trace elements were determined in steel simultaneously. The emission intensities were integrated and ratioed to an iron internal standard. Scott[159] reported the use of a high voltage spark to elutriate rock samples into an ICP source. It was possible to determine copper in rock samples. The precision obtained, however, was poor.

Other methods based on sweeping powders into the ICP[160 - 162] have not been very successful because good relative standard deviations were only achieved if the samples and standards were matched closely to obtain quantitative measurements and to reduce matrix effects.

The application of a laser for vaporising solid samples into the ICP appears to be promising. A carbon dioxide laser[163] and a ruby laser[164] have been employed. The radiation of a laser is intense and is able to evaporate any kind of material into the core of an

ICP. Solids such as metals and rocks can be vaporized directly; powders can be placed on tapes or pressed into pellets[114] and subsequently vaporised. Disadvantages of usingalaser include problems arising from inhomogeneity of the bulk material(1 to 30μm spot is vaporized) and the relatively poor shot-to-shot reproducibility of existing lasers.

The work presented in this part of the thesis describes the direct analysis of solid CMT by ICP-OES employing a resistively heated graphite rod as a means of sample introduction device into the ICP. Fortunately, CMT is fairly volatile and can be completely vaporised from the graphite rod. The samples (kindly supplied by Admiralty Marine Technology Establishment) were doped to enable analytical methods to be developed for the direct determination of trace elements in solid CMT.

6.3 Experimental

The instrumental system has been described in section 5.2. For the dual element studies, a Techtron AA4 monochromator(Techtron Pty. Ltd. Melbourne,Australia) was positioned in line with the Monospek 1000 on the other side of the plasma torch box. This monochromator was fitted with a side window type photomultiplier tube (RCA 1P28) whose output was fed into a Servoscribe potentiometric recorder.

For initial studies, solutions of CMT were introduced onto the rod using the sample transfer device shown in Figure 50

6.3.1 The Solid Sample Transfer Device

The device consisted of a glass pipette tip as shown in Fig. 50 . A sintered glass disc on top of a piece of filter paper was placed over one end of the tube. A brass coupling was used to connect the glass piece to a water pump. To collect the solid particles from the container, the water pump was turned on to create a suction which drew the particles into the tube. Then the pipette was inserted through the inlet port onto the cavity of the carbon rod, the particles were dispensed into the cavity after turning the water pump off.
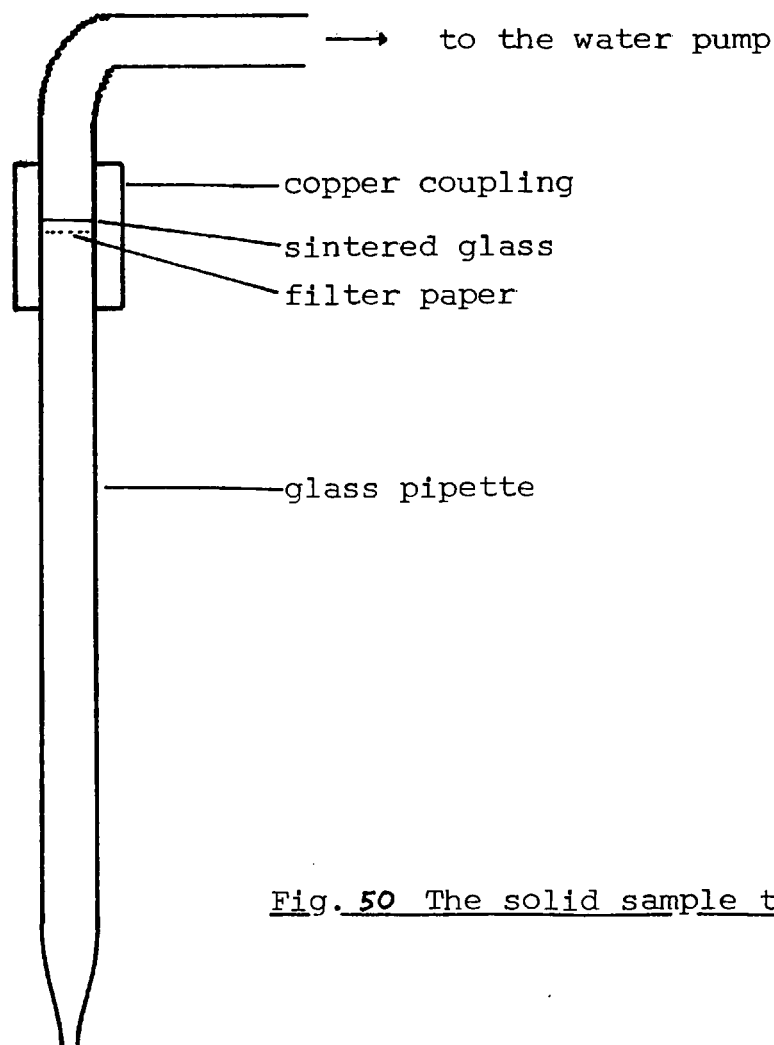
Fig. 50 The solid sample transfer device

The accuracy of the solid transfer process was determined by performing ten replicate weighings of the same particles (470μg). The particles were picked up and deposited onto the weighing pan of a microbalance. The particles were weighed and then transferred onto a a surface in the same way as if the GRV was used. This process was repeated ten times using the same sample. The relative standard deviation of the weighings was calculated to be 0.02. This value indicates that the solid is being transferred totally and efficiently.

6.3.2 The Graphite Rod

In order to locate the particles conveniently and reproducibly, a graphite rod of the shape shown in Fig. 5l was used. It was fashioned by removing a layer
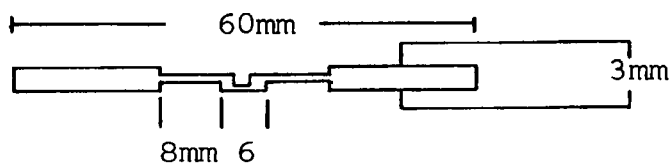
Fig. 5l The graphite rod vaporizer

of graphite of 1mm in depth, a hole was cut in the centre, the graphite on either side of the cavity was removed to give the shape as shown. This structure facilitated a rapid rise of temperature on passing a high current through the rod.

6.3.3 The Optimization of Experimental Conditions

It is common to carry out determinations of solids on a simultaneous multielemental basis (SMEA) as SMEA is

economic in time and in money. Therefore, all the ex-
perimental parameters employed in this study were optimised
in such a way to provided compromise conditions to facilitate
SMEA without great loss in sensitivity for any one element.
These conditions are listed in Table 6.1

Table 6.1   Plasma-Graphite rod vaporizer operating conditions

Net forward RF power	1 kW
Spectrometer slits	35 μm entrance & exit slits
Viewing height	27mm above the load coil
Argon coolant gas flow rate	13 L min^{-1}
Argon plasma gas flow rate	1 L min^{-1}
Nebulizer flow rate	1 L min^{-1}
Nebulizer uptake rate	1 ml min^{-1}
GRV flow rate	1 L min^{-1}
GRV voltage	6 V

For the solution work, a GRV voltage of 6 V (T=2250°C)
was sufficient to vaporize most elements. For elements
such as aluminium and copper, a higher voltage of 7 V
(T = 2500°C) was required to vaporize all of the analyte comp-
letely. For the solids, the vaporization and pyrolysing
temperatures were made variable as some elements were
covolatilized with the matrix while others remained on
the rod after the removal of the matrix and were sub-
sequently vaporized at a much higher temperature.

Table 6.2 shows the GRV heating programme for some elements
present as solid.

Table 6.2 GRV heating programmes

Element	Pyrolyzing temp. C	time sec.	Vaporizing temp. C	time sec.
Mn	—	—	1700	2
Cu	600	40	2500	2
Al	600	40	2500	2
Ag	600	40	2250	2

6.3.4 Procedure for Analysis

1) Solution analysis:

Although cadmium mercury telluride had been analysed for its trace impurities by several independent laboratories using techniques such as secondary ion mass spectrometry, atomic absorption spectrometry using a furnace atomizer and electrochromatography, the results reported differed by as much as 40%[165]. In this study, if the impurity content was sufficiently high, pneumatic nebulization was employed to determine trace concentrations by a standard addition method and the results were compared with those obtained by GRV.

A slice of CMT was cleaned by etching it with warm 2% bromine in methanol. The solid was rinsed thoroughly with analar grade alcohol, then dried in air. It was then ground to a powder with an agate mortar and pestle. 0.1g of the powder was weighed accurately and dissolved in 10ml of aqua regia (prepared by mixing analar grade reagents in the proportions; $1HNO_3:3HCl:4H_2O$). The solution was diluted to make a 0.1% CMT solution. A $10\mu L$ aliquot

of this solution was pipetted onto the carbon rod and was desolvated, pyrolysed (if possible) and vaporized into the plasma. The emission lines used for the elements in this study are shown in Table 6.3. These lines were chosen as they provided best signal to background ratios[166].

Table 6.3

Element	line nm.
Mn	257.6
Al	396.1
Cu	324.7
Ag	328.1

2) Solid analysis

The solid was ground into small particles. ·
Particles of   sizes between $2/2 - 250\mu m$ were selected as larger particles tended to fall out of the pipette and finer ones tended to be carried by the air stream up to the top   of the sampling device or stick to the inner surface of the pipette. The particles were weighed accurately using a microbalance (5 decimal places) and transferred onto the shallow cavity graphite rod and vaporized into the ICP. Emission signals were integrated over the duration of the peak.

The feasibility of using an internal standard was investigated. Both cadmium (228.8nm) and tellurium (208.1nm) were examined as possible internal standards. The Monospek monochromator was used to monitor the atomic emission for the trace elements and the Techtron monochromator was

used to monitor the emission from the internal standard.

6.4   Results and Discussion

1)   Analysis of solutions:

Linear standard graphs were obtained for manganese, silver, aluminium and copper(Figs.52-55).   Table 6.4 presents the results obtained both by nebulization and GRV.

Table 6.4

CMT sample	GRV ppma				Nebulization ppma			
	Mn	Al	Cu	Ag	Mn	Al	Cu	Ag
1206 slice 13	159	—	—	56	148	—	33	56
1206 slice 62	71	—	—	71	—	—	—	—
1059 slice 36	—	25.7	—	—	—	—	—	—

$$ppma = \frac{ppm(weight) \times average\ molecular\ weight\ of\ CMT}{atomic\ weight\ of\ the\ element\ determined}$$

Referring to Figure 53b, curve C was obtained by adding selenium VI (Se VI 1000ppm) to the solutions each containing 0.1% CMT and added silver standard.   Se VI seemed to have an enhancement effect on silver.   In actual fact, when SeVI was covaporized with silver, no enhancement was observed.

On volatilization, the analyte vapour tends to condense into clusters (this is a well established phennomenon causing severe interferences in AAS).   For the ICP-GRV system, the transport efficiency of an analyte

Fig. 52a Determination of Manganese in CMT
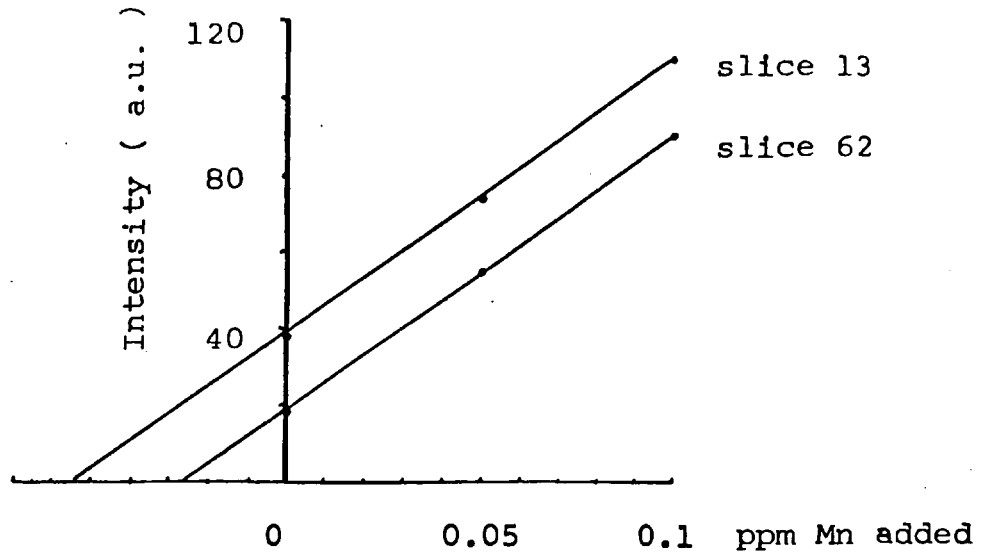
(by nebulization)
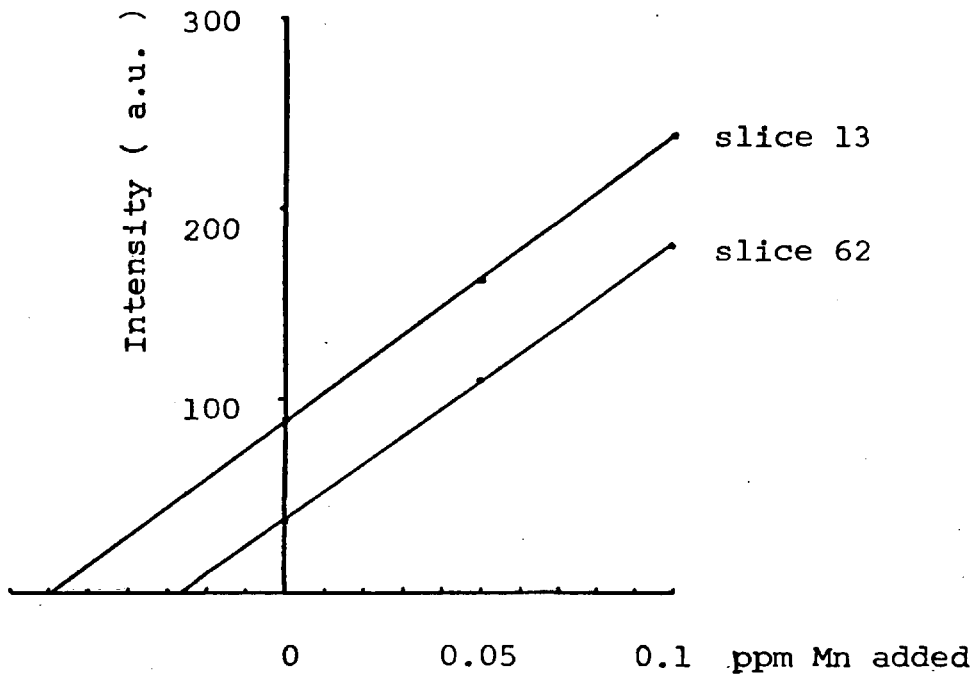
Fig. 52 b Determination of Manganese in CMT

(by electrothermal vaporization)
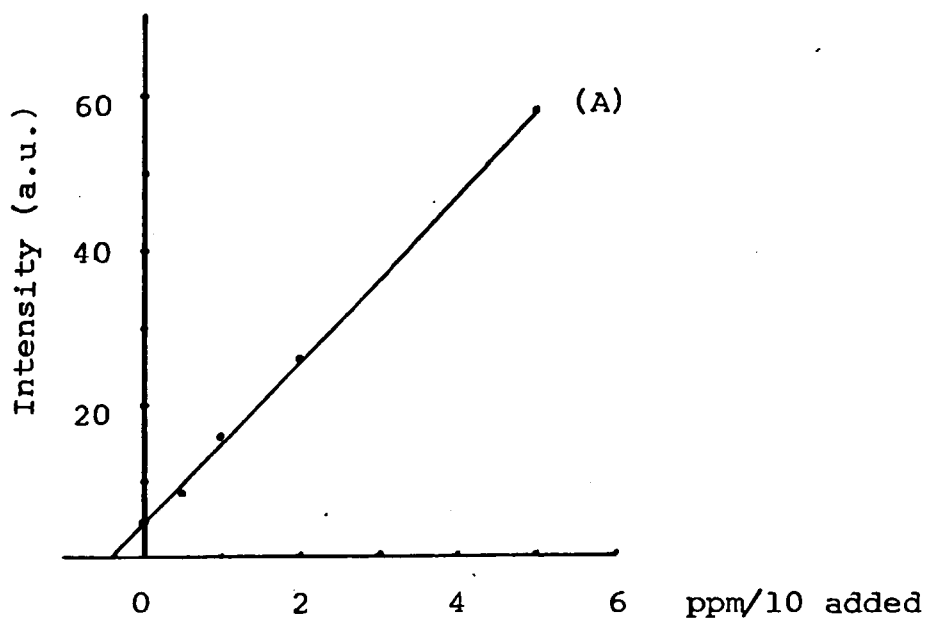
Fig. 53a Standard addition graph obtained for Ag in CMT

(by nebulization)
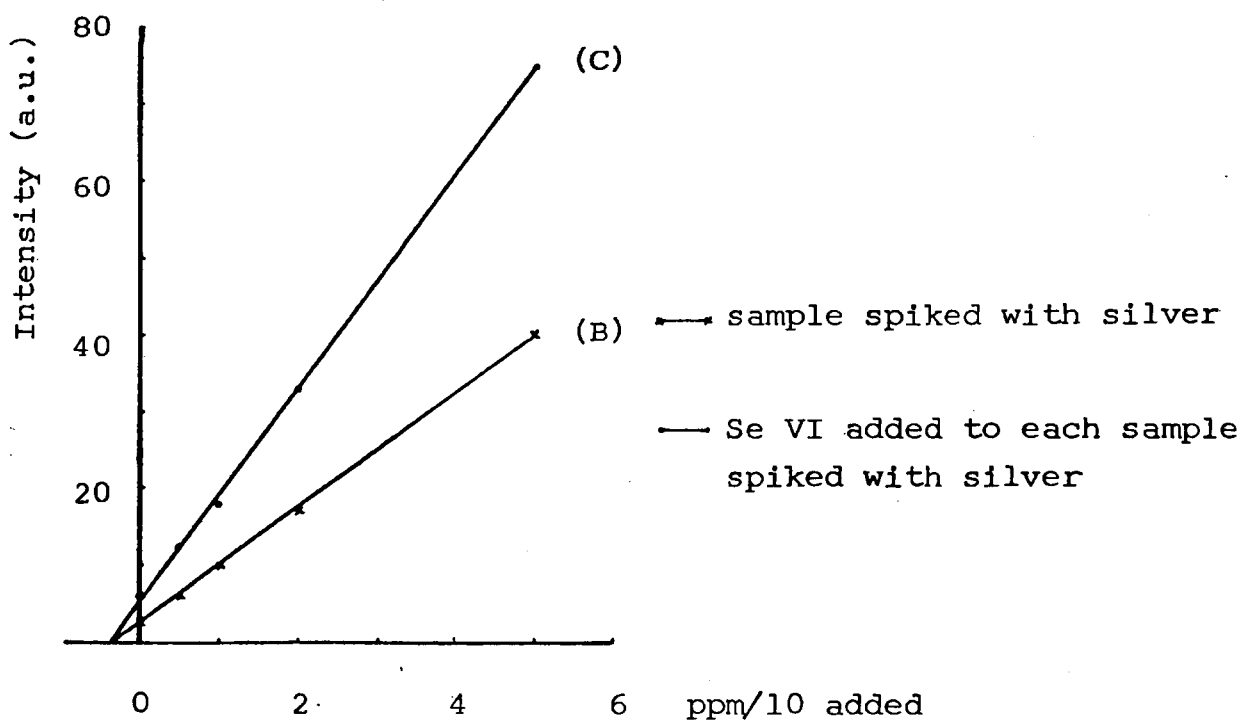
Fig. 53b Standard addition graph obtained for Ag in CMT

(by GRV)
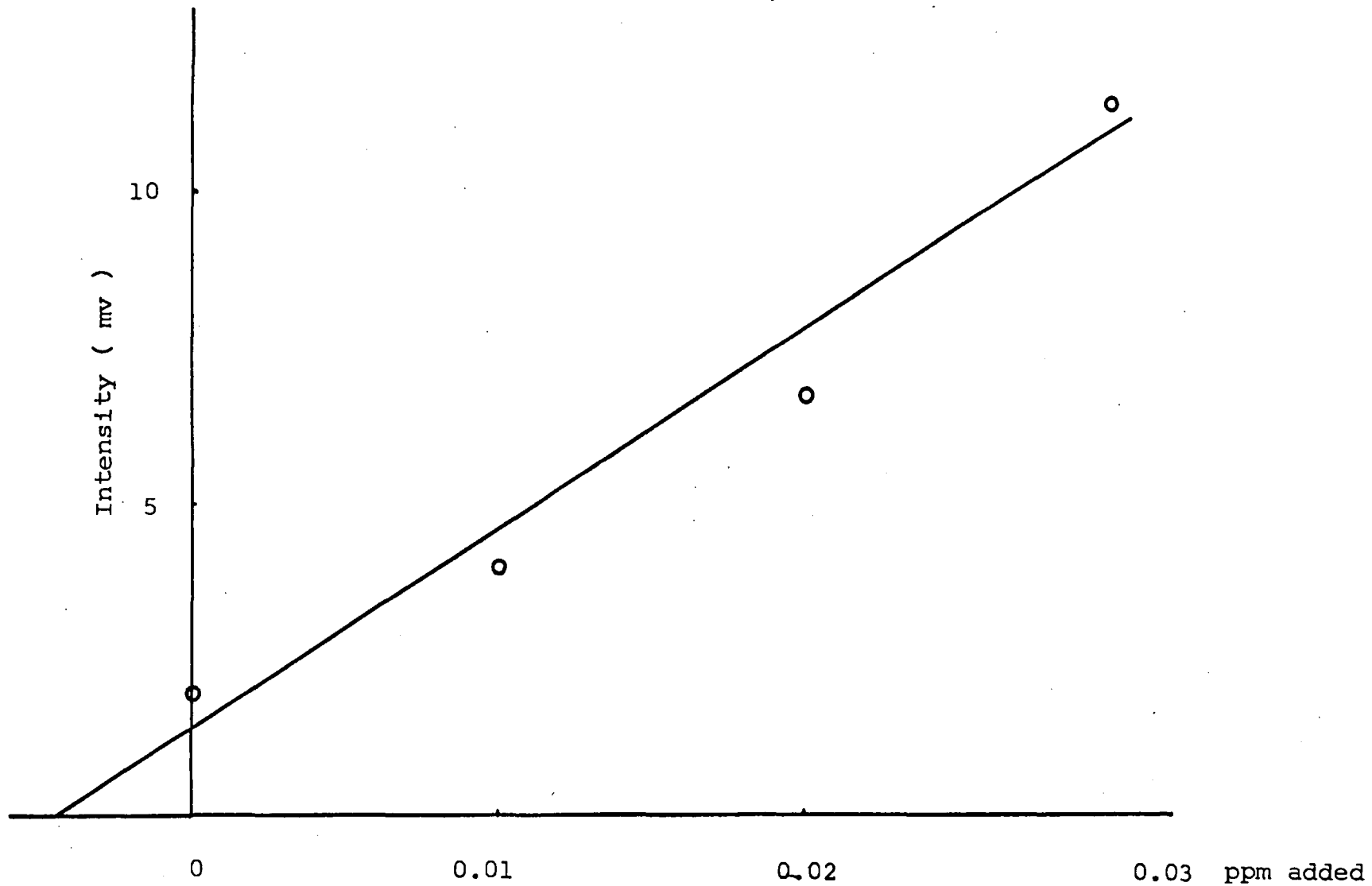
Fig. 54   Determination of Aluminium in CMT by electrothermal vaporization
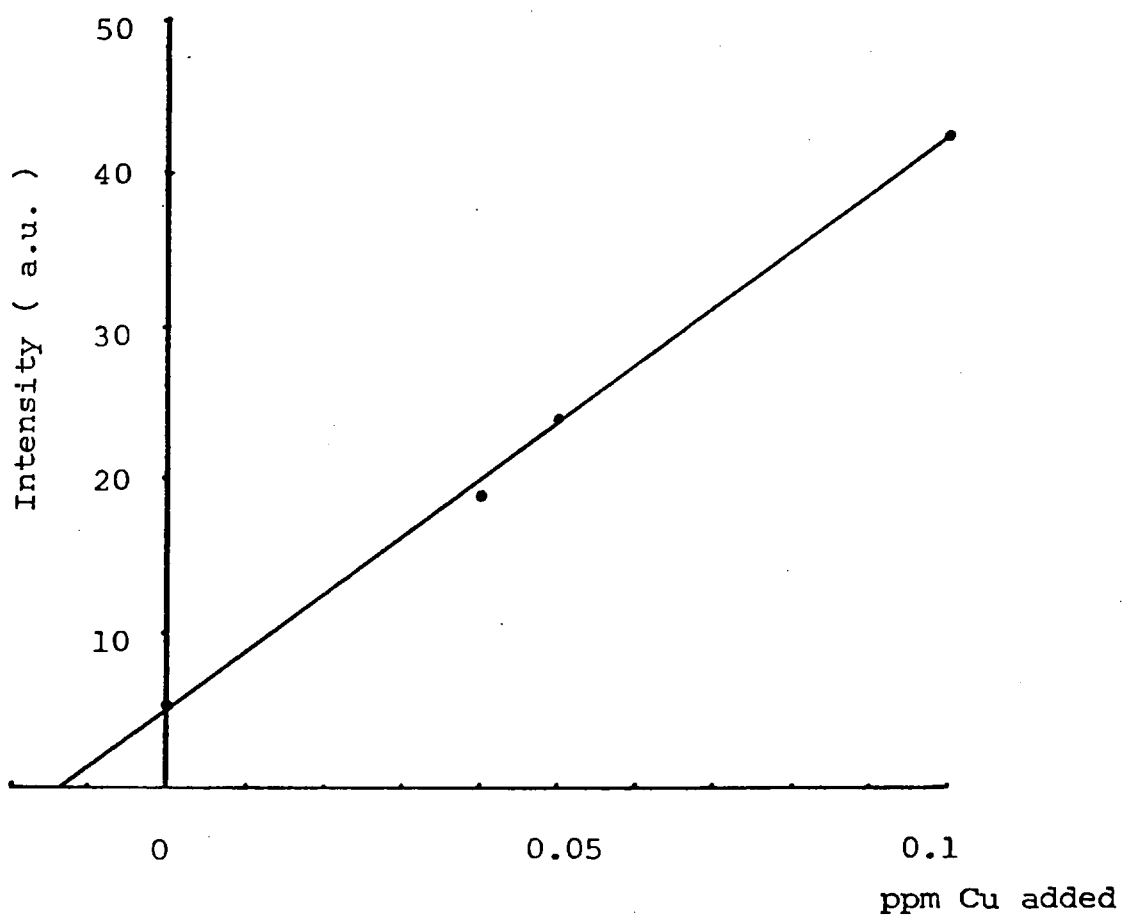
Fig. 55 Determination of Copper in CMT

(by nebulization)

depends partially on the formation of such clusters which can undergo elastic collisions with the walls and hence minimize deposition. In the absence of Se VI, cadmium does not aggregate well because of its volatile nature. When Se VI and cadmium are vaporized simultaneously, nucleation occurs even at 1cm above the rod, these particles appear as billiard balls and bounce their way off the walls and into the plasma. A transport efficiency as high as 80% was calculated for cadmium in the presence of Se VI.

The fact that the intensity of the silver emission is affected by how efficient is the cadmium being carried into the plasma implies that silver is associated with cadmium (the matrix) after vaporization. Hence, the deposition of cadmium will cause a proportionate amount of silver to be deposited. It is possible that addition of Se VI enhances the emission of silver indirectly due to the mechanism described above.

2) Solid Analysis

a) The effect of heat on CMT

By observation of emission at the cadmium, mercury, tellurium and manganese wavelengths, it was possible to show the thermal decomposition of solid CMT (see Fig.56). At a temperature as low as 400°C, mercury and some of the tellurium vaporized from the rod simultaneously. Mercury, being an extremely volatile element, was totally vaporized into the ICP before the atomization cycle. Tellurium volatilized with mercury presumably because of the structure of the CMT crystal
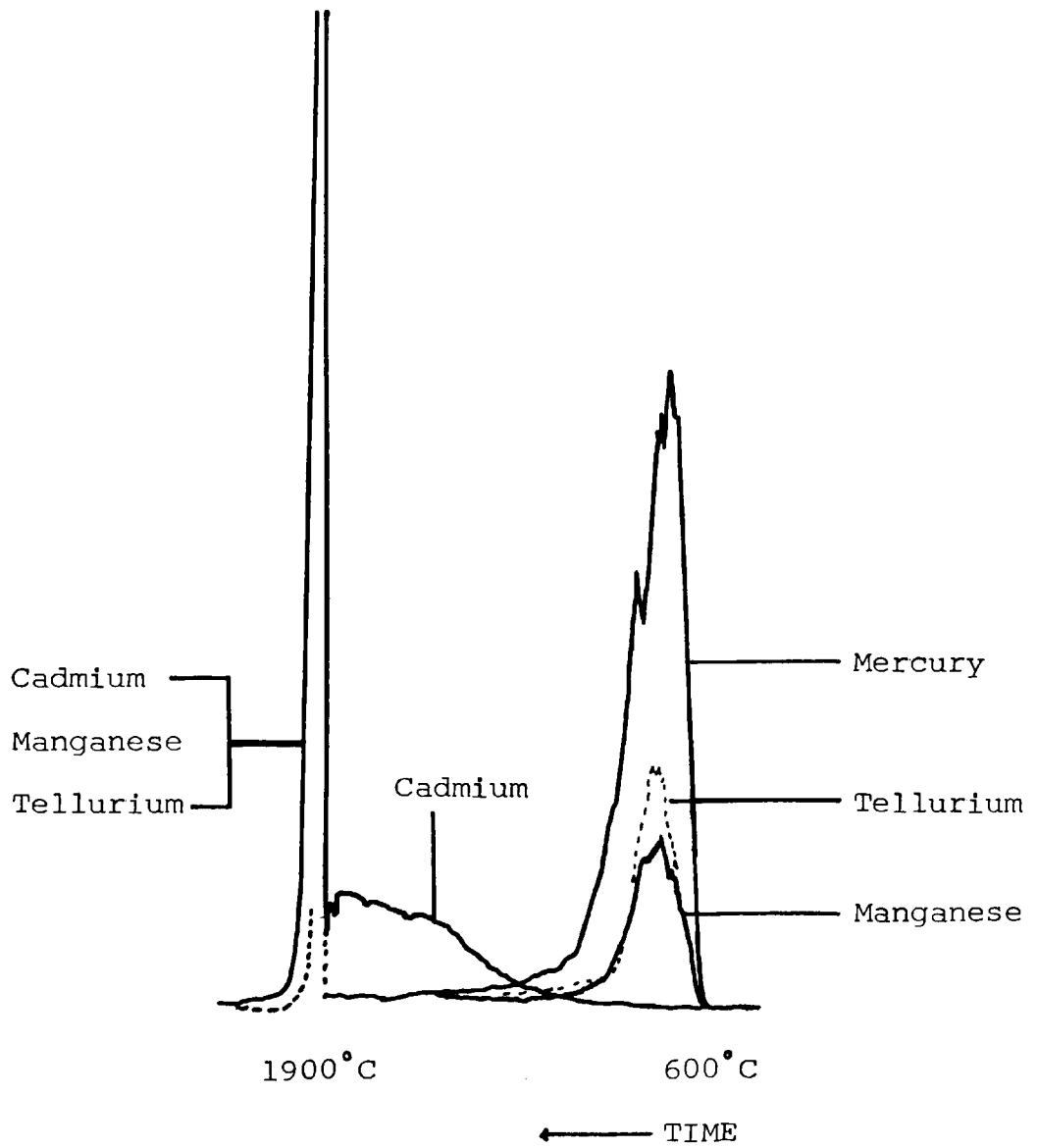
Fig. 56 The thermal decomposition of CMT

lattice as the starting materials for the synthesis of CMT
are mercury telluride (HgTe) and cadmium telluride (CdTe).
Some of the manganese also appeared to be volatilized with
mercury and tellurium. As the temperature of the graphite
rod was raised gradually, cadmium began to vaporize. Upon
vaporization at high temperatures, the matrix and the impurity
which
ʌ remained on the rod after the pre-vaporization cycle were
released rapidly into the ICP resulting in sharp, well
defined peaks. With reference to diagram 56, it is possible
to draw some conclusion about the effect of heat on the
structure of the CMT crystal. At moderately low temperatures
of about 600°C, the CMT crystal lattice breaks up into its
constituents, possibly to CdTe and HgTe. HgTe is very volatile
and is vaporized off the graphite rod as a molecular vapour.
Any impurities or dopants present as interstitial species are
also released with the HgTe vapour. It is fortunate that,
for the GRV-ICP system, the vaporization and excitation
processes are separate. The GRV serves to vaporize the test
material and the ICP functions as an atomizer and at the same
time, furnishes energy to excite the atoms. Therefore any
pre-vaporization losses can be detected and measures can be
taken to eliminate such losses. In furnace atomic absorption
spectrometry, however, the pre-vaporization loss of dopants
and impurities cannot be readily recognised, especially when
these elements are present in molecular form.

b) Optimization of vaporization temperature

The vaporization temperature for vaporizing the CMT
solids affects the shapes of the peaks. At temperatures

A   The release of tellurium before vaporization

B   Vaporization at 1900°C

1900°C   1500°C   1300°C   1100°C   600°C   <600°C
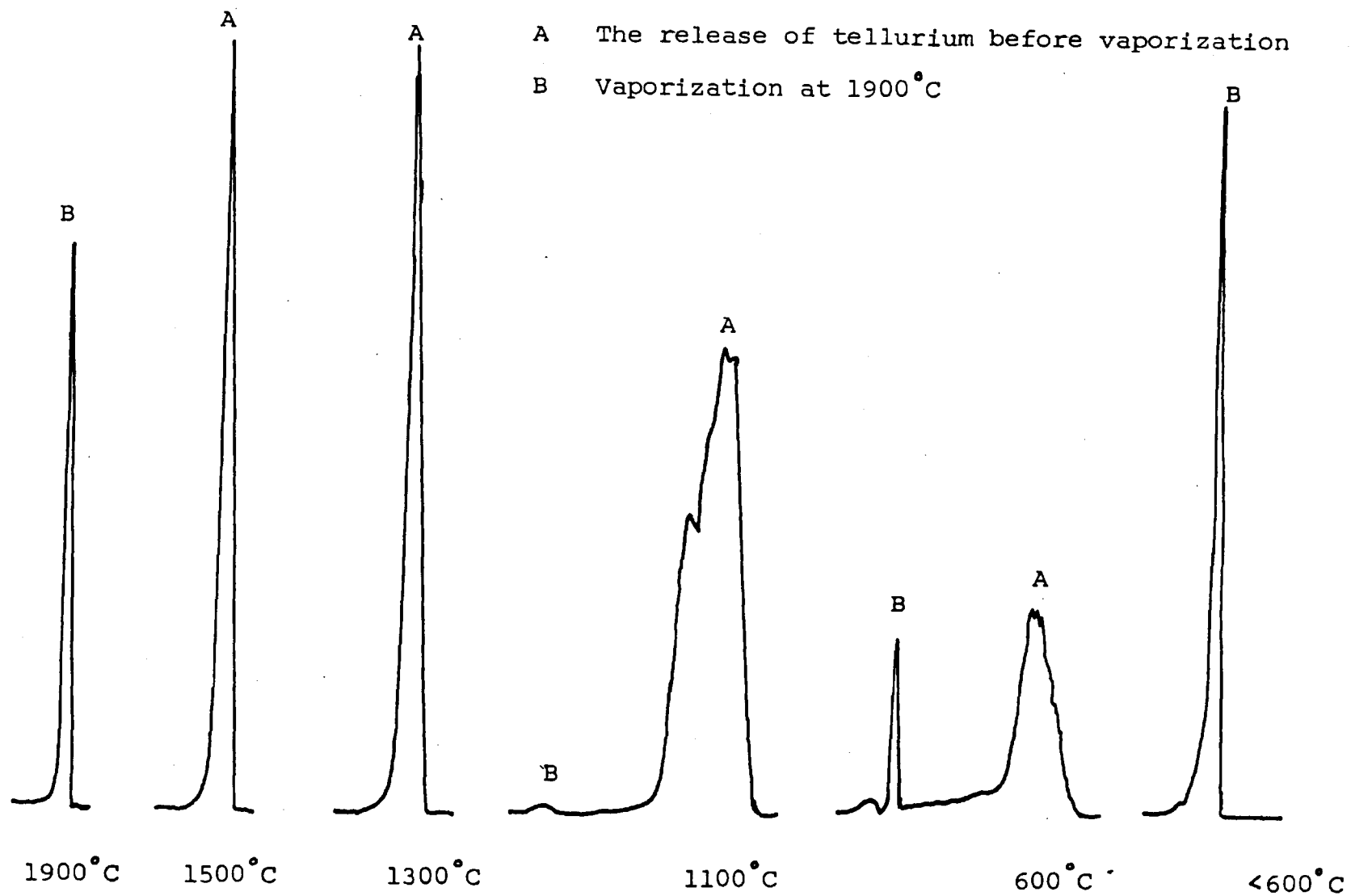
<u>Fig. 57</u> The profiles of tellurium at different temperatures prior to vaporization

30 sec.

TIME

1500°C   1300°C   1100°C   600°C
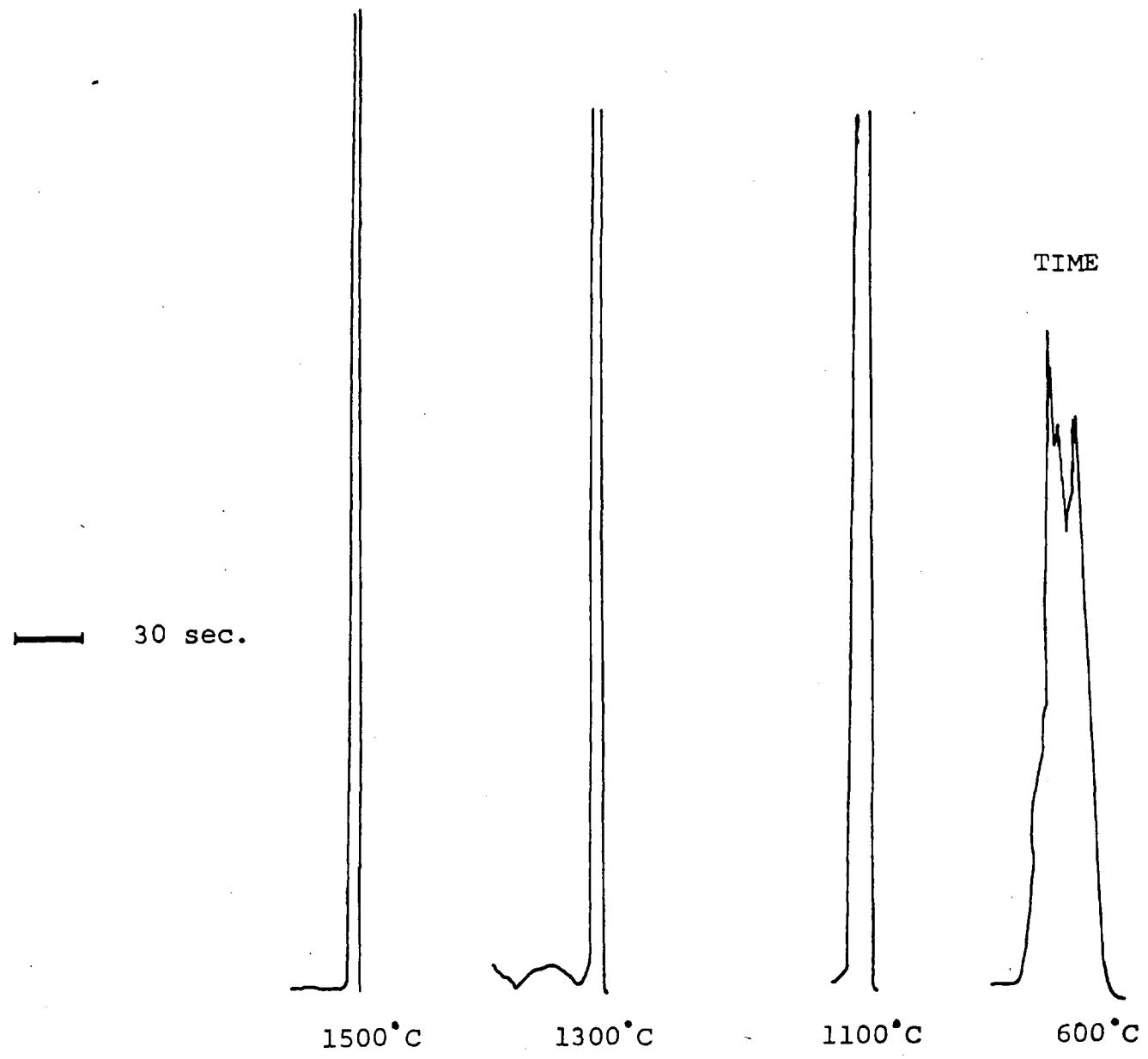
Fig. 58 The profiles of cadmium at different temperatures

149

A — The release of manganese before vaporization

B — Vaporization at 1900°C

← TIME

150

A

A

A

A

B

├── 12 sec.

B

A

B

B

B

B

1700°C   1500°C   1300°C   1100°C   600°C
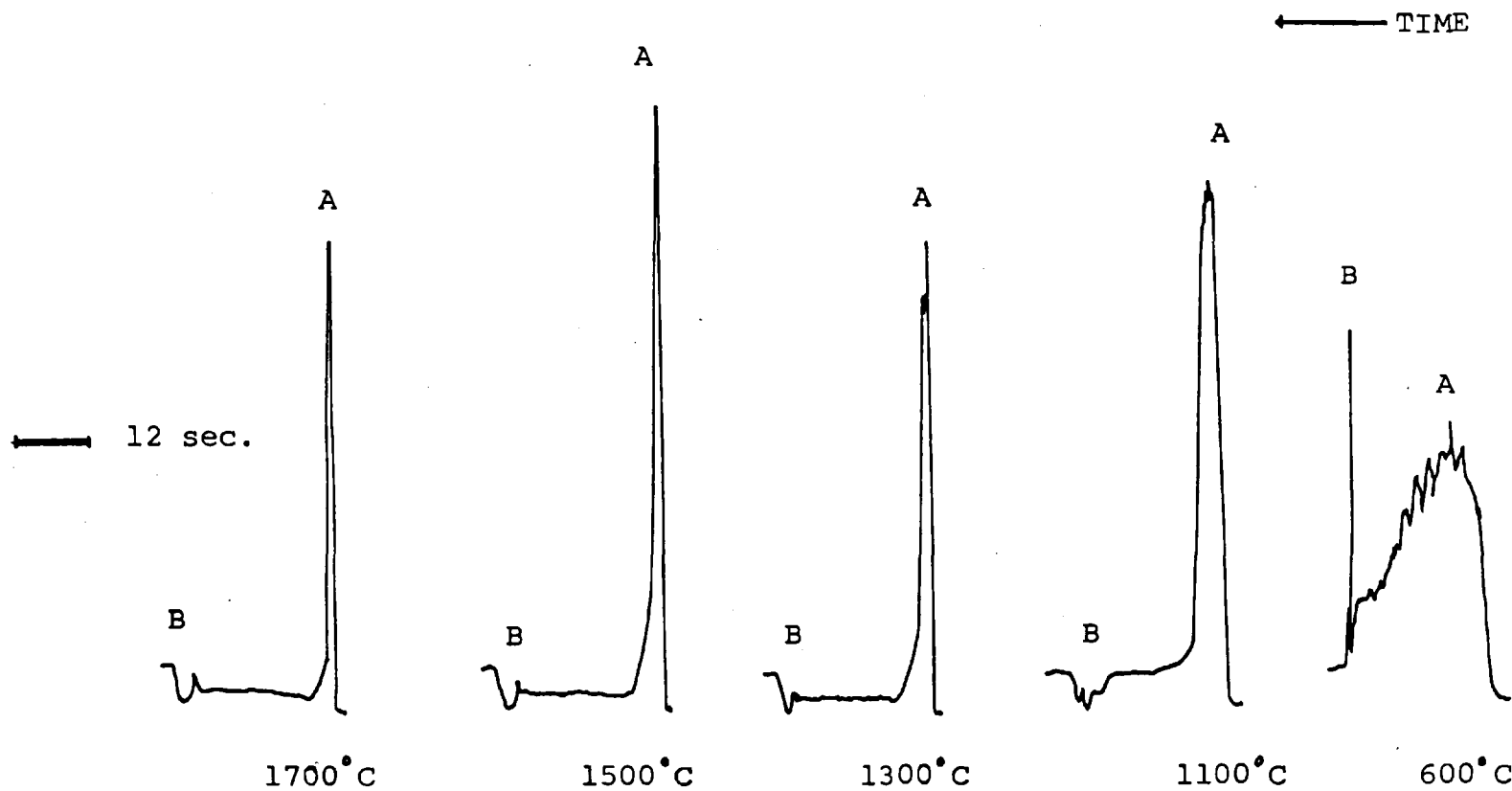
Fig. 59 The profiles of manganese at different temperatures prior to vaporization

A   The release of copper before vaporization

B   Vaporization at 2500°C

1700°C   1500°C   1300°C   1100°C
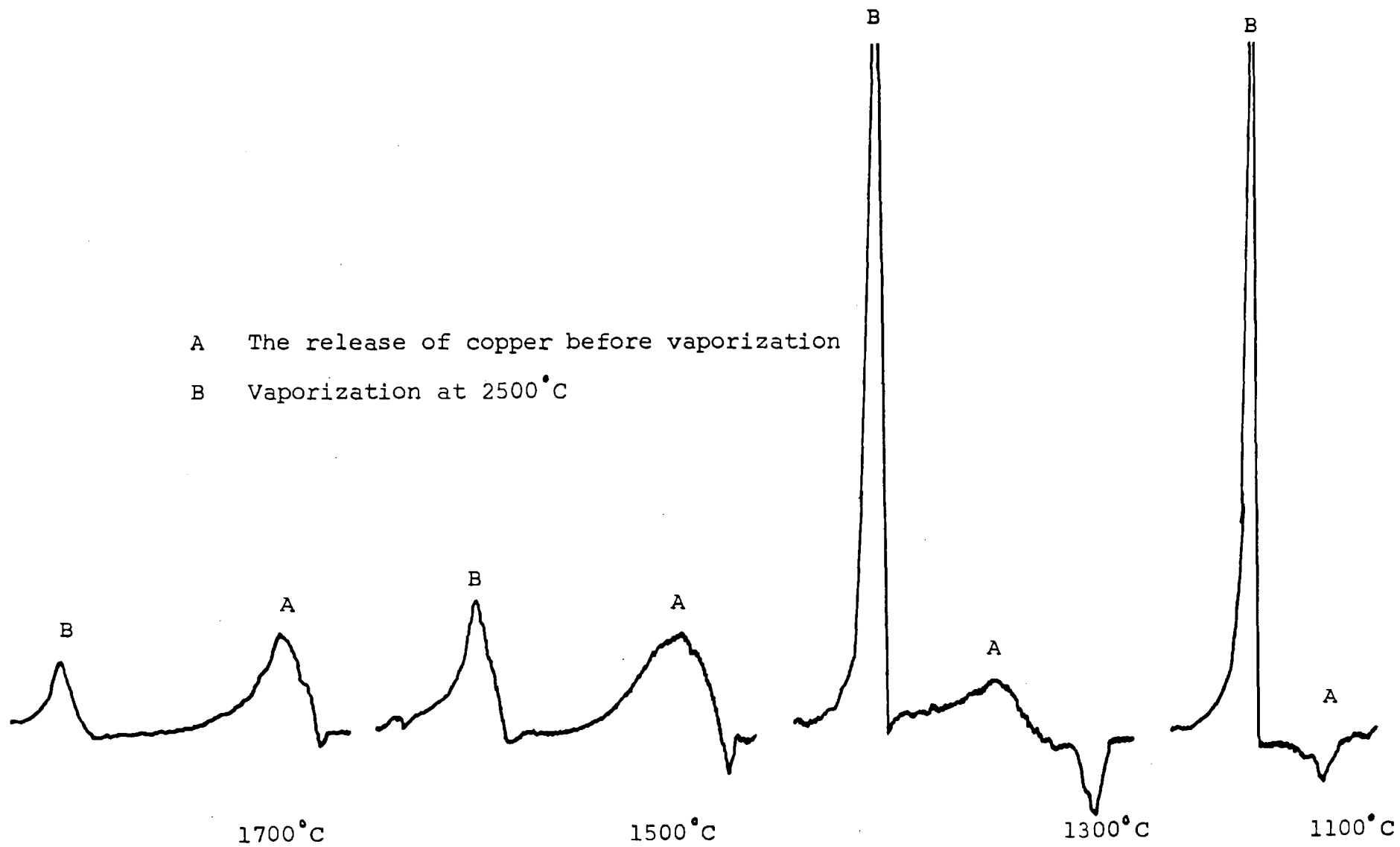
Fig. 60 The profiles of copper at different temperatures prior to vaporization

below 1100°C, the peaks obtained for measuring the emission

signals of some elements were ragged (Figs 57-60) because

a proportion of the solid was vaporized intermittently. At

temperatures around 1100°C, the bulk of the CMT is completely

vaporized into the plasma, however, some elements such as

copper and aluminium remain on the rod and require higher

temperatures for vaporization. As can be seen from the

diagrams, there is a relationship between vaporization temper-

ature and the time duration of the peak. Figure 60a shows

a plot of the vaporization temperature vs the time taken for

the signal to reach half of the peak height value. The graph

indicates an inverse proportionality relation between the

two variables. Another factor affecting the time duration

for the signal peak is the amount of material introduced into

the plasma. But because the solid particles were sieved to

a. size range, the mass variations would be insignificant in

causing gross deviation to the trend. The vaporization temp-

erature also correlates to the rate of expansion of the argon

carrier gas. The higher the temperature, the more rapid is

the rate at which the carrier gas and the analyte entering

the plasma per unit time. Thus resulting in sharp and well
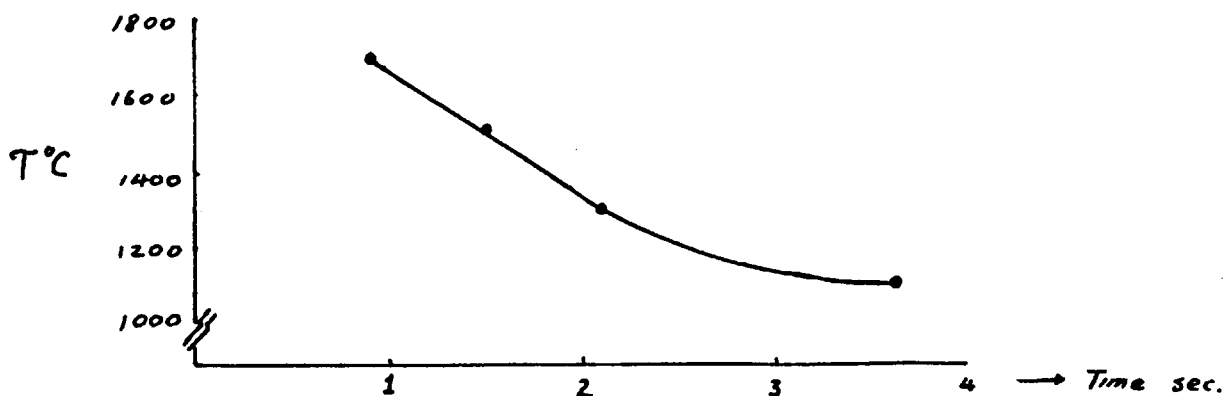
Fig. 60a The relationship between the peak width and
the vaporization temperature.

defined analytical peaks. Peak area measurements were used for relating the relative emission intensity of manganese to the mass vaporized because peak height measurement did not relate to the mass vaporized proportionately.

It was not possible to separate manganese from the matrix by controlling the thermal decomposition of CMT due to *covolitilisation* at temperatures as low as $400°C$. Hence, an optimum rod temperature of $1700°C$ was employed. On the contrary, silver was not vaporized until much higher rod temperature ($2250°C$). Therefore , it was possible to pre-vaporize part of the matrix at low temperature without loss of silver.

c) Procedure for obtaining calibration curves

Ideally, solid particles should be weighed immediately before being dispensed onto the graphite rod using the solid transfer pipette. This was found impractical because each weighing required about 5 minutes, and the complete heating programme took ca 40 seconds only. Thus, the plasma was being left idle for the major part of the experimental time. That was not a cost effective way of obtaining information. The most convenient means was to weigh the solid particles in batches before carrying the experiments. Thus, one or two particles were weighed into boat-shape paper containers. Caution was taken in handling the weighing procedure as the balance was extremely sensitive to dust or sweat adhered to the container. The weighings were usually carried out in draught-free, noise-free conditions. The particles were deposited into the cavity of the graphite rod (Fig. 51) and

were vaporized under the conditions shown in Table *6.1*.

The emission signal of the element under test was monitored under the compromise conditions as listed in Table *6.1* . A calibration curve was constructed by plotting the relative emission intensity (the area under the peaks) against the weight of CMT vaporized. These graphs are shown in Figs. *61a, 61b, 62*

d) Statistical analysis of the experimental results

In quantitative spectrophotometric analysis, often, the effect that some variables exert on another is determined to check the validity of a new assay method against a series of standards. A quantity of sample (X) is measured, after performing a reaction, a response (Y) is then measured. In spectroscopic analysis (X) is usually the concentration of the analyte present in standard samples and (Y) is the corresponding absorption or emission of radiation in relative units. Mathematically, the relationship can be expressed as

$$Y = f(x) \qquad\qquad (6.1)$$

If the relationship is linear, equation (6.1) becomes

$$Y = a + bx \qquad\qquad (6.2)$$

where a is the intercept with the Y-axis and b is the slope of the line: the change in Y per unit change in X. The value a usually represents the blank in an analysis and must be accounted for.

The study of the effect of an interrelated variable upon another is termed regression analysis. Linear regression applies to the regression of Y upon X using equation (6.2) which is the best estimate of the line of regression. In Fig. *61b*, the data points shown are scattered and we want to
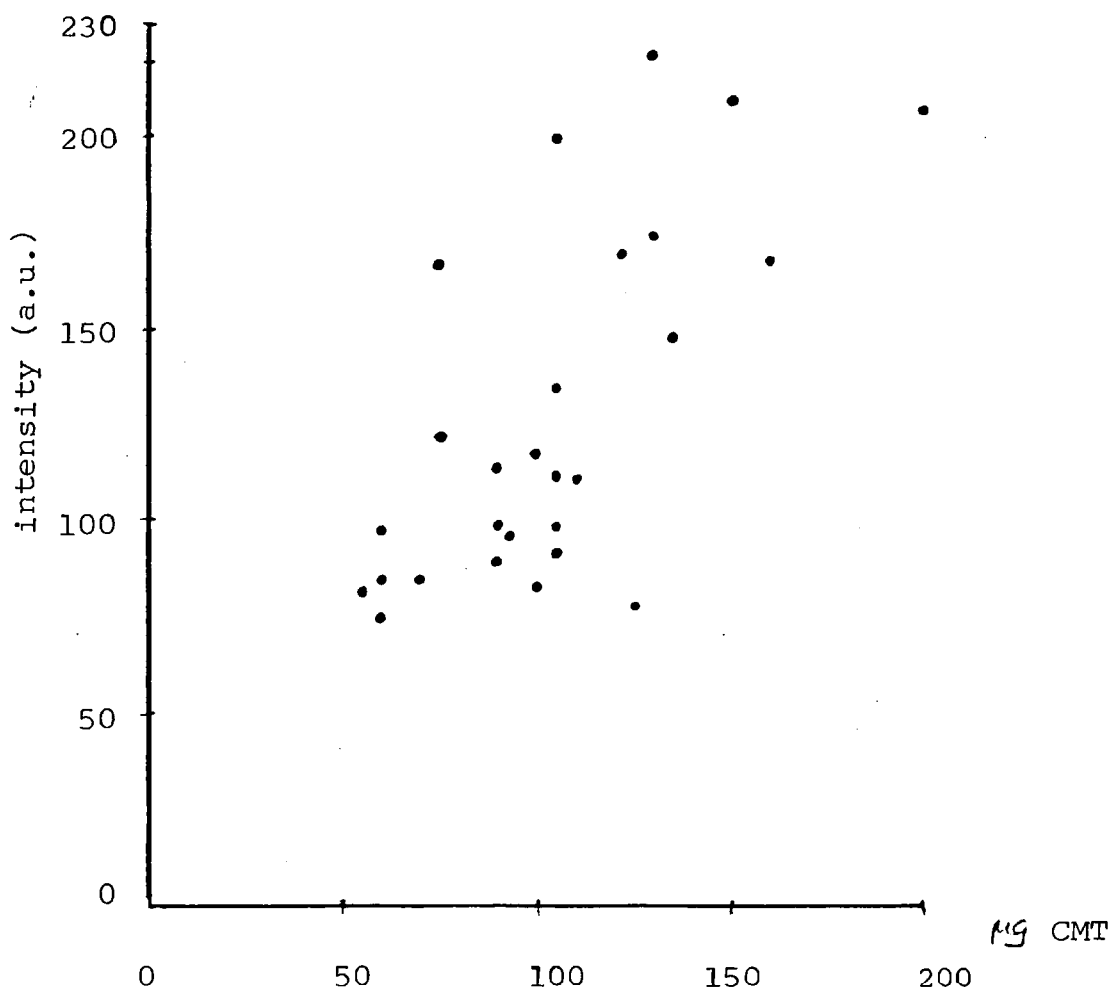
Fig. 61a   The relationship between manganese emission
intensity vs. mass of CMT vaporized.
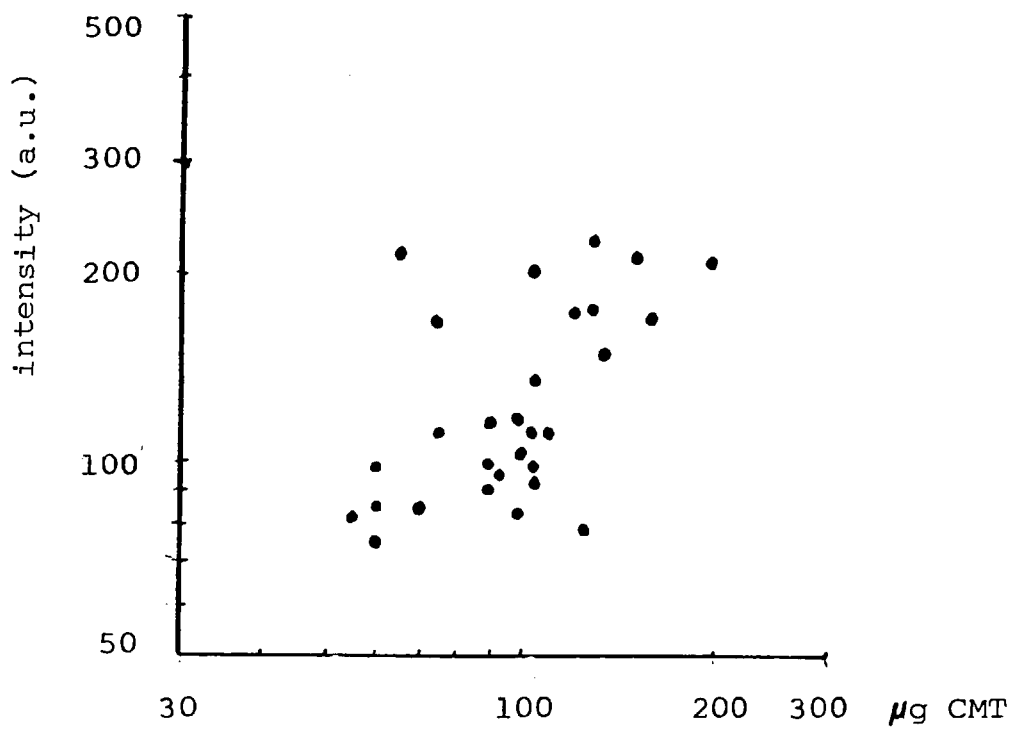
Fig. 61 b   The relationship between the relative
emission intensity(manganese) vs. mass of CMT
vaporized on double logarithmic scale.
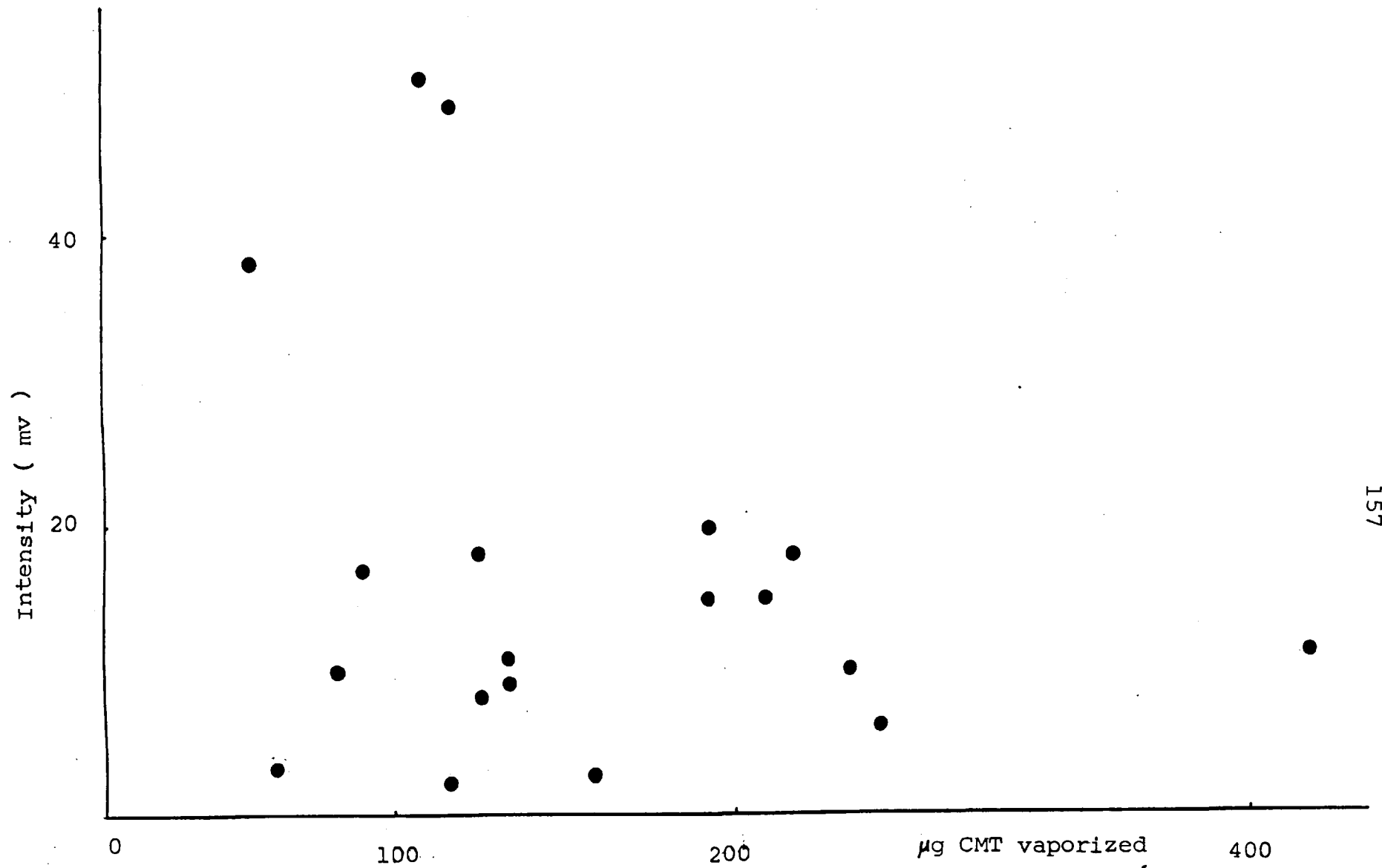
Fig. 62 Relative emission intensity at Ag atomic line vs sample mass vaporized

know if emission intensity is directly proportional to mass
vaporized as this is the basis of quantitative analysis.
The technique of linear regression is useful in this case
in providing some meaning to the data collected. After having
estimated the best straight line through the points, some
tests can then be carried out to assess the validity of the
straight line approximation(see appendix 1). Table 6.5
summarises the statistical results.

To examine if the calibration graph could be
classified as a straight line, a least square method is
employed to fit the best straight line through all the points.
Then, the gradient (b) and the correlation coeffient (f) of
the straight line are calculated. In an ideal case, when
all the data point lie perfectly on the straight line, the
slope and correlation coefficient will be equal to 1. But
in the case for the manganese calibration curve, (b) and (f)
are 0.82 and 0.61 respectively. At a first glance, it appears
that the straight line approximation is not correct. But
by applying the r test, (appendix 1), it can be assumed that
the correlation coefficient of 0.61 is valid, to a 99.9%
degree of certainty

If the calibration graph could be classified as a
straight line, then the intensity to weight ratios (I/wt)
should not deviate too much from the mean of the ratios.
The mean ($\bar{x}$) and the standard deviation are calculated to be
1.311 and 0.526 respectively. Statistically, it is valid
to reject some of the values from a set of data if the values
lie outside the range of $\bar{x} \pm 2.5\sigma$. The standard deviation (σ)

calculated on the remaining ratios is 0.389. In fact, σ measures how far sample values deviate from $\bar{x}$ and is therefore a measure of precision. The value σ = 0.389 indicates that there is a considerable deviation of sample values from $\bar{x}$.

Table 6.5

range of I/wt ratios	0.48-3.32 (n=33)	0.48-2.626 (n=30)
standard deviation	0.526	0.389
variance	0.268	0.147
mean	1.311	1.249
R.S.D.	40%	31%
Linear regression		
Y intercept	46.7	32.0
slope	0.82	0.914
correlation coeff.	0.61	0.69

Why is that the data points show a large spread about the straight line? There are several possible factors causing this deviation.

1) Loss of analyte on vaporization.

2) Deposition of the aerosol on the walls.

3) Inhomogeneous distribution of the trace element in the crystal.

4) Errors in taking the readings of the weighing.

1) On rapid heating (from 100-1700 C), it was thought possible that the energy gained by the CMT particle was sufficient to cause sputtering of the CMT from the rod, a process which may also be enhanced by the thermal expansion of the layer of gas surrounding the shallow cavity rod. To reduce sputtering, a deep cavity rod was constructed as shown in Fig. 63
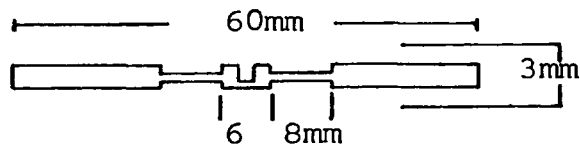
Fig. 63 The graphite rod vaporizer

Using the deep cavity rod, calibration curves were obtained for manganese and silver by plotting their respective emission intensities vs weight of sample vaporized. These graphs are shown in Figs. 64 - 65. The data obtained for manganese were evaluated statistically and the results are presented in Table 6.6 There is an improvement of about 40% in the R.S.D. using the deep cavity rod as it has greater sample confinement capability than the shallow cavity type.

Table 6.6

range of I/wt ratios	2.6-1.0 (n=28)
standard deviation	0.354
mean	1.536
variance	0.121
R.S.D.	23%

Linear regression	
Y intercept	38.8
slope	1.1
correlation coeff.	0.90

As the correlation coeffients are nearly equal to 1, it is 99.9% certain that the straight line approximation is valid(see appendix 1). It is worth noting that in evaluating data statistically, the larger the population, the more meaningful is the result.

2) Deposition of aerosol on tube walls

In order to conduct an experiment designed to give an estimated degree of sample deposition, it was necessary to assume that the test element and the matrix behave in a similar manner. Cadmium was chosen to give an indication of the extent of analyte deposition because its determination by ICP-OES is very sensitive at sub ppm level.

After vaporizing a known weight of sample containing of about 30 particles into the plasma at 1700°C; the dome, the glass connecting piece and the P.V.C. tubing were washed with 5ml of aqua regia. The washing was diluted to 50ml with distilled water and the cadmium concentration in the solution was determined by nebulization. No matrix effects were observed on the emission intensity of cadmium. Calculations showed that approximately 2.4% of the cadmium was deposited onto the dome and the tube walls. Thus, it can be inferred that deposition of cadmium does not play a significant role in causing poor reproducibility.

The insignificant amount of deposition suggests that,
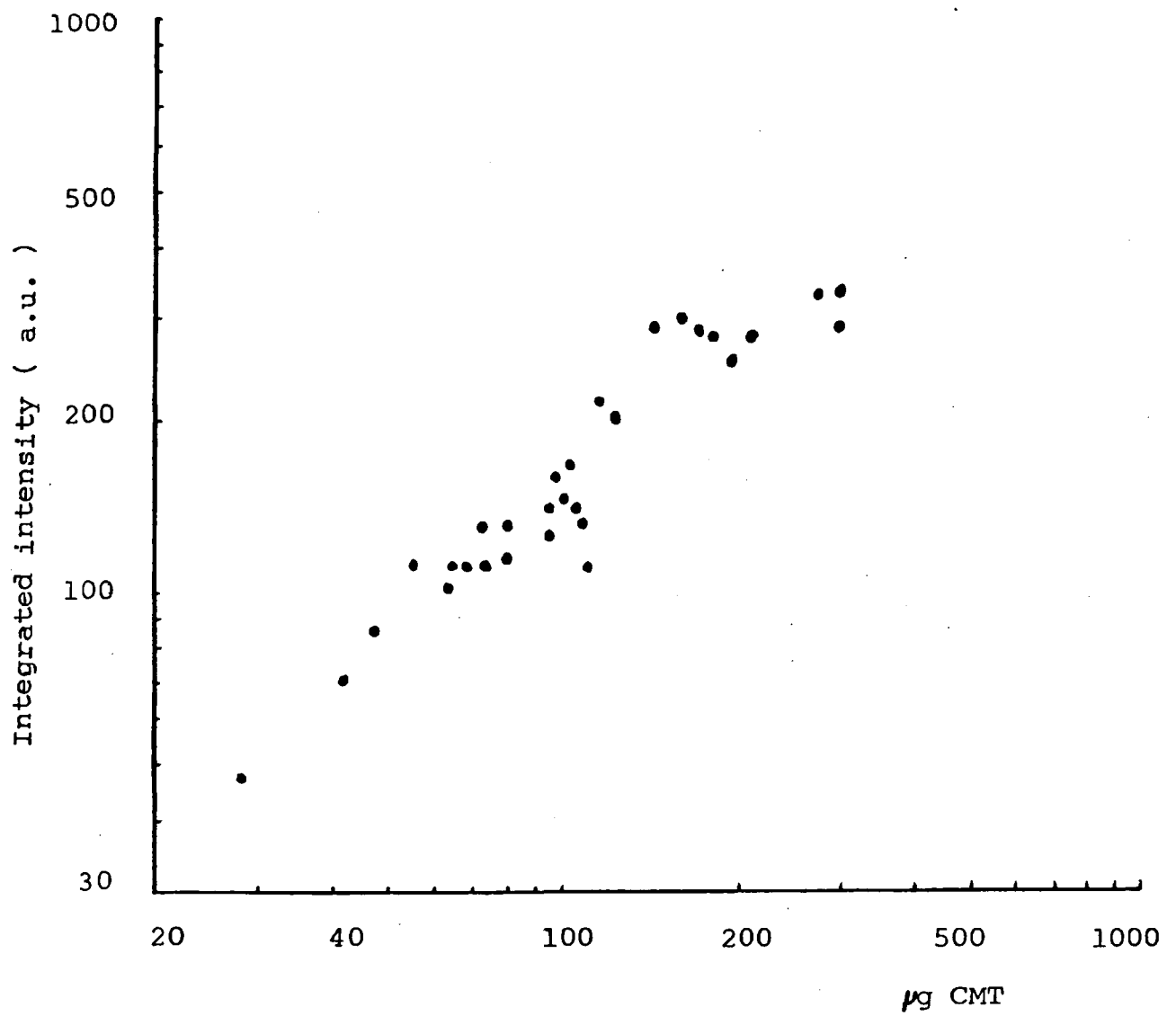
Fig. 64 Relative emission intensity at Mn atomic line vs
sample mass vaporized from a deep cavity graphite
vaporizer
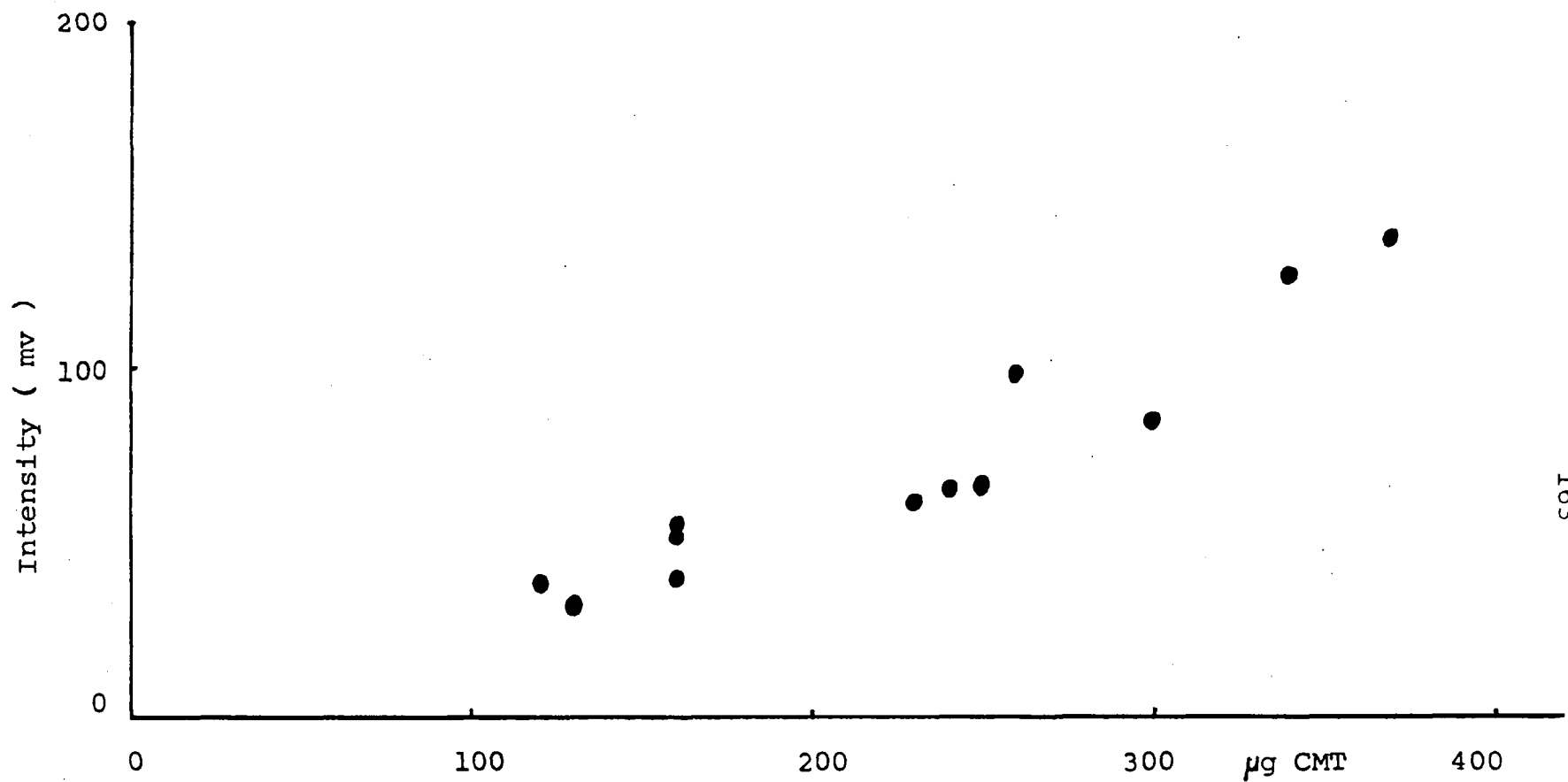
Fig. 65a Relative emission intensity at Ag atomic line vs sample mass vaporized
from a deep cavity graphite vaporizer
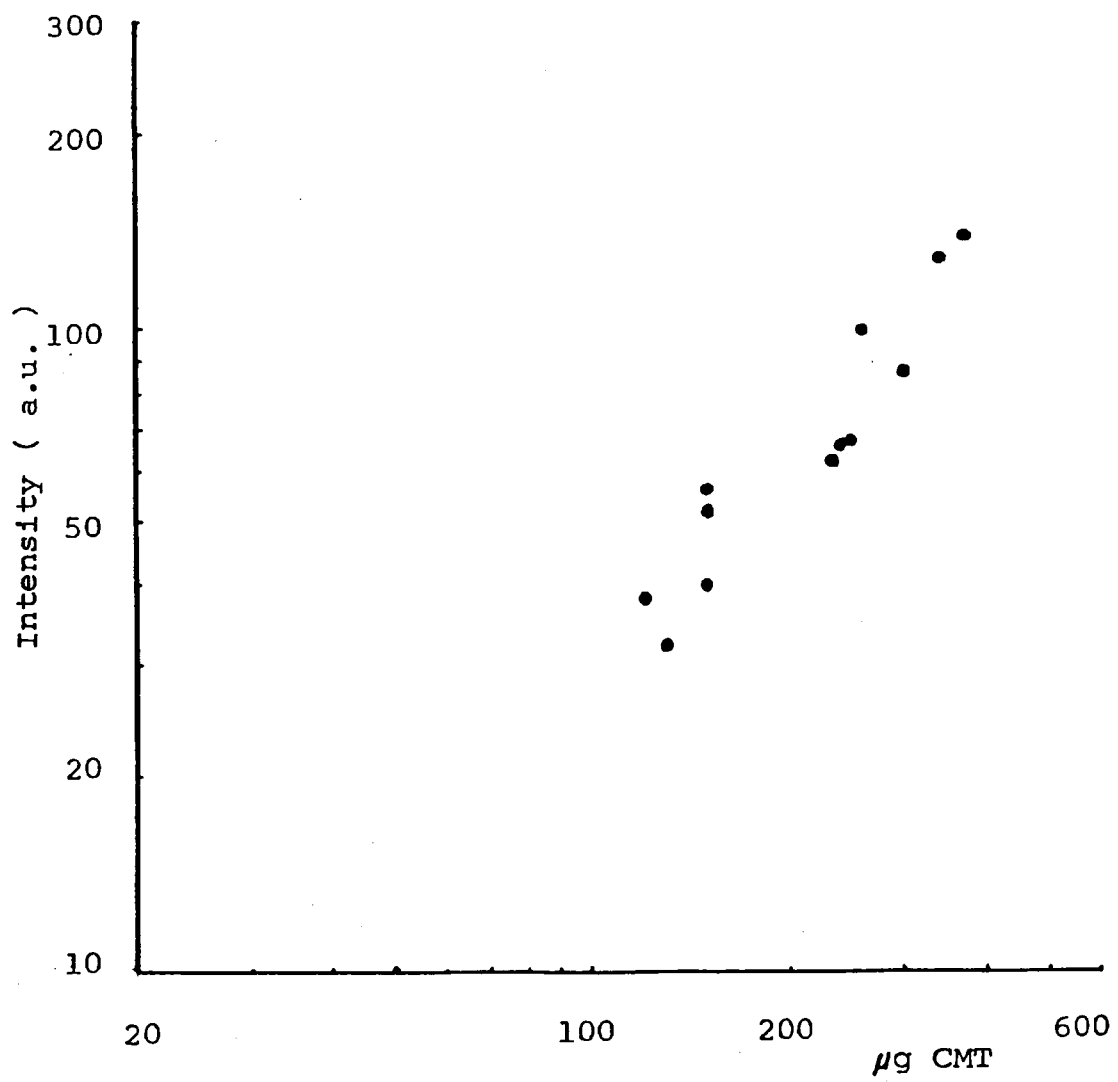
Fig. 66b Calibration for silver on log-log scale

perhaps, in a way, tellurium was behaving like Se VI in assisting the aggregation of cadmium atoms. This presumption was investigated by comparing the emission intensities for cadmium with those for cadmium in the presence of 1000ppm tellurium (made by dissolving tellurium metal in dilute nitric acid). However, tellurium did not seem to contribute any enhancing effect. This could be attributed to the fact that tellurium was not present in the oxidation state which was the most effective in assisting aggregation (Se VI was more effective than Se IV in improving the transport efficiency of cadmium).

The author postulates that since CMT was vaporized at 1700°C, it may be probable that cadmium was released in a molecular vapour form, either as Cd-Cd or Cd-Te rather as atoms. Hence, there was minimal deposition.

3) Inhomogeneous distribution of trace elements in CMT

In the preparation of doped CMT, the dopants are added to the starting materials before the synthesis. It is possible that during crystallisation, the dopants are orientated non-uniformly in the lattice, thus causing concentration variation in the crystal. In order to establish the fact, the following experiment was conducted.

Particles of the milligram range were weighed accurately and dissolved in 150ml of aqua regia. The solutions were each made up to a volume of 2ml with distilled water. 3μl of each solution was vaporized from a deep well cavity rod. The graph of relative silver emission vs mass of CMT dissolved shows poor precision

(Fig.66), even though the R.S.D. for each point was <u>ca</u>

5%. The concentrations reported for aluminium, silver

and manganese by several independent laboratories showed

a range of R.S.D. from 40 to 100%! [165] Based on these

results, it was concluded that the three elements are

distributed inhomogeneously in the CMT crystal.

4) <u>Errors in taking the readings during weighing</u>

If there were any errors, they would be compensated

by plotting the points on a log-log scale.
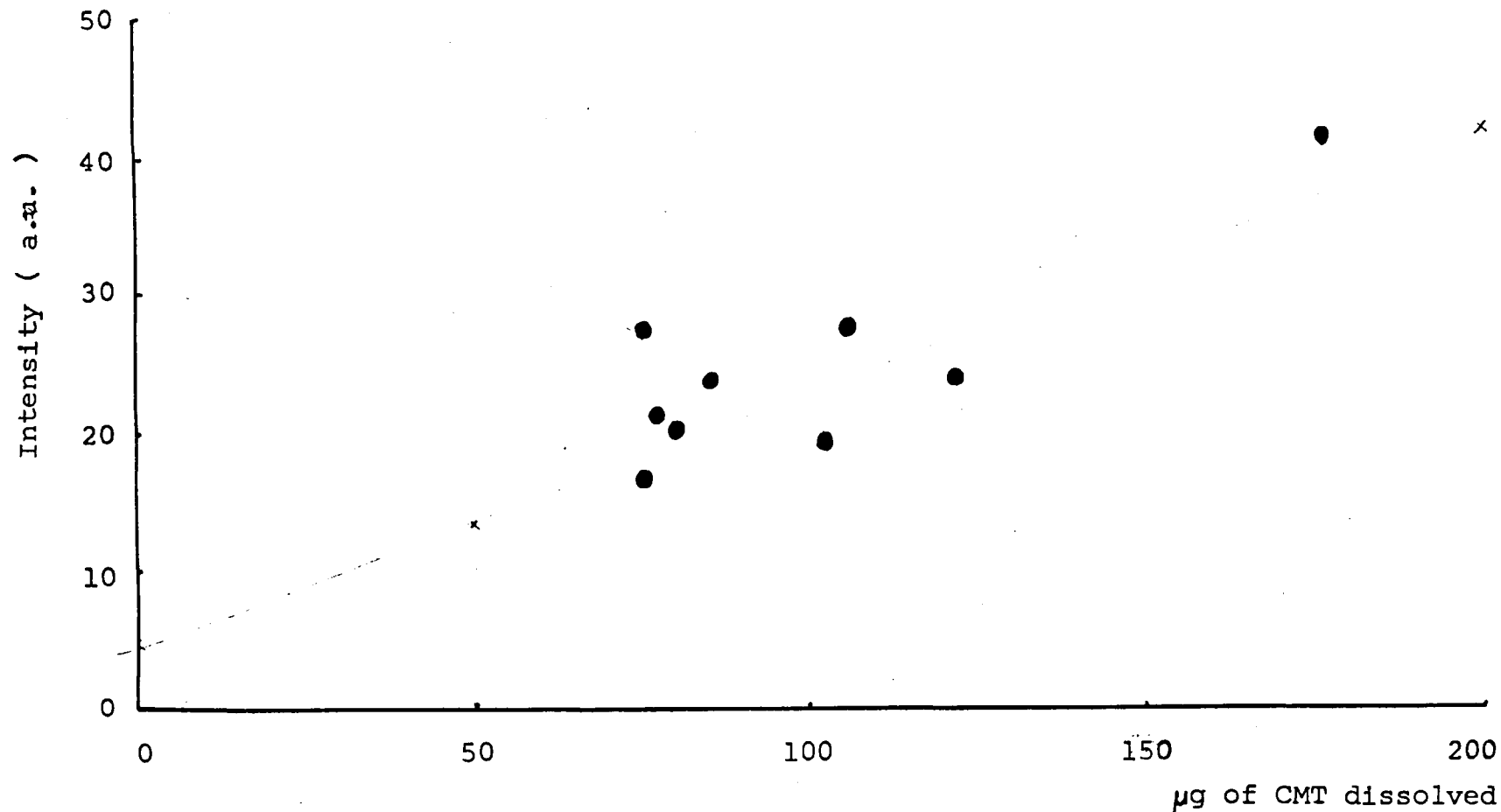
Fig. 66   Relative emission intensity at Ag atomic line vs mass of CMT dissolved

for 3μl sample vaporised from a deep well rod

6.5   Internal Standardisation

In emission and absorption spectrometry, an in-
ternal standard procedure is sometimes employed to reduce
errors and to compensate for small changes in experimental
parameters. The changes occur in the rate at which sample
is supplied to the flame and in flame conditions. These
alterations include change in sample viscosity and surface
tension, nebulizer performance, variation of fuel oxidant
concentration ratio or change in flame geometry due to
external disturbance. The internal standardisation pro-
cedure usually adopted for solution analysis is to add
to each of the sample and standard solutions a known
amount of an internal standard element and to monitor
its line emission intensity and that of the analyte element
for each solution. The measurement of the two signals may
be accomplished simultaneously.

In the present study, as the process for weighing
out micrograms of samples was tedious, an internal standard-
isation procedure was investigated to ascertain the feasibility
of calibrating the solid by relating the mass of sample
vaporized to the ratio of internal standard signal <u>vs</u>
analyte signal. Cadmium and tellurium were investigated
as possible internal standards because they are present
as the matrix elements. Owing to the wide linear cali-
brations, solid sample dilution is not necessary. The
instrumentation used has been described in section 6.3..

6.5.1   Procedure

Solid particles were deposited in the deep-cavity

rod using the solid sampling pipette. The particles were vaporized under the experimental conditions listed in Table 6.1 and the emission signals for cadmium(or tellurium) and manganese were recorded on strip chart recorders and the area under the peaks was integrated using the 'cut-and-weigh' method

6.5.2 Results and Discussion

Using the procedure described in section 6.5.1 the intensities ratios computed for cadmium to manganese and tellurium to manganese are presented in Tables 6.7, 6.8

Table 6.7

weight of CMT vaporized μg	I_{Cd}/I_{Mn}
230	2.39
515	2.48
230	2.60
355	2.42
240	2.60
570	2.60

Table 6.8

weight of CMT vaporized μg	I_{Te}/I_{Mn}
260	2.75
130	1.14
200	10.82
165	8.38
180	7.44
110	8.89

Table 6.8 contd.	
120	8.07
90	3.65
150	8.50

The statistical analysis on the ratios is summarised in Table 6.9

Table 6.9

	Cd/Mn	Te/Mn
standard deviation	0.0975	3.25
mean	2.515	6.63
R.S.D.	3.9%	49%
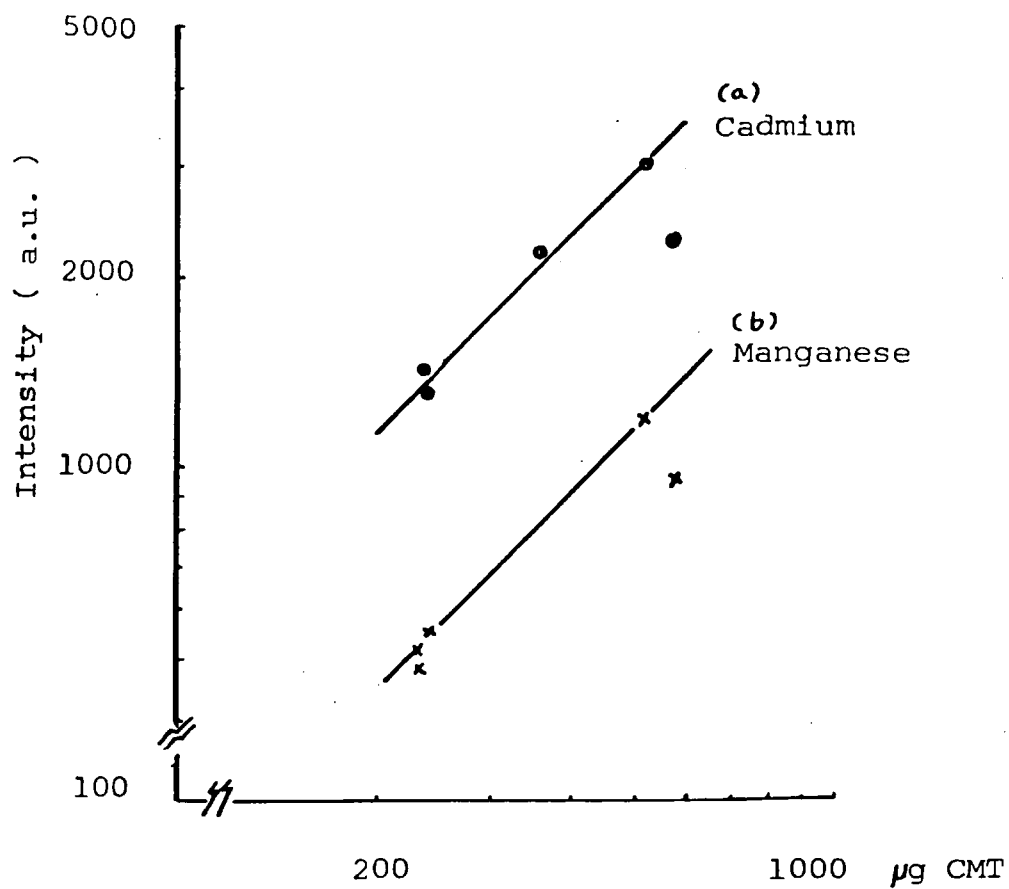
Fig. 67 Calibration curves for cadmium and manganese
(dual analysis)

Graphs 67a and 67b present the calibration curves obtained
for cadmium and manganese respectively from which the
data in Table 6.7 were derived. The graphs show that there
is one point which deviated from both of the straight lines.
This deviation could be due to sample loss due to sputtering.
However, when the ratio I_{Cd}/I_{Mn} was calculated, the value
was not significantly different from the mean. Therefore,
the internal standard approach has proved to be useful
to reduce errors. A calibration curve of relative cadmium
emission intensity vs mass of CMT vaporized is shown in
Fig. 68 . The graph is linear up to 295μg of CMT. This
mass corresponds to 44μg of cadmium and the upper limit
of the linear calibration is 100μg.
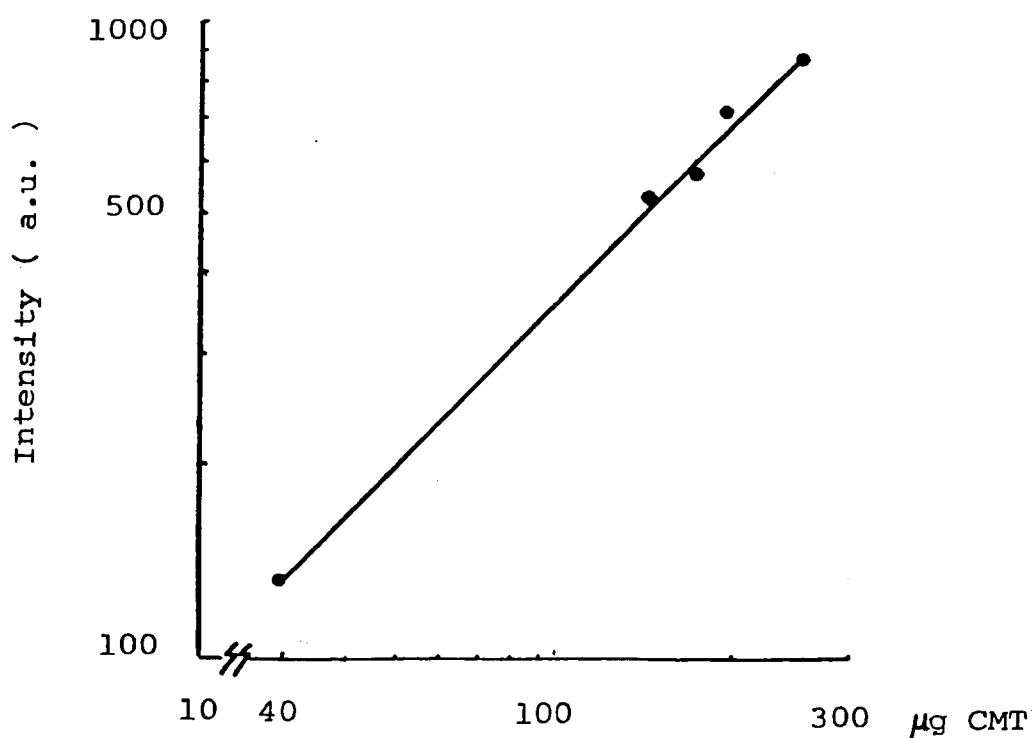
Fig. 68   Calibration graph for Cd in CMT

The high relative standard deviation obtained for tellurium

internal standardisation approach was first thought to

be associated with the temperature at which the solid

was vaporized from the rod. The effect of vaporization

temperature on the I_{Te}/I_{Mn} ratios was examined. Table 6.10

shows that there is no relationship between the reproducibility

of the intensity ratios and temperatures for vaporization.

Table 6.10

Temperature °C	R.S.D. %
1500	47
1700	49
1900	50
2250	51
2500	45

The behavior of tellurium (present in CMT) in

the plasma was investigated by measuring the emission

intensity for known weights of solid. A calibration

thus obtained is shown in Fig.69 which resembles a scatter

diagram. Further investigation showed that tellurium

obeyed the linear emission vs mass relationship up to

50µg only which corresponds to 100µg of CMT. Therefore,

although tellurium is distributed homogeneously(the

composition of cadmium has been reported to vary), it

is not recommended for use as an internal standard

because the particles usually exceed 100µg in weight.
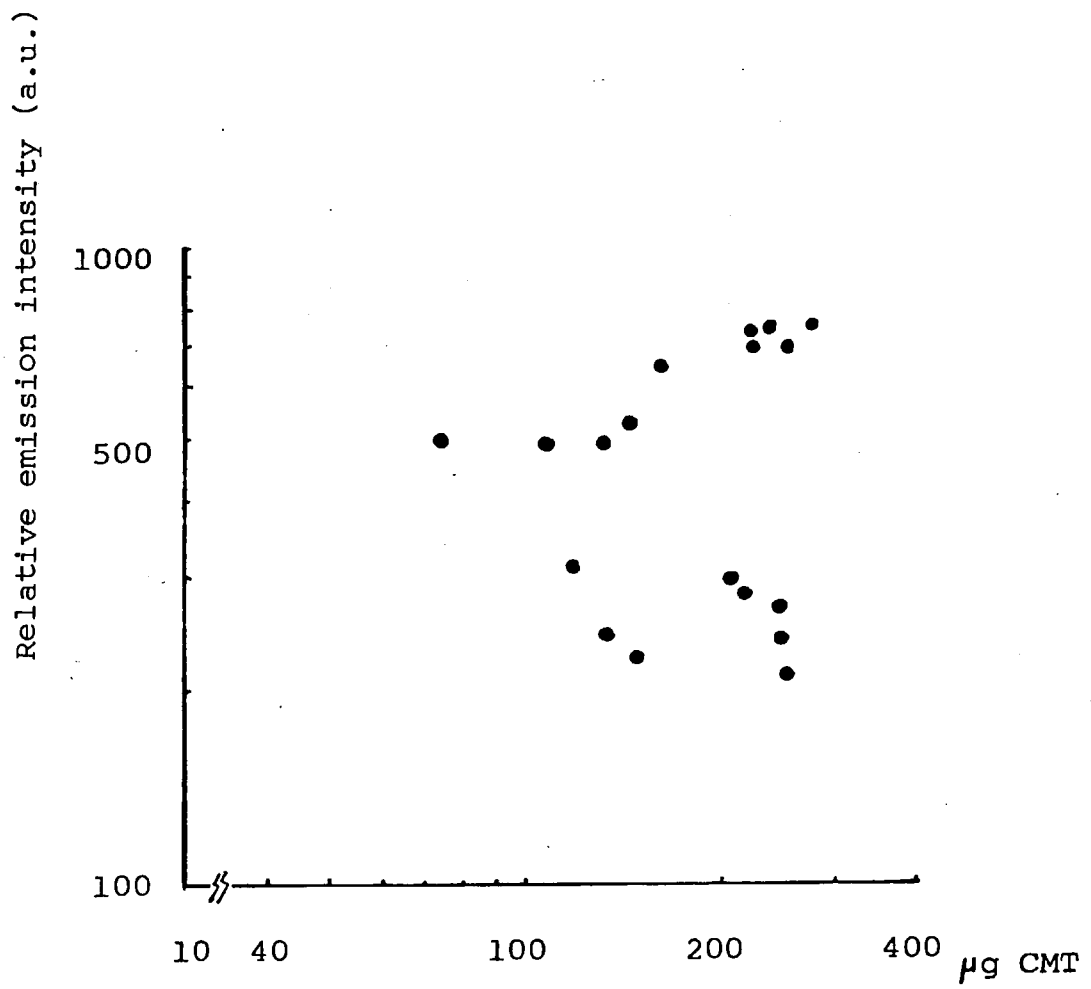
Fig. 69 Calibration graph for tellurium in CMT
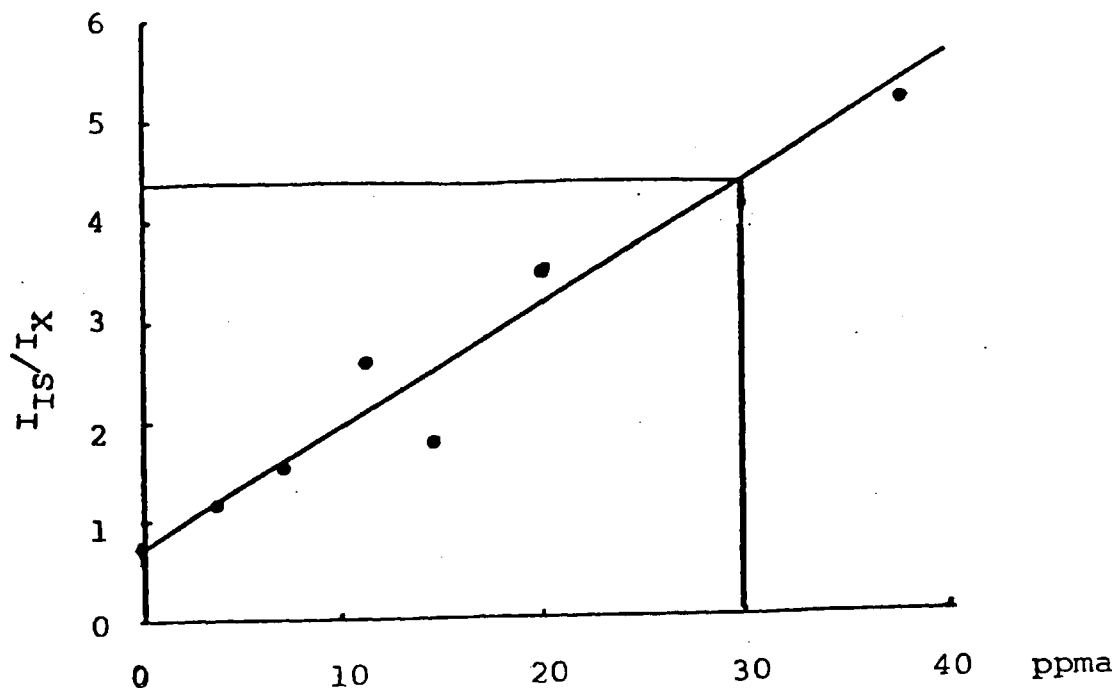
Fig. 70 A hypothetical calibration graph for internal standardisation

6.5.3 A Hypothetical Calibration

In order to determine the concentration of a trace element, it is necessary to construct calibration curves relating the I_{IS}/I_X ratios to some known standards. I_{IS} is the emission intensity of the internal standard and I_X is the emission intensity of the trace element of interest. A hypothetical calibration curve obtained in this manner is shown in Fig.70 . After having performed a statistical analysis on the data to approximate the points to a straight line(the approximation has to satisfy some statistical tests- coefficient of correlation and the r test), then the concentration of the unknown can be found from the calibration curve. The value of which m is an estimate of the true value μ which lies within

the range $\bar{X} - 1.96\hat{\sigma} \leqslant \mu \leqslant \bar{X} + 1.96\sigma$ for a 95% confidence level. $\hat{\sigma}$ is the estimated value of the exact standard deviation and $\hat{\sigma} = S/\sqrt{n}$ where S is the standard deviation of the sample mean. The value of 1.96 corresponds to a particular confidence level sought and can be retrieved from tables.

Conclusion and Suggestions for Further Work

The utility of the graphite rod vaporizer, originally developed for discrete liquid sample introduction, has been extended to solid sample introduction into the ICP. The graphite rod vaporizer has a distinct advantage over some other solid sampling devices in that there are no problems associated with the degree of vaporization and atomization of non-uniform sized particles. In our GRV-ICP instrument, the entire amount of the solid deposited onto the rod is vaporized as a fine aerosol which penetrates the plasma where it is subsequently dissociated, atomized and excited.

The relationship between the relative emission intensity and the mass vaporized has been established to be linear indicating that although the trace elements may be distributed inhomogeneously in the semiconductor crystals examined, the problem is not too serious. A plot of relative emission intensity vs. the concentration of calibrated solid standards would give an indication of the accuracy of the solid sampling procedure employed in this study. But the unavailability of doped standards restricted further examination.

The method of internal standardisation has been investigated. Cadmium proves to be a possible internal standard for the determination of manganese. Further investigation is required to extend the internal standardisation technique to other trace elements.

The magnitude of the area under the emission signal peaks was determined by the 'cut-and-weigh' method. This was far from satisfactory because not only was the procedure time consuming, it was also prone to human errors which occur in the tracing and cutting stages and in the judgement of the level of noise. Some of these errors may be minimized by increasing the chart paper speed so that the thickness of the trace line and the inexactness of the cutting become relatively insignificant as compared to the massive area weighed. Nonetheless, the 'cut-and-weigh' method is imprecise and impractical when a large number of data is handled. Therefore, an electronic circuit for integrating varying signals is frequently employed. A typical circuit is depicted in Figure 71 [181].

Fig. 71 an integrated circuit diagram
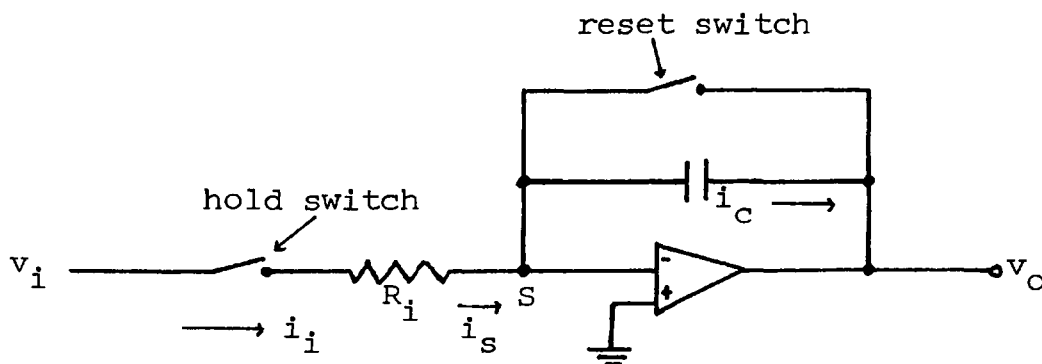
Where $\wedge\!\wedge\!\wedge$, $\|$, and $\triangleright$ denote resistor, capacitor and operational amplifier respectively. By applying Kirchoff's Law,

$$i_i = i_s + i_f \qquad (6.3)$$

because the input impedance of an operational amplifier is always made extremely high, $i_s \ll i_f$ and

$$i_i = i_f \qquad (6.4)$$

The point s is at virtual ground, thus, the output v_o is the voltage across the capacitor. The charge Q of a capacitor is directly proportional to the applied voltage, ie,

$$q = Cv \tag{6.5}$$

Differentiating equation (6.5) gives

$$\frac{dq}{dt} = C \frac{dv}{dt} \tag{6.6}$$

By definition, the current i is the rate of change of charge, therefore, equation (6.6) becomes

$$i = C \frac{dv}{dt} \tag{6.7}$$

Thus, substiting equation (6.7) and Ohm's law (I = V/R) into equation (6.4) gives

$$V_i/R_i = - C \frac{dv_o}{dt} \tag{6.8}$$

$$\text{or} \quad dv_o = - \frac{V_i}{R_i C} dt \tag{6.9}$$

$$\text{and} \quad V_o = - \frac{1}{R_i C} \int_0^t v_i \, dt \tag{6.10}$$

Thus, the output is the time integral of the input voltage. The definite integral is obtained by opening the reset switch and closing the hold switch (Fig. 71) at time zero. Then, when the hold switch is opened at time t, the integration is stopped, thus holding v_o at a constant level for measurement. Closing the reset switch then discharges the capacitor so that a new integration can be started. Figure 72 shows an emission peak and its time integral obtained with an operational amplifier.

The type of integrators described above works well for signals whose background (reference voltage) is constant

with respect to time. But the emission signal observed in the plasma followed by electrothermal vaporization at elevated temperatures takes the form as shown in Fig 73 a
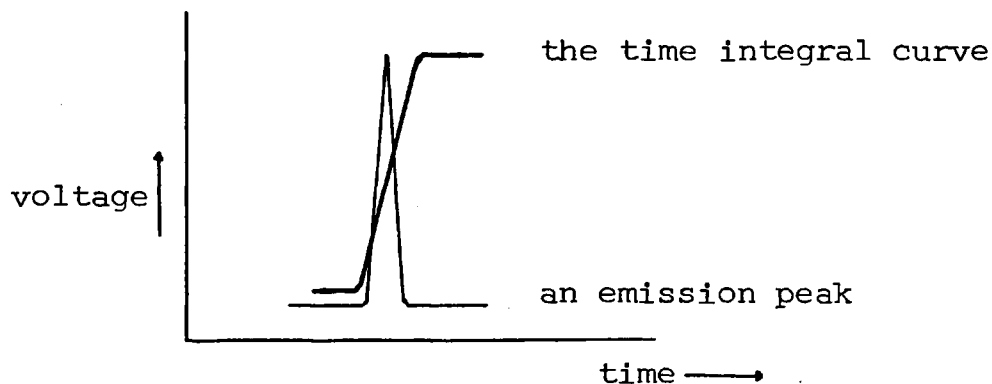
Fig. 72 Diagram of a signal and its integral

Fig. 73a a typical emission signal obtained by ICP-OES.

Fig. 73b the background change in the ICP.

Upon vaporization, there is a decrease in background intensity due to a momentarily increase of argon from the GRV entering the plasma caused by thermal expansion. Then, as the rod cools, the intensity increases because the carrier gas contracts in volume and eventually returns to its normal level as the flow rate stablises (Fig. 73b)[147]. These fluctuations are reproducible and do not present any problem in measuring the

peak height of the emission signals which always appear at

the bottom of the trough when a piece of connecting tubing

(between the GRV and the injector tube) of the length 0.5

metres is used. The peaks thus obtained cannot be integrated

in the normal manner because of the problem of where to take

the reference point for integration. If the reference voltage

was taken at the normal background of the plasma, only the

portion of the peak above that voltage would be integrated.

If the trough was taken as the reference point, then the

integrator would never stop integrating. Fortunately, the

signal could be separated from the pressure pulse by lengthening

the connecting tubing to ca 10.5 metres[147]. In this case,

the background intensity of the plasma altered immediately

when the GRV vaporization cycle was initiated, and after

a time delay, the analyte emission signal profile appeared

over a constant background and could thus be integrated.

The temperature of the graphite rod is not constant

at a set applied voltage. If a ramp generator is attached

to the Shandon Southern programmer to regulate the temperature

it will provide greater flexibility as the temperature and

time for each stage of the heating cycle may be controlled

precisely and accurately.

Finally, the potential of the ICP used as an excitation

source for simultaneous multielement analysis should be

exploited in the analysis of semiconductors.

APPENDIX $(167 - 171)$

Statistics can be defined as the science of class-
ifying and manipulating data in order to draw inferences.
Before any analysis, the Data have to be collected, or-
ganised and presented in a form displaying its distinctive
features. The simplest way is to organise the data in a
Frequency table which is a list of each possible value
the data could have and its total number of occurrence-
the frequency. If the population is large, the variables
can be divided into groups as shown in Table A.1
A histogram obtained by plotting frequency vs the group
interval is shown in Fig. 74

Table A. 1

Group interval	Frequency
0.95-1.14	3
1.15-1.34	5
1.35-1.54	8
1.55-1.74	6
1.75-1.94	3
1.95-2.14	2
2.15-2.34	0
2.35-2.54	0
2.55-2.74	1

More often, it is easier to understand the data
if it is presented diagrammatically or graphically. The
commonly used types are the bar charts, pie charts, his-
tograms and frequency pologon.

Although organised data is more meaningful in

Fig. 74 A Histogram

Frequency (number of occurrence)
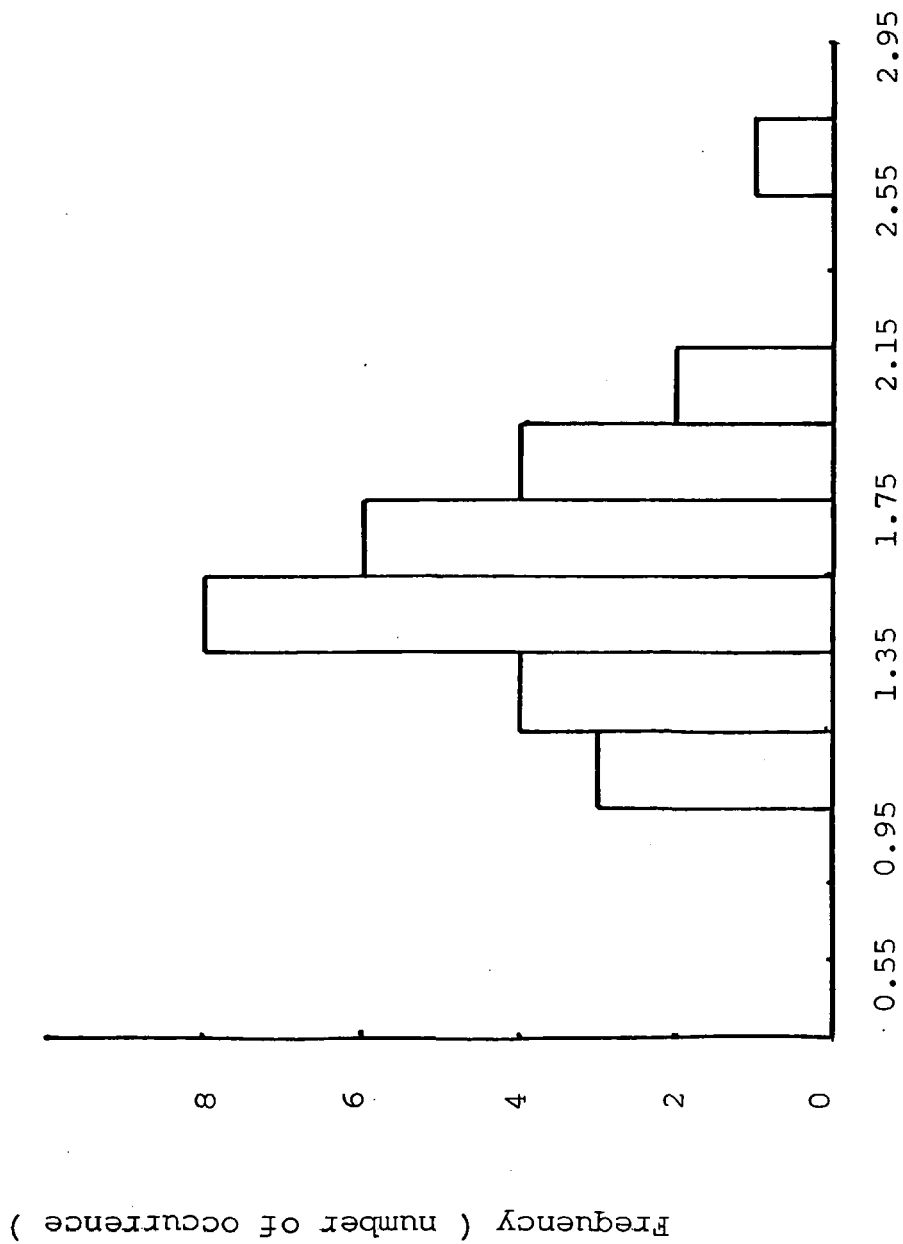
presentation form than unorganised data, there are other ways to describe a set of data which can reveal the underlying trend. Numerical methods are therefore applied.

The Mean:

Quite often, it is desirable to represent a set of data by a number. The number frequently employed is the mean which is a value about which the set of data tends to cluster. Given a set of n number $\left[x_1, x_2, \ldots \right.$ $\left. x_n \right]$, the mean $\bar{x}$ is defined as $\bar{x} = 1/n \left[x_1 + x_2 + \ldots + x_n \right]$ $= 1/n \sum_{i=1}^{n} x_i$ where Σ means the 'sum of'. To calculate $\bar{x}$, all values in the data are included. Another method to calculate the average is the median. For a given total of N values of a variable, arranged in order of magnitude, the median is the $\left[(N+1)/2 \right]$ th value. Thus, the median is unaffected by the upper and lower extremes of the value.

The standard deviation:

Although the mean gives an estimate of the centre of distribution, but it may not accurately reflect the distribution of the values, whether the numbers are close together or far apart. A useful measure of this scatter is called the standard deviation S. Mathematically, standard deviation is defined by the formula $S = \sqrt{\dfrac{\Sigma (x - \bar{x})^2}{n - 1}}$.

For a small population, $(n - 1)$ is used instead of n because it gives an 'unbiased' estimate of the standard deviation of the population. For large population, $(n - 1)$ tends to n, therefore, n is used in the calculations. The square of the standard deviation is also a measure of dispersion. It is called the variance S^2 which is

defined as $S^2 = \dfrac{\Sigma(x - \bar{x})^2}{n - 1}$. Throughout this thesis,

the term relative standard deviation (R.S.D.≅ the coefficient

of variance) has been used. It is defined as R.S.D.= $S/\bar{x}$.

By use of the relative standard deviation, the dispersion

of different frequency distribution can be compared.

The coefficient of correlation:

Coefficient correlation r is a number which

measures the degree of association between two related

sets of data. The coefficient correlation is defined

in such a way that it has a miximum value of +1 and a

minimum value of -1. When the sample points lie exactly

in a straight line with a positive gradient, there is

perfect correlation, r = +1. When the sample points lie

exactly in a straight line with a negative gradient, there

is perfect negative correlation, r = -1. When there is

no tendency for the points to lie in a straight line,

there is no correlation, r = 0. The value r can lie

between +1 or -1. In order to decide whether the value

reflects correlation or not in the population, one applies

a procedure for a check on the validity of r calculated.

That is to compare it with r_{test} value (test correlation

coefficient). The following procedure is applied:

1) Decide how valid one would require r to be,for instance,

   95%.

2) Locate the r_{test} value from tables (an example is shown

   in Table A2 (182)).

3) If the correlation coefficient calculated is greater

   than r_{test}, then, the straight line approximation is valid.

For example, if r is 0.99 and this is compared with the r_{test} value at 95% certainty for 5 samples. From tables A2 r_{test} = 0.878. Therefore $r > r_{test}$ and it is safe to assume that r is valid to a 95% degree of certainty.

Table A2 "r_{test}" Values

# of Samples	degrees of Freedom	80 %	90 %	95 %	99 %	99.9 %
3	1	0.951	.988	.997	1.000	1.000
4	2	0.800	.900	.950	.990	.999
5	3	0.687	.805	.878	.959	.991
6	4	0.608	.729	.811	.917	.974
7	5	0.551	.669	.755	.875	.951
8	6	0.507	.621	.707	.834	.925
9	7	0.472	.582	.666	.798	.898
10	8	0.443	.549	.632	.765	.872
11	9	0.419	.521	.602	.735	.847
12	10	0.398	.479	.576	.708	.823
13	11	0.380	.476	.553	.684	.801
14	12	0.365	.457	.532	.661	.780
15	13	0.351	.441	.514	.641	.760
16	14	0.338	.426	.497	.623	.742
17	15	0.327	.412	.482	.606	.725
18	16	0.317	.400	.468	.590	.708
19	17	0.308	.389	.456	.575	.693
20	18	0.299	:378	.444	.561	.679
21	19	0.291	.369	.433	.549	.665
22	20	0.284	.360	.423	.537	.652
23	21	0.277	.352	.413	.526	.640
24	22	0.271	.344	.404	.515	.629
25	23	0.265	.337	.396	.505	.618
26	24	0.260	.330	.388	.496	.607
27	25	0.255	.323	.381	.487	.597
28	26	0.250	.317	.374	.479	.588
29	27	0.245	.311	.367	.471	.579
30	28	0.241	.306	.361	.463	.570
31	29	0.237	.301	.355	.456	.562
32	30	0.233	.296	.349	.449	.554
42	40	0.202	.257	.304	.393	.490
62	60	0.165	.211	.250	.325	.408
122	120	0.117	.150	.178	.232	.294

Linear Regression:

If the variables are significiently correlated, they can be represented by a straight line from which it is possible to predict which value of the Y variable corresponds ideally to any given value of the X variable. The equation fitting the straight line has a general formula of y = a + bx where y and x are dependent variables, a is the intercept on the y axis and b is the slope of the line.

Probability:

In situations in which there is random variation, probablity is used to measure the chance of an experiment resulting of a particular outcome. A probablity equal to 1 represets certainty. A probability equal to 0 represents impossibility. Hence, all other probabilities lie less than 1 and greater than zero.

Confidence level:

Suppose that it is impossible or impractical to examine the whole population and a random fraction of the population is chosen to be examined and if the mean of the variable in the population is calculated. How can one be sure that the calculated mean is equal or close to the mean of the whole population? In statistics, a range of values is given which includes the true value, this range of values is called an interval estimate. When the interval estimate is assigned with a probablity, then it is called a confidence level.

If the mean of the sample is $\bar{x}$ and if it is used as the best estimate of the mean of the population $\mu = \bar{x}$, then for a sample size n greater than 30, one can be reasonably sure that the true mean is not more than 1.96 standard deviations away from the sample mean at a 95% confidence interval. Using S (standard deviation for the mean) as an estimate for σ ($\sigma = S/\sqrt{n}$) , then the 95% confidence interval can be expressed as

$\bar{x} - 1.965\sigma \leq \mu \leq \bar{x} + 1.965\sigma$ Similarly, the 99% confidence interval is $\bar{x} - 2.58\sigma \leq \mu \leq \bar{x} + 2.58\sigma$.

(1) Bunsen R.
Ann. Chem. (Liebigs) 138, 257, (1866).

(2) Kirchhoff G., Bunsen R.
Pogg. Ann. d. Phys. U Chem. 110, 161, (1860)

(3) Beckmann E.
Z. Elektrochem. 5, 327, (1899).

(4) Beckmann E.
Z. Physik. Chem. 34, 593, (1900).

(5) Beckmann E.
Z. Physik. Chem. 35, 442, (1900).

(6) Gouy G.L.
Ann. Chim. Phys. 18, 5, (1879).

(7) Kniseley R.N., Amenson H., Butler C.C., Fassel V.A.
Appl. Spectrosc. 28, 285, (1974).

(8) Meinhard J.E.
ICP Inf. Newsl. 2, 163, (1977).

(9) Babington R.S.
Pop. Sci. May, 102, (1973).

(10) Fry R.C., Denton M.B.
Anal. Chem. 49, 1413, (1977).

(11) Sudendorf R.F., Boyer K.W.
Anal. Chem. 50, 1769, (1978).

(12) Savage R.N., Hiefje G.M.
Rev. Sci. Instrum. 49, 1418, (1978).

(13) Hoare H.C., Mostyn R.A.
Anal. Chem. 39, 1153, (1967).

(14) Wendt R.A., Fassel V.A.
Anal. Chem. 37, 920, (1965).

(15) Boumans P.W.J.M., de Boer F.J.
Proc. Anal. Div. Chem. Soc. 12, 140, (1975).

(16) Boumans P.W.J.M., de Boer F.J.
Spectrochim Acta 27B, 391, (1972).

(17) Boumans P.W.J.M., de Boer F.J.
Spectrochim Acta 30B, 309, (1975).

(18) Boumans P.W.J.M., de Boer F.J.
Spectrochim Acta 31B, 355, (1976).

(19) Catterick T., Hickman D.A.
Analyst(London) 104, 516, (1979)

(20) Dickson G.W., Fassel V.A.
Anal.Chem. 41 1021, (1969).

(21) Barnett W.B., Fassel V.A., Kniseley R.N.
Spectrochim. Acta 25B, 139, (1970).

(22) Greenfield S., Jones I.L., McD. McGeachin H., Smith P.B.
Anal.Chim. Acta 74, 225, (1975).

(23) Olson K.W., Hass W.J.Jr., Fassel V.A.
Anal. Chem. 49, 632, (1977).

(24) Lang R.J.
      J. Acoust. Soc. Am. 34, 6, (1962)

(25) Boucher R.M., Kreuter J.
      An. Allergy 26, 591, (1969)

(26) Stupar J., Dawson J.B.
      Appl. Opt. 7, 1351, (1968)

(27) Robin J.
      ICP Inf. Newsl. 3, 249, (1977)

(28) Issaq H.J., Morgenthaler P.
      Anal. Chem. 47, 1748, (1975)

(29) Denton M.B., Malmstadt H.V.
      Anal. Chem. 44, 241, (1972)

(30) Korte N.E., Moyers J.E., Denton M.B.
      Anal. Chem. 45, 530, (1973)

(31) L'Vov B.V.
      Spectrochim. Acta 24B, 53, (1969)

(32) Massmann H.
      Spectrochim Acta 23B, 53, (1968)

(33) King A.S.
      Astrophysical J. 21, 236, (1905)

(34) King A.S.
      Astrophysical J. 27, 353, (1908)

(35) King A.S.
      Astrophysical J. 28, 239, (1913)

(36) Woodriff R., Stone R.W., Held A.M.
      Appl. Spectrosc. 22, 408, (1968)

(37) Woodriff R., Ramelow G.
      Spectrochim. Acta 23B, 665, (1968)

(38) Woodriff R., Stone R,W.
      Appl. Opt. 7 1337, (1968)

(39) Headridge J.B., Smith D.R.
      Talanta 18, 247, (1971)

(40) West T.S., William Y.K.
      Anal.Chim.Acta 45, 27, (1969)

(41) Alder J.F., West T.S.
      Anal. Chim. Acta 51, 365, (1970)

(42) Gregoire D.C., Chakrabarti C.L.
      Anal. Chem. 49, 2018, (1977)

(43) Krasilschik V.Z., Lifshits M.G.
      Zavod. Lab. 43, 692, (1977)

(44) Sturgeon R.E., Chakrabarti C.L.
      Anal. Chem. 49, 90, (1977)

(45) Manning D.C., Ediger R.D.
      At. Abs. Newsl. 15, 42, (1976)

(46) Donega H.M., Burgess T.E.
      Anal. Chem. 42, 1521, (1970)

(47) Maruta T., Takeuchi T.
Anal. Chim. Acta 62, 253, (1972)

(48) Maruta T., Takeuchi T.
Anal. Chim. Acta 66, 5, (1973)

(49) Williams M., Piepmeier E.H.
Anal. Chem. 44, 1342, (1972)

(50) Cantle J.E., West T.S.
Talanta 20, 459, (1973)

(51) Chauvin J.V., Newton M.P., Davis D.G.
Anal. Chim. Acta 65, 291, (1973)

(52) Newton M.P., Davis D.G.
Anal. Chem. 47, 2003, (1975)

(53) Goode S.R., Montaser A., Crouch S.R.
Appl. Spectrosc. 27, 355, (1973)

(54) Garnys V.P., Smythe L.E.
Anal. Chem. 51, 62, (1979)

(55) Syty A.
CRC Critical Review in Anal. Chem. 4, 155, (1974)

(56) Sycha V., Kolihiva D., Vyskovilova O., Hlavac R. Puschell P.
Anal Chim Acta 105, 263, (1979)

(57) Alder J.F., Gunn A.M., Kirkbright G.F.
Anal. Chim. Acta 92, 43, (1977)

(58) Gunn A.M., Millard D.L., Kirkbright G.F.
Analyst 103, 1066, (1978)

(59) Millard D.L., Shan H.C., Kirkbright G.F.
Analyst 105, 1502, (1980)

(60) Snook R.D.
AWRE report (1979)

(61) Nixon D.E., Fassel V.A., Kniseley R.N.
Anal. Chem. 46, 210, (1974)

(62) Fassel V.A.
Flameless atomic absorption analysis: an update
ASTM STP 618

(63) Dahlquist R.L., Knoll J.W., Hoyt R.E.
Paper presented at 26th. Pittsburgh Conference on
Analytical Chemistry and Applied Spectroscopy,
Cleveland, Ohio March 1975

(64) Aldous K.M., Dagnall R.M., Sharp B.L.
Anal. Chim. Acta 54, 233 (1971)

(65) Runnels J.H., Gibson J.H.
Anal. Chem. 39, 1598, (1967)

(66) Taylor H.E., Gibson J.H., Skogerboe R.K.
Anal. Chem. 42, 1569, (1970)

(67) Greenfield S., Smith P.B.
Anal. Chim. Acta 59, 341, (1972)

(68) Kniseley R.N., Fassel V.A., Butler C.C.
Clin. Chem. 19, 807, (1973)

(69) Fry R.C., Northway J.J., Denton M.B.
      Anal. Chem. <u>50</u>, 1719. (1978)

(70) Uchida H., Matsui H., Uchida T., Zida C.
      Spectrosc. Lett. <u>11</u>, 1, (1978)

(71) West C.D., Hume D.N.
      Anal. Chem. <u>36</u>, 412, (1964)

(72) Dalton E.F., Malanoski A.J.
      At. Abs. Newsl. <u>10</u>, 92, (1971)

(73) Melton T.R., Hoover W.L., Ayers J.L., Howard P.A.
      Soil Sci. Soc. Am. Proc. <u>37</u>, 558, (1973)

(74) Azad J., Kirkbright G.F., Snook R.D.
      Analyst <u>104</u>, 232, (1979)

(75) Azad J., Kirkbright G.F., Snook R.D.
      Analyst <u>105</u>, 79, (1980)

(76) Chi R.C., Banon G.R., Baumgamer P.A.W.
      Anal. Chem. <u>44</u>, 1476, (1972)

(77) Lichte F.C., Skogerboe R.K.
      Anal. Chem. <u>44</u>, 1480, (1972)

(78) Goulden P.D., Brooksbank P.
      25th Pittsburgh Conference on Analytical Chemistry
      and Applied Spectroscopy, Cleveland, Ohio March 1975

(79) Vijan P.N., Wood G.R.
      At. Abs. Newsl. <u>13</u>, 33, (1974)

(80) Thompson M., Pahlavanpour B., Walton, Kirkbright G.F.
      Analyst <u>103</u>, 568, (1978)

(81) Thompson M., Pahlavanpour B.
      Anal. Chim. Acta <u>109</u>, 251, (1979)

(82) Alder J.F., Mermet J.M.
      Spectrochim. Acta <u>28B</u>, 421, (1973)

(83) Alder J.F., Bombelka R.M., Kirkbright G.F.
      J. Physics <u>11B</u>, 235, (1978)

(84) Mermet J.M., Jarosz J.
      J. Quant. Spectrosc. Radiant. Transfer <u>17</u>, 237, (1977)

(85) Mermet J.M.
      Spectrochim. Acta <u>30B</u>, 383, (1975)

(86) Kirkbright G.F., Snook R.D.
      Anal. Chem. <u>51</u>, 1938, (1979)

(87) Aggett J., West T.S.
      Anal. Chim Acta <u>55</u>, 349, (1971)

(88) Garnys V.P., Smythe L.E.
      Talanta <u>22</u>, 881, (1975)

(89) Cormier M.J., Hercules D.M., Lee J., Editors
      "Chemiluminescence and bioluminescence' Plenum Press,
      London, N.Y. 1973

(90) Seitz W.R., Neary M.P.
      Anal. Chem. <u>46</u>, 188A, (1974)

(91) Paul D.B.
      Talanta 25, 377, (1978)

(92) Salet G.
      Acad. Sci. (paris), 68, 404, (1869)

(93) Fowler A., Vaidya W.A.
      Proc. Roy. Soc. London Ser. A 132, 310, (1931)

(94) Gaydon A.G.
      'The Spectroscopy of Flames' John Wiley and Sons Inc.
      N.Y. 1959

(95) Crone (Private communication to Gaydon & Whittingham)
      Pro. Roy. Soc. A 189, 313, (1974)

(96) Bulewicz E.M., Sugden T.M.
      Trans. Farad. Soc. 54, 1855, (1958)

(97) Syty A., Dean J.
      Appl. Opt. 7, 1331, (1968)

(98) Sugden T.M., Demerdache A.
      Nature 195, 596, (1962)

(99) Lam Thanh M., Peyron M.
      J. Chim. Phys. 60, 1289, (1963)

(100) Lam Thanh M., Peyron M.
      J. Chim. Phys. 61, 452, (1964)

(101) Fenimore C.P., Jones G.W.
      Combustion and Flames 8, 133, (1964)

(102) Aldous K.M., Dagnall R.M., West T.S.
      Analyst 95, 1130, (1970)

(103) Prager M., Seitz W.R.
      Anal. Chem. 49, 148, (1975)

(104) Syty A.
      At. Abs. Newsl. 12, 1, (1963)

(105) Willis J.B.
      Spectrochim. Acta 23A, 811, (1968)

(106) Dagnall R.M., Thompson K.C., West T.S.
      At. Abs. Newsl. 6, 117, (1967)

(107) David D.J.
      Spectrochim. Acta 20, 1185, (1964)

(108) Kirkbright G.F., Ward A.F., West T.S.
      Anal. Chim. Acta 62, 241, (1972)

(109) L'Vov B.V.
      Pure and Appl. Chem. 23, 11, (1970)

(110) Crider W.L.
      Anal. Chem. 37, 1770, (1965)

(111) Dagnall R.M., Thompson K.W., West T.S.
      Analyst 92, 506, (1967)

(112) Belcher R., Bogdanski S.L., Townsend A.
      Anal. Chim. Acta 67, 1, (1973)

(113) Belcher R., Bogdanski S.L., Knowles D.J., Townsend A.
      Anal. Chim. Acta 79, 292, (1975)

(114) Everette G.L., West T.S.
Anal. Chim. Acta 68,387, (1974)

(115) Hamouda A.
Ph.D. Thesis, Univ. of London, 1978

(116) Kargosha K.
Ph.D. Thesis, Univ. of London, 1979

(117) Gilbert M.
Symposium on Combustion, 6th , New Haven, (1957)

(118) Dĕdina J., Rubĕska
Anal. Chim. Acta 35B, 119, (1980)

(119) Alkemade T.I., Herrmann R.
Fundamentals of Analytical Flame Spectroscopy
Adam Hilger Ltd., England p.177 (1979)

(120) Mizany A.Z.
J. Chromatog. Sci. 8, 151, (1970)

(121) Sugijama T., Suzuki Y., Takeuchi T.
J. Chromatog. 80, 61. (1973)

(122) Veillon C., Park J.Y.
Anal. Chim. Acta 60, 293, (1972)

(123) Fredriksson S.A., Cedergren A.
Anal. Chim. Acta 100, 429, (1978)

(124) Dippel W.A., Bricker C.E., Furman
Anal. Chem. 26, 553, (1954)

(125) Thomas L.C., Chamberlain G.J.
'C lorimetric chemical analytical methods' 8th Edn.
The Tinbometer Ltd., Salisbury, U17- 1974

(126) Brite D.W.
Anal. Chem. 27, 1815, (1955)

(127) Davis A., Dinan F.J., Lobbett E.J., Chazin J.D, Tufts L.E.
Anal. Chem. 36, 1066, (1964)

(128) Dagnall R.M., Thompson K.C., Wesr T.S.
Analyst 93, 72, (1968)

(129) Brody S.S., Chaney J.E.
J. of Gas Chromtog. 4,42, (1966)

(130) Patterson P.L., Howe R.L., Abu-Shumays A.
Anal. Chem. 50, 339, (1978)

(131) Bowman M.C., Beroza M.
Anal. Chem. 40, 1448, (1968)

(132) Everett G.L.
Ph.D. Thesis, Univ. of London, 1975

(133) Campbell D.
U.S. National Technical Information Service PB-252 952
(1976)

(134) Driedger A. Seitz W.R.
Anal. Chem. 51, 1197, (1979)

(135) Aldous K.M., West T.S., Dagnall R.M., Pratt S.J.
Anal. Chem. 41, 1851, (1969)

(136) Aldous K.M., Dagnall R.M., West T.S.
       Analyst 95, 417, (1970)

(137) Belcher R., Bogdanski S.L., Townsend A.
       Anal. Lett. 2, (1974)

(138) Greenfield S., Jones I.L.W., Berry C.T.
       Analyst 89, 713, (1964)

(139) Wendt R.H., Fassel V.A.
       Anal. Chem. 37, 920, (1965)

(140) Fassel V.A., Kniseley R.N.
       Anal. Chem. 46, 1158A, (1974)

(141) Fassel V.A., Kniseley R.N.
       Anal. Chem. 46, 1110A, (1974)

(142) Greenfield S., McGreachin H. McD., Smith P.B.
       Talanta 22, 1, (1975)

(143) Boumans P.W.J.M.
       Phillips Tech. Rev. 34, 305, (1974)

(144) Boumans P.W.J.M., Barnes R.M.
       ICP Inform. Newsl. 3, 445, (1978)

(145) Bombelka R.M.
       Ph.D. Thesis, Univ. of London, 1978

(146) Millard D.L.
       Ph.D. Thesis, Univ. of London, 1979

(147) Gunn A.M.
       Ph.D. Thesis, Univ. of London, 1979

(148) Dickson G.W., Svobada V.
       Anal. Chem. 41, 1021, (1969)

(149) Boumans P.W.J.M., de Boer F.J.
       Spectrochim Acta 30B, 109, (1975)

(150) Abdallah M.H., Demiaszonek R., Jarosz J., Mermet J.M.,
       Robin J., Trassy C.
       Anal. Chim. Acta 84, 271, (1976)

(151) Kniseley R.N., Fassel V.A., Butler C.C.
       Clin. Chem. 19, 807, (1973)

(152) Kirkbright G.F., Ward A.F., West T.S.
       Anal. Chim. Acta 62, 241, (1972)

(153) Gunn A.M., Kirkbright G.F., Opheim L.N.
       Anal.Chem. 49, 1492, (1977)

(154) Alder J.F., Mermet J.M.
       Spectrochim. Acta 28B, 421, (1973)

(155) Hoult D.W.
       Atomic Spectroscopy 1, 82, (1980)

(156) Wallace G.F.
       Atomic Spectroscopy 1, 38, (1980)

(157) Gunn A.M.
       Thesis, London University, (1979), p.186

(158) Dahlquist R.L.
       ICP Inf. Newsl. $\underline{1}$, 148, (1975)

(159) Scott R.H.
       Spectrochim. Acta $\underline{33B}$, 123, (1978)

(160) Greenfield S, Jones I.L., Berry C.T.
       Analyst $\underline{89}$, 713, (1964)

(161) Dagnall R.M., Smith D.J., West T.S., Greenfield S.
       Anal. Chim. Acta $\underline{54}$, 397, (1971)

(162) Hoare H.C., Mostyn R.A.
       Anal. Chem. $\underline{39}$, 1153, (1967)

(163) Abercrombie F.N., Silvester M.D., Stoute G.S.
       Paper No.40, presented at the 28th Pittsburgh
       Conference, Cleveland, Ohio, March 1977; ICP
       Inf. Newsl. $\underline{2}$, 309, (1977)

(164) Salin E.D., Carr J., Horlick G.
       Paper No. 563, presented at the 30th Pittsburgh
       Conference, Cleveland, Ohio, March, 1979; ICP
       Inf. Newsl. $\underline{4}$, 401, (1979)

(165) Clegg J.B., Mullin J.B., Timmins K.J., Blackmore G.W.
       Everett G.L., Snook R.D.
       J. of Materials Science
       in press.

(166) Boumans P.W.J.M
       Spectrochim. Acta $\underline{34B}$, 59, (1979)

(167) Yamane T.
       Statistics-An Introductory Analysis. 3rd Edn.
       Harper International Edition

(168) Byrkit D.R.
       Elements of Statistics 2nd Edn. D. Van Nostrand
       Company

(169) Naiman A., Rosenfeld R., Zirkel G.
       Understanding Statistics 2nd Edn. McGraw-Hall Company

(170) Hine J., Wetherill G.B.
       A programmed text in statistics Books 1-4, Chapman & Hall

(171) The Open University Mathematics Foundation Course
       Unit 16
       Probability and Statistics I

(172) Kirkbright G.F., Shan H.C., Snook R.D.
       Atomic Spectroscopy $\underline{1}$, No.4, 85, (1980)

(173) Kirkbright G.F., Sargent M.
       "Atomic Absorption and Fluorescence Spectroscopy"
       Academic Press, London (1974)

(174) Alkemade C.Th.J.
       Anal. Chem. $\underline{38}$, 1252, (1966)

(175) Larson G.F., Fassel V.A., Winge R.K., Kniseley R.N.
       Appl. Spec. $\underline{30}$, 384, (1976)

(176) Winge R K. Fassel V.A., Kniseley R.N., DeKalb E.,
       Hass W.J.
       Spectrochim. Acta $\underline{32B}$, 327, (1977)

(177)   Fassel V.A., Katzenberger J.M., Winge R.C.
        Appl. Spec. __33__, 1, (1979)

(178)   Hassel K.D., Rose D.A., Warren J.
        ICP Inf. Newsl. __4__, 261, (1978)

(179)   Greer D.G., Bydalek T.J.
        Environ. Sci. Tech. __7__, 153, (1973)

(180)   Patterson P.L., Howe R.L., Abu-Shumays A.
        Anal. Chem. __50__, 339, (1978)

(181)   Skoog D.A., West D.M.
        Principles of Instrumental Analysis, 2nd. edn.
        Saunders College, Philadelphia 1980.

(182)   Texas Instruments Calculator Handbook (TI 51-III)
        Texas Instruments, Manton Lane, Bedford, MK41 7PU

(183)   Prager M.J., Seitz W.R.
        Anal. Chem. __47__, 148, (1975)